AN ANALYSIS OF THE EFFECTS OF LOW ENERGY ELECTRON RADIATION ON $Al_xGa_{1-x}N$/GaN MODULATION-DOPED FIELD-EFFECT TRANSISTORS

THESIS

James M. Sattler, Second Lieutenant, USAF

AFIT/GE/ENP/04-02

DEPARTMENT OF THE AIR FORCE
AIR UNIVERSITY

AIR FORCE INSTITUTE OF TECHNOLOGY

Wright-Patterson Air Force Base, Ohio

APPROVED FOR PUBLIC RELEASE; DISTRIBUTION UNLIMITED

The views expressed in this thesis are those of the author and do not reflect the official policy or position of the United States Air Force, Department of Defense, or the United States Government.

AFIT/GE/ENP/04-02

AN ANALYSIS OF THE EFFECTS OF LOW ENERGY ELECTRON RADIATION ON $Al_xGa_{1-x}N/GaN$ MODULATION-DOPED FIELD-EFFECT TRANSISTORS

THESIS

Presented to the Faculty

Department of Physics

Graduate School of Engineering and Management

Air Force Institute of Technology

Air University

Air Education and Training Command

In Partial Fulfillment of the Requirements for the

Degree of Master of Science in Electrical Engineering

James M. Sattler, BSEE

Second Lieutenant, USAF

March 2004

APPROVED FOR PUBLIC RELEASE; DISTRIBUTION UNLIMITED

AFIT/GE/ENP/04-02

AN ANALYSIS OF THE EFFECTS OF LOW ENERGY ELECTRON RADIATION ON $Al_xGa_{1-x}N/GaN$ MODULATION-DOPED FIELD-EFFECT TRANSISTORS

James M. Sattler, BSEE
Second Lieutenant, USAF

Approved:

James C. Petrosky (Chairman)	12MAR04 date
Paul Kladitis (Member)	12 MAR04 date
Gary C. Farlow (Member)	12 March '04 date

AFIT/GE/ENP/04-02

Abstract

The effects of radiation on $Al_xGa_{1-x}N$/GaN MODFETs is an area of increasing interest to the USAF as these devices become developed and integrated in satellite-based systems. Irradiation is also a valuable tool for analyzing the quantum-level characteristics and properties that are responsible for device operation.

$Al_xGa_{1-x}N$/GaN MODFETs were fabricated and irradiated at liquid nitrogen temperatures by 0.45 –1.2 MeV electrons up to doses of 6×10^{16} e^-/cm^2. Following irradiation, low temperature *I-V* measurements were recorded providing dose-dependent measurements. Temperature-dependent *I-V* measurements were also made during room temperature annealing following irradiation.

I-V measurements indicate radiation-induced changes occur in these devices creating increased gate and drain currents. These increased currents are only maintained at low temperatures (T < 300 K). It is believed that the increase in gate current is caused by an increase in the electron trap concentration of the $Al_xGa_{1-x}N$ layer. This increase in trap concentration directly increases the trap-assisted tunneling current resulting in the observed increase in gate current. The mechanism causing the increase in drain current is unknown. Several theories explaining this increase are presented along with the additional research necessary to illuminate the correct theory. This is the first experiment involving electron radiation of $Al_xGa_{1-x}N$/GaN MODFETs.

AFIT/GE/ENP/04-02

To my parents

Acknowledgments

The results of any endeavor are not a product of mere chance; they are a testament to the long and difficult road traversed during the course of the endeavor. The journey itself, being paved with frustration, disappointment, determination, and perseverance, would be at best dissatisfying, and at worst impossible were it not for the efforts and encouragement of advisors, co-workers, family, and friends. Consequently, it is essential that credit for the results of this endeavor, be shared with those persons who provided support to the researcher throughout the journey.

LTC James Petrosky, my advisor, provided me with vital technical knowledge as well as the tools and experience to carry out this difficult project. Additionally, and perhaps more importantly, he was an outstanding guide in the strange new land of professional research and experimentation. His ability to see and articulate the "big picture" to a young and inexperienced engineer prevented the research effort from straying off course.

Dr. Gary Farlow of the Wright State University was responsible for providing the means by which the experiments were carried out. Without the timeless efforts he provided towards maintaining and running the Van de Graff facility during the experiments, there would be no results to present.

Lieutenant Neil Moser of the AFRL Sensors Directorate was responsible for fabricating and testing the transistors that were used in this research. Additionally, he and

his co-worker, Dr. Robert Fitch provided crucial information that yielded a better understanding of the transistors and their operation.

Larry Callaghan was responsible for wafer dicing and packaging. His consistently quick turn-around on packaging requests proved to be integral, allowing experiments to be conducted when needed.

My Mother, Father, Brothers, and other family members and friends continuously provided me with the support and encouragement that kept me going when things seemed at their worst. Their ability to make me smile and even laugh during those bleak moments cannot be credited enough.

Finally, and most importantly, I give thanks to God and my savior Jesus Christ for giving me the strength, wisdom, and patience needed to complete this effort.

James M. Sattler

Table of Contents

Page

Abstract iv

Acknowledgments vi

List of Figures x

List of Tables xv

List of Symbols xvi

List of Abbreviations xix

I. Introduction 1

- Background 1
- Problem Statement 6
- Hypothesis 6
- Objectives 6
- Scope 7
- Approach 7
- Assumptions 9
- Results 9
- Sequence of Presentation 10

II. Literature Review 12

- Purpose 12
- The Need for GaN Heterostructures 12
- Radiation Effects on $Al_xGa_{1-x}N$/GaN Heterostructures 17
- Research Justification 21

III. Theoretical Considerations 22

- $Al_xGa_{1-x}N$/GaN MODFETs 22
- Radiation Interactions 32

IV. Experimental Procedures 38

- Transistor Fabrication 38
- Packaging 43
- Pre-Irradiation Characterization 47
- Irradiation Experiments 50

V. Experimental Results 60

First Experiment I-V Measurements....60
Second Experiment I-V Measurements....64
Analysis and Discussion....75

VI. Conclusions and Recommendations....83

Conclusions....83
Recommendations for Further Work....84

Appendix A – TIGER Code Simulations....86

Appendix B – Visual Basic Data Acquisition Program....95

Appendix C – Experimentally Induced MODFET Damage....102

Appendix D – Additional Experimental Plots....109

Bibliography....117

Vita....120

List of Figures

Figure Page

1. Semiconductor Device Family Tree; MODFET Lineage 4

2. Trapped Electron Radiation Belts for Energies Greater than 1 MeV [9] 5

3. Intrinsic Carrier Concentration as a Function of Temperature for Various Semiconductors [5] 13

4. Historical Progress in $Al_xGa_{1-x}N$/GaN HEMT Power Densities [12] 17

5. Applications of GaN-based HEMTs [12] 17

6. Common-Source DC *I-V* Curves; Pre-Irradiation (Solid Curves), Post 10^{11} cm^{-2} Fluence (Dashed Curves), and Post 10^{12} cm^{-2} Fluence (Dotted Curves) [15] 19

7. Basic $Al_xGa_{1-x}N$/GaN MODFET Structure 23

8. Band Structure of $Al_xGa_{1-x}N$/GaN Interface [16] 25

9. Important Properties of III-Nitride Materials [12] 26

10. Schematic Representation of the FET Model Used for Drain Current Derivation [21] 28

11. Proposed Mechanism for DC Drain Current Compression [12] 32

12. Electron Stopping Power in $Al_xGa_{1-x}N$ and GaN as Calculated by XGEN 34

13. Electron Range in $Al_xGa_{1-x}N$ and GaN as Calculated by XGEN 35

14. Single Reticle Layout 39

15. AFRL/SNDD UV Exposure System Used for Photolithography 40

16. FatFET Layout 41

17. Cross Section A-1 (Not to Scale) 42

18. AFRL/SNDD DC/RF Transistor Tester 43

19. Unpackaged Reticles from JS01A 44

20. Reticle Labeling System 44

21. Packaged Reticles 46

22. JS01A Reticle Identification Map Showing Locations of Irradiated Samples 46

23. Building 470 Experimental Setup for Pre-Irradiation *I-V* Characterization 48

24. Cold Head and Sample Mount Assembly [10] 48

25. AFIT Probe-Stand Used for Pre- and Post-Irradiation *I-V* Characterization 49

26. AFIT Probe-Stand Testing of JS01A 49

27. Wright State University Van de Graff Generator 51

28. Cold Head/Sample Mount with Sample Showing Internal Feed-Through Lines Soldered to Sample Leads.....53

29. Cold Head Mounted to VDG Beam Chamber Showing External Feed-Through Lines Connected to Instrumentation Lines 54

30. Schematic of WSU VDG Experimental Setup 54

31. Cold Head Operation Under Cryogenic Conditions 55

32. Sample A0410 2X150X1.2 Transistor, SNDD vs. AFIT Room Temperature *I-V* Curves 62

33. Sample A0410 2X150X1.2 Transistor, Percent Change from SNDD to AFIT Room Temperature *I-V* Curves.....62

34. Sample A0313 2X150X1.2 Transistor Pre- and Post-Irradiation Room Temperature *I-V* Curves (1.2 MeV Electrons) 63

35. Sample A0313 2X150X1.2 Transistor Percent Change from Pre- to Post-Irradiation Room Temperature *I-V* Plots (1.2 MeV Electrons) 63

36. Sample A0408 FatFET First Irradiation: Change in *I-V* Curves at LiN Temperature (0.45 MeV Electrons) 65

37. Sample A0408 FatFET First Irradiation: Change in Gate Leakage Currents at LiN Temperature (0.45 MeV Electrons) 65

38. Sample A0408 FatFET Second Irradiation: Change in *I-V* Curves at LiN Temperature (0.45 MeV Electrons) 66

39. Sample A0408 FatFET Second Irradiation: Change in Gate Leakage Currents at LiN Temperature (0.45 MeV Electrons) 66

40. Sample A0409 FatFET First Irradiation: Change in *I-V* Curves at LiN Temperature (0.45 MeV Electrons) 68

41. Sample A0409 FatFET First Irradiation: Change in Gate Leakage Currents at LiN Temperature (0.45 MeV Electrons) 68

42. Sample A0409 FatFET Second Irradiation: Change in *I-V* Curves at LiN Temperature (0.45 MeV Electrons) 69

43. Sample A0409 FatFET Second Irradiation: Change in Gate Leakage Currents at LiN Temperature (0.45 MeV Electrons) 69

44. Sample A0408 FatFET First Irradiation, LiN Temperature I-V Curves Minus Gate Leakage 72

45. Sample A0409 FatFET First Irradiation, LiN Temperature I-V Curves Minus Gate Leakage 72

46. Sample A0408: Magnitude of Change in Drain and Gate Currents for First Irradiation (1×10^{14} e^-/cm^2 at 0.45 MeV) 73

47. Sample A0409: Magnitude of Change in Drain and Gate Currents for First Irradiation (3×10^{14} e^-/cm^2 at 0.45 MeV) 73

48. Sample A0409 FatFET Room Temperature Pre- and Post-Irradiation *I-V* Curves .. 74

49. Sample A0409 FatFET Pre- and Post-Irradiation Gate Leakage Currents 74

50. Dose Deposited in Source and Drain Regions by 10^{14} e^-/cm^2 (0.45 MeV) 89

51. Dose Deposited in Source and Drain Regions by 10^{14} e^-/cm^2 (0.8 MeV) 89

52. Dose Deposited in Source and Drain Regions by 10^{14} e^-/cm^2 (1.2 MeV) 90

53. Dose Deposited in Gate Region by 10^{14} e^-/cm^2 (0.45 MeV) 90

54. Dose Deposited in Gate Region by 10^{14} e^-/cm^2 (0.8 MeV) 91

55. Dose Deposited in Gate Region by 10^{14} e^-/cm^2 (1.2 MeV) 91

56. Dose Deposited in Region Between Source and Gate or Drain and Gate by 10^{14} e^-/cm^2 (0.45 MeV).....92

57. Dose Deposited in Region Between Source and Gate or Drain and Gate by 10^{14} e^-/cm^2 (0.8 MeV).....92

58. Dose Deposited in Region Between Source and Gate or Drain and Gate by 10^{14} e^-/cm^2 (1.2 MeV).....93

59. Dose Deposited in $Al_{0.27}Ga_{0.73}N$ Region Along the 2DEG (0.45 MeV).....94

60. Dose Deposited in GaN Region Along the 2DEG (0.45 MeV).....94

61. Sample A0313 FatFET Irradiation Experiment Drain Damage 103

62. Sample A0314 FatFET Irradiation Experiment Drain Damage 103

63. Sample A0315 FatFET Irradiation Experiment Drain Damage 104

64. Sample A0316 FatFET Irradiation Experiment Drain Damage 104

65. Sample A0408 2X150X1.2A FET Pre-Irradiation Picture.....106

66. Sample A0408 2X150X1.2A FET Post-Irradiation Experiment Damage.....106

67. Sample A0409 2X150X1.2A FET Pre-Irradiation Picture.....107

68. Sample A0409 2X150X1.2A FET Post-Irradiation Experiment Damage.....107

69. Sample A0408 2X150X1.2 Transistor, SNDD vs. AFIT Room Temperature *I-V* Curves 109

70. Sample A0408 2X150X1.2 Transistor, Percent Change from SNDD to AFIT Room Temperature *I-V* Curves.....109

71. Sample A0409 2X150X1.2 Transistor, SNDD vs. AFIT Room Temperature *I-V* Curves 110

72. Sample A0409 2X150X1.2 Transistor, Percent Change from SNDD to AFIT Room Temperature *I-V* Curves.....110

73. Sample A0411 2X150X1.2 Transistor, SNDD vs. AFIT Room Temperature *I-V* Curves.....111

74. Sample A0411 2X150X1.2 Transistor, Percent Change from SNDD to AFIT Room Temperature *I-V* Curves.....111

75. Sample A0412 2X150X1.2 Transistor, SNDD vs. AFIT Room Temperature *I-V* Curves.....112

76. Sample A0412 2X150X1.2 Transistor, Percent Change from SNDD to AFIT Room Temperature *I-V* Curves.....112

77. Sample A0314 2X150X1.2 Transistor Pre- and Post-Irradiation Room Temperature *I-V* Curves (0.8 MeV Electrons).....113

78. Sample A0314 2X150X1.2 Transistor Percent Change from Pre- to Post-Irradiation Room Temperature *I-V* Plots (0.8 MeV Electrons).....113

79. Sample A0315 2X150X1.2 Transistor Pre- and Post-Irradiation Room Temperature *I-V* Curves (0.8 MeV Electrons).....114

80. Sample A0315 2X150X1.2 Transistor Percent Change from Pre- to Post-Irradiation Room Temperature *I-V* Plots (0.8 MeV Electrons).....114

81. Sample A0409 FatFET Third Irradiation: Change in *I-V* Curves at LiN Temperature (0.45 MeV Electrons).....115

82. Sample A0409 FatFET Third Irradiation: Change in Gate Leakage Currents at LiN Temperature (0.45 MeV Electrons).....115

83. Sample A0409 FatFET Fourth Irradiation: Change in *I-V* Curves at LiN Temperature (0.45 MeV Electrons).....116

84. Sample A0409 FatFET Fourth Irradiation: Change in Gate Leakage Currents at LiN Temperature (0.45 MeV Electrons).....116

List of Tables

Table Page

1. Properties of Wurtzite GaN [10] 14

2. Advantages of GaN-Based Transistors [12] 15

3. Bandgaps of Various Semiconductors [5] 23

4. Maximum Energy Transferred to Gallium and Nitrogen Lattice Atoms for Given Incident Electron Energies 37

5. First Irradiation Experiment Summary (09-10 December 2003) 57

6. Second Irradiation Experiment Summary (28 January 2004) 59

List of Symbols

Symbol	Description	Unit
c	Speed of Light	m/s
C_p	Specific Heat	cal/mol·K
$D(z)$	Displacement Field	$C \cdot cm^{-3}$
$\varepsilon(z)$	Position-Dependent Dielectric Constant	unitless
ε_ρ	Static Dielectric Constant	unitless
ε_∞	High Frequency Dielectric Constant	unitless
E	Electric Field	V/m
E_C	Conduction Band Energy Level	eV
E_{e^-}	Incident Electron Energy	eV
E_F	Fermi Level	eV
E_i	ith Quantized Energy Level	eV
E_{trans}^{max}	Maximum Elastic Collisional Transfer Energy	eV
E_V	Valance Band Energy Level	eV
F	Energy Level	eV
$\hbar$	Reduced Planck's Constant ($h/2\pi$)	J·s
I_D, I_d	Drain Current	A
I_{DS}	Source-to-Drain Current	A
I_g	Gate Current	A
κ	Thermal Conductivity	W/cm·K
k_B	Boltzman's Constant	eV/K

λ_B	de Broglie wavelength	m
λ_D	Debye Length	nm
μ_e	Bulk Electron Mobility	$cm^2/V\cdot s$
μ_H	Bulk Hole Mobility	$cm^2/V\cdot s$
μ_0	Low Field Mobility	$cm^2/V\cdot s$
$m(z)$	Position-Dependent Effective Mass	kg
m_{e^-}	Electron Rest Mass	kg
m_{atom}	Target Atom Mass	kg
n	Index of Refraction	unitless
$n(z)$	Position-Dependent Electron Charge Concentration	cm^{-3}
$n_s(x)$	Sheet Charge Density	cm^{-2}
N_D^+	Ionized Donor Concentration	cm^{-3}
N_A^-	Ionized Acceptor Concentration	cm^{-3}
φ	Electron Wave Function	unitless
Φ	Electron Fluence	e^-/cm^2
$p(z)$	Position-Dependent Hole Charge Concentration	cm^{-3}
P	Total Polarization	$C\cdot cm^{-2}$
P_{pz}	Piezoelectric Polarization	$C\cdot cm^{-2}$
P_{sp}	Spontaneous Polarization	$C\cdot cm^{-2}$
q	Elementary Charge	C
ρ	Density	g/cm^3
R_D	Drain Resistance	Ω

R_S	Source Resistance	Ω
T	Temperature	K
$v(x)$	Electron Mean Velocity	cm/s
v_{sat}	Electron Saturation Velocity	cm/s
$V(z)$, $V(x)$	Position-Dependent Electrostatic Potentials	V
V_D	Drain Bias	V
V_D^e	Drain-Channel Boundary Potential	V
V_{DS}	Drain-Source Bias	V
V_G	Gate Bias	V
V_S	Source Bias	V
V_S^e	Source-Channel Boundary Potential	V
W	Molecular Weight	g/mol
W	Transistor Gate Width	μm
χ	Electron Affinity	eV
x	Mole Fraction of Aluminum in AlGaN or AlGaAs	unitless

List of Abbreviations

Abbreviation	Description
2DEG	Two-Dimensional Electron Gas
AFRL	Air Force Research Laboratories
Al	Aluminum
$Al_xGa_{1-x}N$	Aluminum Gallium Nitride
$Al_xGa_{1-x}As$	Aluminum Gallium Arsenide
AlN	Aluminum Nitride
BJT	Bipolar Junction Transistor
C-V	Capacitance-Voltage
DC	Direct Current
DLTS	Deep Level Transient Spectroscopy
EL	Electroluminescence
EMA	Effective Mass Theory
FET	Field-Effect Transistor
Ga	Gallium
GaAs	Gallium Arsenide
GaN	Gallium Nitride
GPIB	General Purpose Interface Bus
HEMT	High Electron Mobility Transistor
HFET	Heterojunction Field-Effect Transistor
InN	Indium Nitride

I-V	Current-Voltage
LED	Light Emitting Diode
LEO	Low Earth Orbit
LiN	Liquid Nitrogen
MEO	Medium Earth Orbit
MODFET	Modulation-Doped Field-Effect Transistor
MOSFET	Metal Oxide Field-Effect Transistor
MOS-HFET	Metal-Oxide-Semiconductor Heterostructure Field-Effect Transistor
MOVPE	Metal-Organic Vapor-Phase Epitaxy
N	Nitrogen
NIEL	Non-Ionizing Energy Loss
PEARL	Passivated Emitter Rear Locally Diffused
PL	Photoluminescence
PPC	Persistent Photoconductivity
RF	Radio Frequency
RTD	Resistive Temperature Device
Si	Silicon
SiC	Silicon Carbide
SiN	Silicon Nitride
SMU	Source Measurement Unit
SNDD	Sensors Directorate Aerospace Components and Subsystems Technology Electron Devices Branch

UV	Ultraviolet
VDG	Van de Graff
V_N	Nitrogen Vacancy
WSU	Wright State University
ZnSe	Zinc Selenide

AN ANALYSIS OF THE EFFECTS OF LOW ENERGY ELECTRON RADIATION ON $Al_xGa_{1-x}N$/GaN MODULATION-DOPED FIELD-EFFECT TRANSISTORS

I. Introduction

Background

Over the past 30 years, dependence on semiconductor electronics has increased tremendously as the world has demanded smaller, faster, more powerful, and lower cost electronics. Today, semiconductor devices are essential in almost every commercial product that contains electronic components. Their widespread implementation can be attributed to their numerous desirable attributes, which include their small size, low-power consumption, and low production cost. However, compared to traditional electronics, semiconductor devices are more susceptible to radiation-induced degradation and failure. Fortunately, at or near the earth's surface, the background radiation is extremely small. However, there exist several environments in which we use semiconductor-based electronics that must operate in much higher levels of radiation. It is in these environments that problems have arisen and continue to arise, as semiconductor devices and circuits deteriorate or fail altogether.

There currently exists a wide range of semiconductor devices in operation and many more are being researched and developed for future use. Semiconductor devices differ generally, owing to two distinct properties: semiconductor material composition

and design of the device. Semiconductor devices have different susceptibilities to different types of radiation. The magnitude of these susceptibilities depends directly on the material and the design. Solar cells, for example, are constructed to be affected by electromagnetic radiation so that they can convert that radiation into electricity. However, the efficiency of a specific solar cell is directly related to the design of that solar cell. For example, an amorphous silicon solar cell has a much lower efficiency than a silicon passivated emitter rear locally diffused (PEARL) solar cell. Solar cell efficiencies also depend on the material used because semiconductors have different intrinsic properties such as bandgap and mobility. Thus, it is easy to see how both distinct device properties (material and design) can significantly affect a device's susceptibility to radiation.

Throughout the microelectronics revolution, silicon has been the semiconductor material of choice, primarily due to its natural abundance and ability to form an oxide. This has led to an extremely advanced state of fabrication technology for silicon that has resulted in silicon's dominance of the commercial semiconductor market [1]. The second most popular material for building semiconductor devices is gallium arsenide (GaAs) [2]. This is due primarily to the superior electron transport properties and optical properties that GaAs material exhibits over silicon [1]. Within the past 10 years, advances in semiconductor growth technology have provided for the pursuit of devices fabricated from wider bandgap III-V semiconductor materials. Materials such as diamond, silicon carbide (SiC), and gallium nitride (GaN), which were previously used as insulators, have now become practical wide bandgap semiconductors, which can be used to fabricate faster, more robust, devices and sensors [3].

Due in large part to the wide bandgap GaN possesses, as well as other intrinsic material properties such as its high electron drift velocity and high thermal conductivity, GaN-based devices have been theorized to be more resilient than silicon and GaAs-based devices in high temperature, high power, and high frequency conditions [3], [4], [5], [6]. Based on these ideas and some preliminary findings, GaN-based devices are being proposed for implementation into a wide variety of modern applications such as high-speed computer development and aircraft/spacecraft sensors and detectors. Additionally, because of its wide bandgap and high nitride displacement energies, GaN-based devices are believed to be more radiation tolerant than GaAs-based devices [7]. Preliminary research conducted by Ionascut-Nedelcescu, *et. al*. aids in confirming the idea that GaN-based devices are more radiation tolerant than GaAs-based devices [8]. However, no literature studies were found on the effects that electron radiation has on $Al_xGa_{1-x}N$/GaN modulation-doped field-effect transistors (MODFETs).

Transistors are one specific classification of semiconductor devices, for which there are two primary designs: the bipolar junction transistor (BJT) and the field effect transistor (FET). BJTs operate in a radically different manner than FETs and consequently the effects that radiation has on transistors will vary dramatically between the two general designs. Most studies of GaN-based transistors focus on the heterojunction field-effect transistor (HFET), which is a specific type of FET involving the joining of two dissimilar semiconductor materials such as GaN and AlGaN. In the family of HFETs, there exists a specific transistor design called the MODFET. A MODFET, also referred to as a high electron mobility transistor (HEMT), utilizes a two-

dimensional electron gas (2DEG) that is formed along the interface between the two dissimilar semiconductors. This 2DEG is essentially a thin quantum well that confines carriers and allows for extremely fast carrier transport. Figure 1 shows a family tree of semiconductor devices with the lineage of the MODFET outlined in dashed lines.

The MODFET is believed to be the fastest of all transistors and consequently used in high-frequency applications [1]. The monopoly that MODFETs own on high frequency (~ terahertz) operation makes them a prime candidate for implementation into many modern high-frequency applications. Some of these applications involve the integration of GaN-based MODFETs into satellite systems required to operate in earth orbit for several years. During this time in orbit, the satellite and the GaN-based MODFET will be

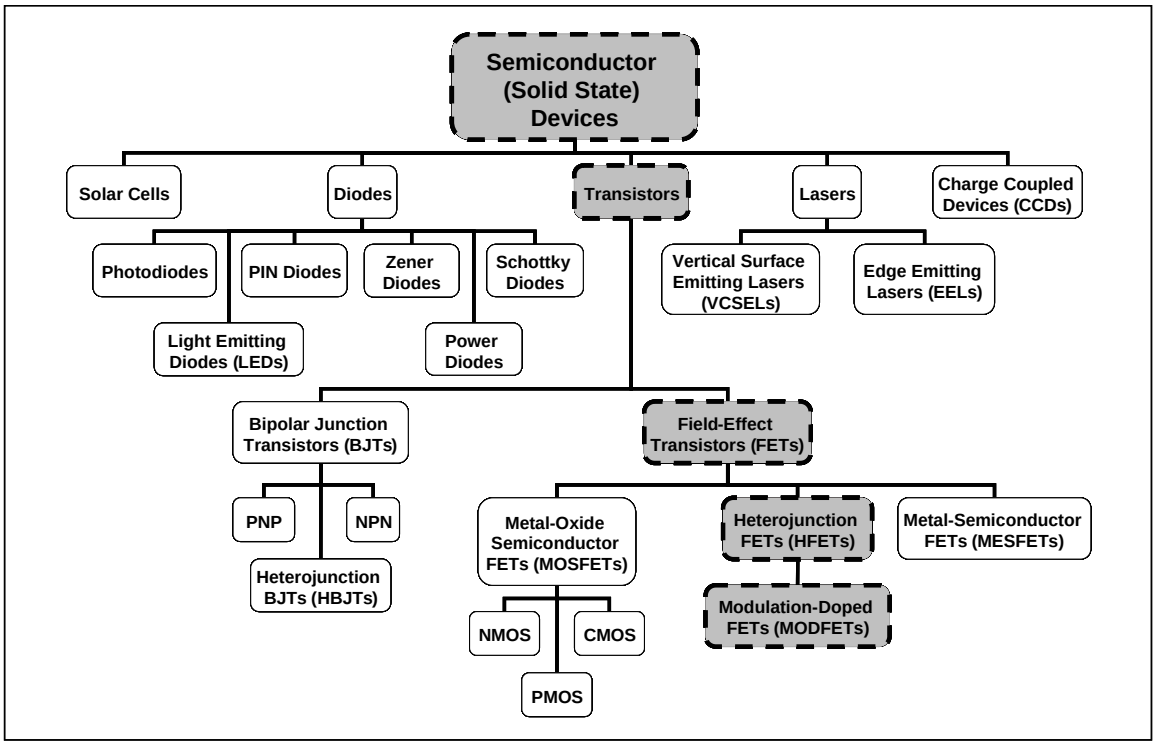

Figure 1. Semiconductor Device Family Tree; MODFET Lineage

exposed to a wide range of radiation including protons, electrons, alpha particles, and heavy ions. The majority of electron radiation that exists in earth orbit is due to the earth's radiation belts. Furthermore, it is known that most electrons trapped in the earth's radiation belts possess energies around a few million electron volts (MeV) [9]. Figure 2 shows a cross-section of the earth's electron radiation belts taken in the earth's magnetic axis and showing contours of equal electron flux for energies greater than 1 MeV [9]. For reference, a low earth orbit (LEO) satellite would be positioned at approximately 1.3 earth radii; a satellite with a medium earth orbit (MEO) would be positioned at approximately 2.6 earth radii; a satellite with a geostationary orbit would lie at approximately 6.6 earth radii. Figure 2 helps to show that any satellite operating in low earth orbit, medium earth orbit, or geostationary orbit with an inclination less than ~60º would be exposed to high electron fluxes and correspondingly high doses.

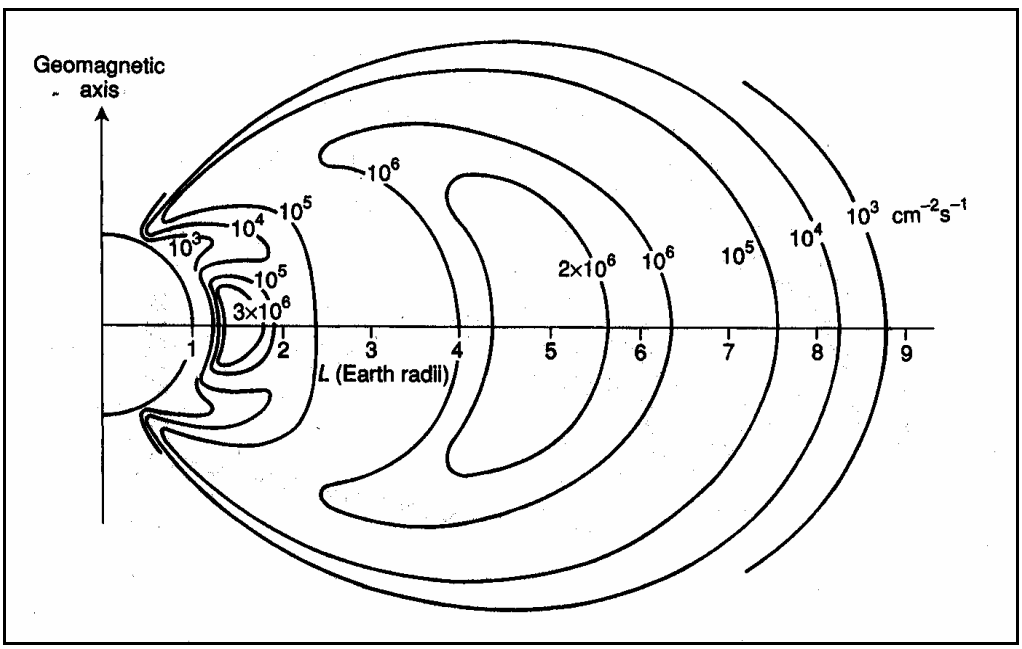

Figure 2. Trapped Electron Radiation Belts for Energies Greater than 1 MeV [9]

Thus, for any GaN-based MODFET to be successfully integrated into a satellite system incorporating one of these orbits, the MODFET must be able to operate in the presence of ~1 MeV electron radiation. The first step toward achieving this goal must be to determine experimentally the specific effects that ~1 MeV electrons have on the operation of $Al_xGa_{1-x}N$/GaN MODFETs. This brings us to the statement of the problem that this thesis will investigate.

Problem Statement

What are the effects that ~1 MeV electrons have on the operation of $Al_xGa_{1-x}N$/GaN MODFETs with regard to the integrity of the 2DEG?

Hypothesis

Defects created by electron radiation along the $Al_xGa_{1-x}N$/GaN interface will reduce carrier mobility in the 2DEG, which will cause source-drain channel conduction to drop severely, rendering the MODFET inoperable.

Objectives

1. Identify device-level electron radiation effects using *I-V* measurements.
2. Determine fluences and doses that change MODFET operation and induce MODFET failure.
3. Use MODFET failure data to determine dose effects on 2DEG.

Scope

This research is limited to a specific study on the effects that ~1 MeV electrons have on the electrical characteristics of $Al_xGa_{1-x}N$/GaN MODFETs. This study will consist of current-voltage (*I-V*) measurements. These measurements will be conducted at liquid nitrogen (LiN) temperatures resulting in the need to perform temperature dependent *I-V* measurements. Other possible relevant measurements such as capacitance-voltage (C-V), Hall-effect, or deep level transient spectroscopy (DLTS) will be considered outside the scope of this thesis. Throughout the research effort, emphasis will be placed on relating the *I-V* measurements to the behavior and integrity of the 2DEG. The research effort will be concluded when successful correlation is achieved between the applicable theory, modeling, and experimental measurements.

Approach

The general research approach included theoretical development, modeling, and experimental measurements. Theoretical development occurred consistently throughout the research effort. Modeling consisted of running TIGER codes on software models of the transistor materials. These codes simulate electron irradiation of the transistor materials based on a Monte Carlo simulation method, the results of which provide energy deposition information. The experimental measurements involved first fabricating the $Al_xGa_{1-x}N$/GaN MODFETs using the GaN Baseline 1.0 Process practiced by the Air Force Research Labs (AFRL) Sensors Directorate Aerospace Components and Subsystems Technology Electron Devices Branch (SNDD). The transistors were then

tested, packaged, and prepared for irradiation experiments that would take place at the Wright State University (WSU) Van de Graff (VDG) facility.

The first experimental approach was to irradiate three transistors (one at a time) at LiN temperatures while conducting *in-situ I-V* measurements. It was subsequently determined that this experimental approach was flawed because three out of three irradiated transistors were destroyed via an unforeseen experimental side effect. This side effect was determined to be related to charge collection and discharge and was not in any way related to a legitimate radiation effect.

The second experimental approach was to irradiate a single transistor at LiN temperatures without conducting *in-situ I-V* measurements. Following the irradiation the *I-V* measurements would be taken with the device held at LiN temperatures. Again, it was subsequently determined that this approach was flawed because the irradiated transistor was destroyed in the same manner as the previous.

The final experimental approach was to irradiate two transistors (one at a time) at LiN temperatures without conducting *in-situ I-V* measurements. Similar to the second approach, following the irradiation the *I-V* measurements would be taken with the device held at LiN temperatures. The key difference between this approach and the second approach was that the VDG was disconnected from the current integrator during irradiation, thus closing the cold head's ground loop. This seemingly minor change resulted in valid measurements that allowed the devices to be irradiated up to a total dose of 3.67×10^{15} e^{-}/cm^{2} without being destroyed. Pre-irradiation and post-irradiation *I-V* measurements were compared to analyze the irradiation effects on the transistors.

Assumptions

There were two important assumptions made in the process of this research.

1. The VDG electron beam deposited a uniform dose over the entire transistor. (This assumption has been known to be valid in previous unrelated experiments)
2. The drain currents measured by the SNDD test instrumentation form a linear relationship with gate width.

The latter assumption allows the drain currents measured from transistors operated in dual-gate mode, to be scaled by 50% resulting in drain currents that would have been measured had the device been operated in single-gate mode. This is necessary for comparisons between pre-irradiation and post-irradiation *I-V* curves for the unoperated transistors irradiated under the first two experimental approaches.

Results

$Al_xGa_{1-x}N$/GaN MODFETs were successfully fabricated and shown to be radiation tolerant after receiving various total doses up to 6×10^{16} e^-/cm^2. This tolerance was demonstrated using a wide variety of transistor designs (varying gate widths, gate lengths, source-drain distances, etc.) that showed no significant changes between room temperature pre-irradiation and post-irradiation *I-V* measurements. Consistent increases in both drain and gate current were observed for two different irradiations; these increases were not dose dependent. Furthermore, these increases annealed out at room temperatures.

Transistors operated during irradiation were destroyed by the creation of open circuits at the drain contacts. Another consistent and more peculiar effect was observed

relating to the destruction of transistors that were wire-bonded to package leads with the leads left floating during irradiation. These transistors experienced irreversible damage in which both gates as well as the drain were completely severed resulting in open-circuits. A theory describing the mechanism behind this destruction is presented, however the exact reason is unknown.

The novel contributions of this research are as follows:

- Performed first known electron irradiation of $Al_xGa_{1-x}N$/GaN MODFETs
- Demonstrated inability to perform practical *in-situ* measurements
- Measured radiation-induced, order of magnitude increases in gate current
- Measured radiation-induced increases in drain current up to 7 mA
- Showed elimination of gate/drain current increases through room temperature anneal
- Correlated gate leakage increases to enhancement of trap-assisted tunneling through the $Al_xGa_{1-x}N$ layer caused by radiation-induced trap creation in the $Al_xGa_{1-x}N$ layer
- Presented two theories explaining drain current increase

Sequence of Presentation

This thesis is divided into six chapters and four supporting appendices. Chapter one introduces the thesis by providing big-picture information important to any reader attempting to obtain an initial understanding of the research effort. Chapter two presents a clear, concise literature review that provides detailed background information that stems from previously conducted research as well as justification for this research effort.

Chapter three details the theory behind $Al_xGa_{1-x}N/GaN$ MODFET operation as well as relevant radiation interaction theory. Chapter four provides important experimental procedures including details of the fabrication process and irradiation experiments. Chapter five presents the results of the irradiations and provides relevant discussion. Finally, conclusions and recommendations for further work are presented in Chapter six.

II. Literature Review

Purpose

The purpose of this literature review is to provide answers to two questions:

1. Does the literature provide the justification to perform a study on electron radiation effects on the 2DEG in $Al_xGa_{1-x}N$/GaN MODFETs?
2. Has there been similar research efforts conducted that would void any need for this proposed experiment?

The Need for GaN Heterostructures

The most exciting and potentially useful III-V material is GaN and its alloys with indium nitride (InN) and aluminum nitride (AlN). These GaN-based III-V materials have recently moved to the forefront of modern semiconductor device technology due to their ability to emit and detect yellow, green, blue, and ultraviolet light [4]. Additionally, the ability of GaN-based sensors and transistors to operate in high power and high temperature environments, as well as in high frequency electronics, only enhances their perceived usefulness [4]. These highly attractive properties make the pursuit of GaN-based devices an important endeavor for the military, with particular regard to satellite applications. Figure 3 shows a comparison of GaN to other important semiconductors with respect to the susceptibility of their carrier concentrations to changing temperatures. The information shown in Figure 3 provides one reason why GaN-based devices are more robust than their widely used counterparts (Si and GaAs).

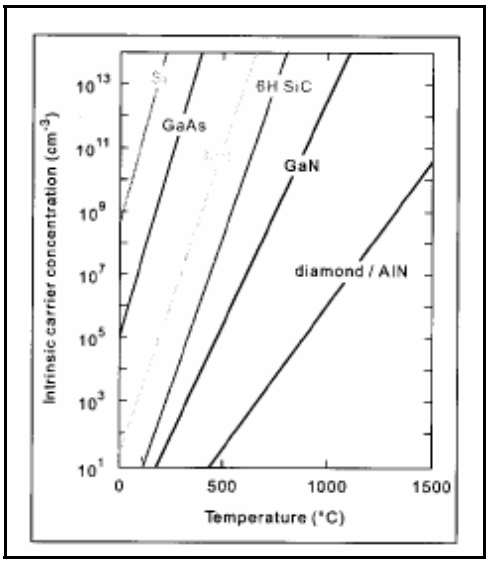

Figure 3. Intrinsic Carrier Concentration as a Function of Temperature for Various Semiconductors [5]

One example of GaN-based device applications exists in the important, but complex world of sensors. Sensors are the quintessential example of devices that must operate in extremely harsh and uncontrolled environments. The military in particular, needs sensors that can go just about anywhere to ensure the protection of our nation's assets. It is in the medium of these difficult requirements that GaN-based devices have risen to the top. GaN is well known for its wide, ~3.26 eV, direct bandgap which has several important benefits [5]. First, the direct bandgap allows for photoemission and photoabsorption, which occur at shorter wavelengths due to the size of the bandgap. Second, the large bandgap minimizes the unwanted effects of optical or thermal charge carrier generation, which can result from large temperature variations as well as specific types of radiation exposures [3]. Third, the strong chemical bonding between constituent atoms both widens the forbidden gap in the electronic density of states, and gives rise to

favorable mechanical, thermal, and chemical properties [3]. Table 1 displays some specific properties of wurtzite GaN.

Another exciting application of GaN-based devices can be found in the area of light emitting diodes (LEDs). Until recently, applications of LEDs were limited by their inability to produce intense light as well as their limited range of wavelengths. However, newer, GaN-based LEDs are emitting wavelengths and intensities that were previously unattainable for LEDs. These new GaN-based blue and green LEDs exhibit brightness levels and longevities that exceed the requirements for outdoor applications [4]. For the first time full color, all semiconductor displays are possible when available red LEDs are combined with these new blue and green LEDs [4]. Furthermore, if these new GaN-based LEDs are used in place of incandescent light bulbs, they would consume 80-90% less power and provide lifetimes over 10 times those of incandescent light bulbs [4]. Many cities around the world have already replaced filtered incandescent traffic lights with LEDs.

Table 1. Properties of Wurtzite GaN [10]

Property (units)	**Symbol**	**Value**
Molecular Weight (g/mol)	W	83.728
Density (g/cm^3)	ρ	6.15
Thermal Conductivity (W/cm·K)	κ	1.3
Specific Heat (cal/mol·K)	C_p	$9.1 + (2.15 \cdot 10^{-3}\ T)$
Static Dielectric Constant	ε_ρ	9.0
High Frequency Dielectric Constant	ε_∞	5.35
Electron Mobility, Bulk (cm^2/V·sec)	μ_e	1000
Hole Mobility, Bulk (cm^2/V·sec)	μ_H	300
Debye Length @ 300K, $N_d=10^{18}$ cm^{-3} (nm)	λ_D	3.586
Index of Refraction @ 1μm	n	2.35
Electron Affinity (eV)	χ	4.1

Perhaps the most important application for GaN-based devices exists in the high-power microwave frequency field. The RF (radio frequency) semiconductor market is currently estimated to be worth $5 billion and is projected to increase dramatically due to increasing communications demands [11]. Silicon-based semiconductors control ~70% of this market, whereas GaAs-based semiconductors control almost the entire remaining market share [11]. However, because GaN-based devices show distinct advantages over silicon and GaAs-based devices, the GaN-based electronics market is expected to reach $500 million over the next 10 years [11], [12]. Furthermore, RF and microwave applications are likely to hold the largest share of the GaN device market [12]. The advantages of GaN-based devices include higher saturation velocities, higher breakdown fields, and a higher range of temperature operation [11]. Table 2 describes the competitive advantages that GaN-based devices and amplifiers posses over silicon and GaAs-based technologies.

Table 2. Advantages of GaN-Based Transistors [12]

Need	Enabling Feature	Performance Advantage
High Power/Unit Width	Wide Bandgap, High Field	Compact, Ease of Matching
High Voltage Operation	High Breakdown Field	Eliminate/Reduce Step Down
High Linearity	HEMT Topology	Optimum Band Allocation
High Frequency	High Electron Velocity	Bandwidth, μ-Wave/mm-Wave
High Efficiency	High Operating Voltage	Power Saving, Reduced Cooling
Low Noise	High Gain, High Velocity	High Dynamic Range Receivers
High Temperature Operation	Wide Bandgap	Rugged, Reliable, Reduced Cooling
Thermal Management	SiC Substrate	High Power Densities with Reduced Cooling Needs
Technology Leverage	Direct Bandgap Allows for Lighting	Driving Force for Technology; Low Cost

As a direct result of improved saturation velocity, breakdown field, and temperature range, GaN-based transistors are being developed with power densities up to 10 W/mm and beyond. For comparison, $Al_xGa_{1-x}As$/GaAs HEMTs posses power densities as high as 1 W/mm [13]. Figure 4 shows the remarkable progress in power density available from $Al_xGa_{1-x}N$/GaN HEMTs.

All of these improvements in transistor operation lead to vast, untapped markets for GaN-based transistors. These markets include both military and commercial applications. Some of these applications include radar electronics (shipboard, airborne, satellite, and terrestrial) and satellite communications electronics [12]. Figure 5 shows some of the military and commercial markets that can be targeted by GaN-based transistors. These findings emphasize the importance of GaN-based transistors for use in high-power microwave frequency applications.

GaN-based devices have many additional applications, however, their importance and usefulness has already been made clear enough for the needs of this research project. GaN-based device technology is only in its infancy and yet is already one of the most important semiconductor research fields. As the technology for producing GaN-based devices advances so too will the list of possible applications. In addition to currently proposed satellite applications, some of these future unknown applications will involve radiation exposures. This fact alone justifies the need for research on the effects that radiation has on these devices.

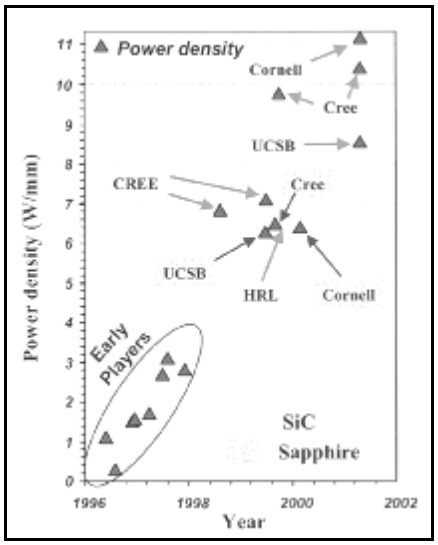

Figure 4. Historical Progress in $Al_xGa_{1-x}N$/GaN HEMT Power Densities [12]

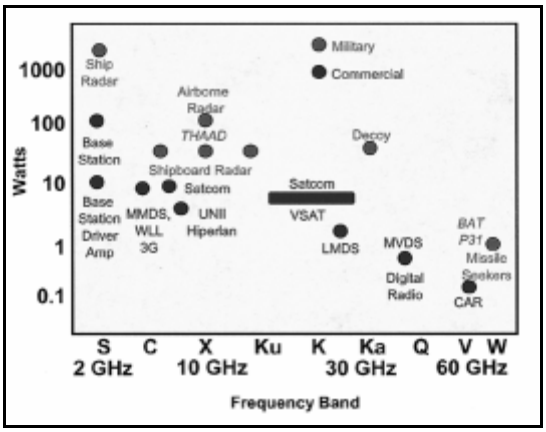

Figure 5. Applications of GaN-based HEMTs [12]

Radiation Effects on $Al_xGa_{1-x}N$/GaN Heterostructures

Although the literature contains several well-conducted studies regarding radiation effects on various $Al_xGa_{1-x}N$/GaN heterostructures, the overwhelming majority of these studies pertain to proton-irradiation. Polyakov, *et. al*. report on the effects of proton implantation on the electrical and recombination properties of n-GaN [14]. The

motivation behind this study is twofold. First, they wish to use proton implantation as a means for device isolation [14]. Second, they wish to use the irradiation as an opportunity to perform a study on the nature of point defects in GaN [14].

Luo, *et. al*. conducted a device specific investigation on the effects that high-energy proton radiation has on $Al_xGa_{1-x}N$/GaN HEMTs [7]. Their motivation was geared toward the application of these devices in low-earth orbit where high levels of proton radiation exist [7]. They report a decrease in extrinsic transconductance, drain-source current threshold voltage, and gate current as a result of irradiation with 40 MeV protons at low-earth orbit dose levels [7]. They conclude that the device operation degradation is due to a decrease in electron concentration in the 2DEG [7]. They also show that post-irradiation annealing to 300°C restores the transconductance and drain current to ~70% of their unirradiated values.

White, *et. al*. examined the effects that 1.8 MeV proton irradiation has on $Al_xGa_{1-x}N$/GaN MODFETs as well as bulk HFET material [15]. Figure 6 shows the MODFET source-drain dc *I-V* characteristics before irradiation and after two successive proton exposures. The effects of the radiation on the device operation can be seen clearly in Figure 6 as well as the increase in radiation impact at higher gate-source voltages. The research conducted by White, *et. al*. led to the conclusion that the proton-irradiation created spatially localized changes in the electronic properties of the heterostructure, which reduce the internal electric field strength while also creating charged defects [15]. These defects directly reduce the charge density along the 2DEG. The reduction in

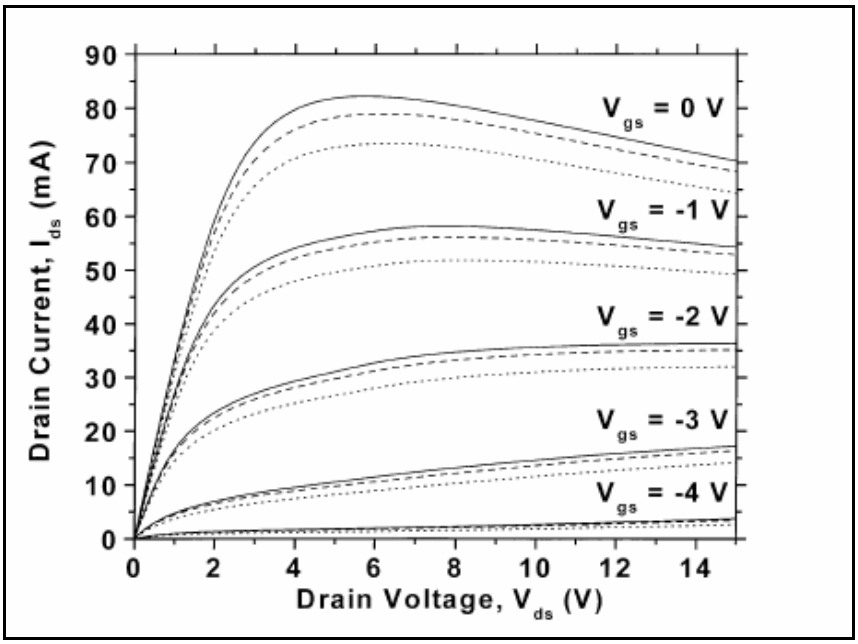

Figure 6. Common-Source DC *I-V* Curves; Pre-Irradiation (Solid Curves), Post 10^{11} cm^{-2} Fluence (Dashed Curves), and Post 10^{12} cm^{-2} Fluence (Dotted Curves) [15]

the internal electric field strength along with the reduction in charge density at the 2DEG interface channel account for the decreases in MODFET saturation current, drain current, and transconductance [15].

Gaudreau, *et. al.* also investigated the effects of proton radiation on $Al_xGa_{1-x}N$/GaN HFETs [16]. This research focused primarily on the carrier transport properties in the 2DEG. Irradiation was shown to reduce the carrier density by a factor of two and the mobility by a factor of one thousand [16]. The researchers concluded that changes in mobility are more dependent on radiation than changes in sheet charge density [16]. This leads to the belief that a system designed such that its performance is based on carrier mobility, may function consistently up to a critical fluence and fail abruptly at higher fluences [16]. The research also concluded that as far as electronic

properties are concerned, $Al_xGa_{1-x}N/GaN$ transistors are more radiation resistant than $Al_xGa_{1-x}As/GaAs$ transistors by approximately two orders of magnitude [16].

Ionascut-Nedelcescu, *et. al.* reported on the radiation hardness of GaN based on three separate irradiation experiments [8]. The first experiment involved the study of irradiated bulk material by photoluminescence (PL) [8]. The second experiment compared the electroluminescence (EL) of GaAs and GaN LEDs [8]. The third experiment investigated the resistivity of the 2DEG [8]. The most significant contribution of this research involved determining the displacement energies of individual gallium atoms in the GaN material [8]. The experiment found a threshold energy of 440 keV corresponding to a gallium displacement energy of 19 ± 2 eV [8]. This was achieved by exposing GaN blue LEDs to relativistic electrons [8].

Finally, Z-Q Fang, D. C. Look, G. C. Farlow, and others published various results from experiments involving electron irradiation of GaN materials [17], [18], [19]. They identified defects created by electron radiation and classified those defects as shallow and deep donors and acceptors. For example, Fang, *et. al.* characterized deep centers in as-grown and electron-irradiated n-GaN on sapphire using DLTS [14]. 1 MeV electrons were found to create V_N-related centers with thermal activation energies of 0.06 eV [17]. Additionally, Look, *et. al.* studied the effects that high-energy (0.7-1 MeV) electron radiation has on GaN and noted that the irradiation produces shallow donors and deep or shallow acceptors at equal rates [18]. Finally, Look, *et. al.* determined that the dominant electrically active defect produced in GaN irradiated by 0.42 MeV electrons, is a 70 meV donor and that this donor is most likely the isolated nitrogen vacancy [19].

Research Justification

As the need for faster and more robust semiconductor devices increases, so too will the need for GaN-based technology. The importance of GaN-based devices exists in various commercial applications such as LEDs and high-power, microwave frequency communications applications. Furthermore, there are several military applications for which GaN-based devices will prove useful including satellite communications, radar electronics, and sensors. However, as GaN-based devices are implemented as solutions for increasing numbers of applications, the need for understanding the effects that radiation has on these devices will only increase. The best example of this is found in the desire to use GaN-based devices on satellites, where the devices will experience various rates and energies of radiation exposures from both proton and electron radiation. Based on these facts, gathered from the literature, a study on the effects that electron radiation has on the 2DEG in $Al_xGa_{1-x}N$/GaN HFETs is justified.

The literature strongly suggests that a great deal of research and experimentation have been conducted on the effects that proton radiation has on GaN-based devices. However, only a handful of research endeavors were found involving electron-irradiation of GaN-based materials. One of these efforts consisted of irradiating GaN LEDs with electrons while many others involved irradiating bulk GaN material. As of this report, no evidence could be found in the literature of research efforts involving irradiated $Al_xGa_{1-x}N$/GaN MODFETs. Consequently, it can easily be concluded that conducting this research effort would involve an investigation that has yet to be undertaken, the results of which may play a crucial role in the advancement of GaN-based technology.

III. Theoretical Considerations

$Al_xGa_{1-x}N$/GaN MODFETs

If the success of semiconductor devices were to be attributed to one distinct property, this property would most assuredly be the bandgap. Bandgap, referring to the difference between conduction and valance energy bands in a material, is the property that describes why some materials are excellent conductors, while other materials are poor conductors. The simplest relationship between bandgap and the ability of a material to conduct is an indirect relationship; in other words, as bandgap increases, conduction decreases. This distinctive material property explains why semiconductors can behave like a wild card, acting as a good conductor under some circumstances and a bad conductor under other circumstances. It is the intelligent implementation of this "wild card" like property that best describes the success of semiconductor devices.

Table 3 displays the bandgaps of several semiconductor materials. One reason that silicon is the most widely implemented semiconductor is made evident in Table 3. Silicon's relatively small bandgap enables it to be easily manipulated back and forth between a conductor and an insulator with relative ease. Of courses, as important as a material's bandgap is, it is still only one piece of a larger puzzle that explains each semiconductor's usefulness.

Until recently, materials like GaN, and SiC were strictly thought of as insulators because their bandgap was too wide to implement in a practical manner [3]. However, recent advances in semiconductor processing technology have enabled engineers to create

Table 3. Bandgaps of Various Semiconductors [5]

Material	Bandgap (eV)
Si	1.11 (Indirect)
GaAs	1.42 (Direct)
GaN	3.26 (Direct)
AlN	6.28 (Direct)
ZnSe	2.67 (Direct)
SiC	2.2 (Indirect)
Diamond	5.5 (Indirect)

devices based on wider bandgap semiconductors. As important as this fact is, it only explains a portion of the successful development of GaN-based transistors. Perhaps the most important property these transistors possess was first discovered in the early stages of the semiconductor revolution. Whereas simple silicon devices make use of one semiconductor material (silicon), more complicated heterojunction devices were quickly understood to possess some exciting and unique properties. With respect to $Al_xGa_{1-x}N$ and GaN, the joining these two dissimilar semiconductors creates a 2DEG that allows for extremely fast carrier action. Figure 7 shows the cross-section for a simple $Al_xGa_{1-x}N$/GaN MODFET based on heterostructure design. The 2DEG can clearly be seen extending from source to drain, passing beneath the gate.

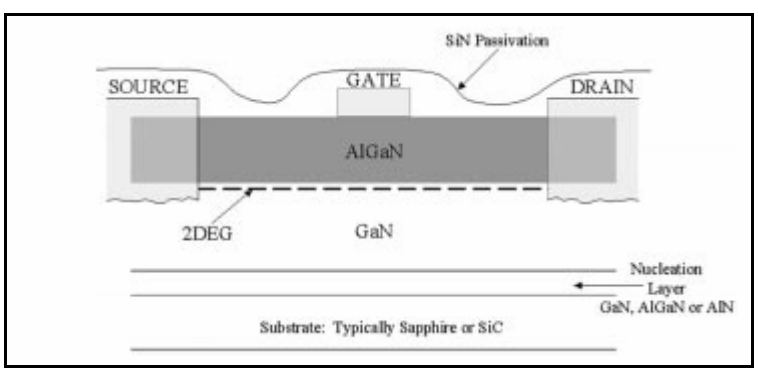

Figure 7. Basic $Al_xGa_{1-x}N$/GaN MODFET Structure [12]

The process by which the 2DEG is formed is of a complicated nature and has yet to be fully understood. Band theory is the most useful tool for understanding the nature of the 2DEG, although it does not paint a complete picture as to why the 2DEG forms. The mechanisms that cause 2DEG formation will be discussed shortly, but first let us examine the band structure of a simple $Al_xGa_{1-x}N$/GaN MODFET. Figure 8 shows this band structure as well as the associated 2DEG created. Figure 8 displays the $Al_xGa_{1-x}N$ layer on the left and the GaN layer on the right, with the 2DEG running along the $Al_xGa_{1-x}N$/GaN interface. It is important to note the axis labels in Figure 8; energy is the vertical axis and position (along the z direction) is the horizontal axis. To better understand Figure 8 in relation to Figure 7, it should be stated that the z-axis would run vertically in Figure 7 (with the $Al_xGa_{1-x}N$ layer on top). Furthermore, it is important to understand that the 2DEG is effectively two-dimensional as the name implies. This is because the quantum well that exists in Figure 8 (extending along an axis directed perpendicular to this page) is only a few angstroms in width corresponding to the length of the Fermi level as it crosses the quantum well in the z direction. The electrons confined by this quantum well travel along the quantum well in a direction parallel to the material interface (perpendicular to the page).

Although the 2DEG can easily be described and made use of in device designs, understanding its origins is drastically more difficult. As recently as 2002, it has been reported that the exact origin of the 2DEG in $Al_xGa_{1-x}N$/GaN MODFETs is unclear and still under debate [20]. The formation of the 2DEG is inherently a two-part process

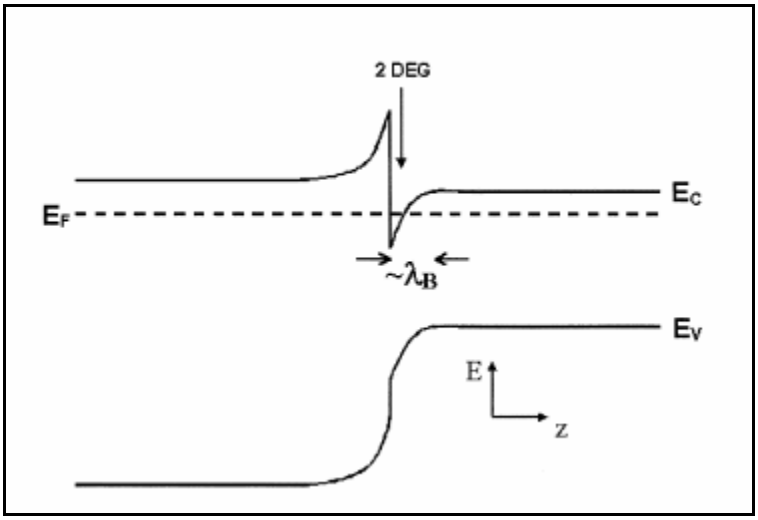

Figure 8. Band Structure of $Al_xGa_{1-x}N$/GaN Interface [16]

involving both the creation of a quantum well and the population of the quantum well with carriers. Morkoc, Di Carlo, and Cingolani describe the debate over the origin of the carriers forming the 2DEG as "the holy grail of GaN/$Al_xGa_{1-x}N$ heterostructures [11]." However, there are many well-known and understood pieces of the 2DEG puzzle. A brief discussion of this understanding follows.

Both GaN and $Al_xGa_{1-x}N$ exhibit large spontaneous polarizations due in part to the large ionicity associated with the covalent metal nitrogen bond [21]. This spontaneous polarization is particularly important in a case like $Al_xGa_{1-x}N$/GaN MODFETs where two nitride semiconductors with varying ionicities are involved [21]. In addition, the Group III-nitride semiconductors (including both $Al_xGa_{1-x}N$ and GaN) posses large piezoelectric coefficients [10], [12], [21], [22]. The piezoelectric nature of both $Al_xGa_{1-x}N$ and GaN becomes relevant in these devices because of the mechanical strain that exists at their interface. This strain is caused by a difference in lattice constants between AlN and GaN,

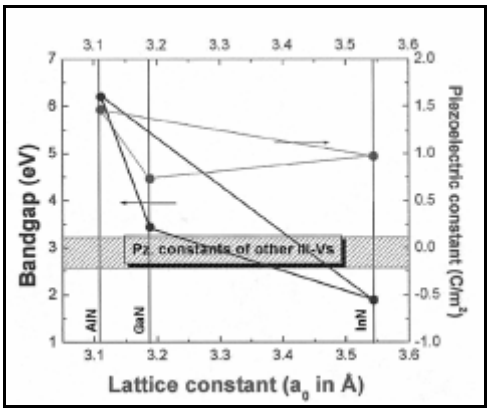

Figure 9. Important Properties of III-Nitride Materials [12]

which is shown in Figure 9. Because AlN has a smaller lattice constant, and because the $Al_xGa_{1-x}N$ layer is much smaller in thickness compared to the GaN layer (nm compared to μm), the result is a large tensile force applied to the $Al_xGa_{1-x}N$ layer. The piezoelectric nature of the $Al_xGa_{1-x}N$ layer, enhanced by the tensile strain, adds to the spontaneous polarization of the $Al_xGa_{1-x}N$ layer to yield a net polarization

$$P(x) = P_{pz} + P_{sp} = -[(3 \cdot 2x - 1 \cdot 9x^2) \times 10^{-6} - 5 \cdot 2 \times 10^{-6} x] C \cdot cm^{-2} \qquad (1)$$

where P_{pz} is the piezoelectric polarization, P_{sp} is the spontaneous polarization, $P(x)$ is the net polarization, and x is the Al mole fraction [12]. This net polarization produces an electric field in the $Al_xGa_{1-x}N$ layer, directed along the z-axis into the GaN layer resulting in positive charge collection in the $Al_xGa_{1-x}N$ layer at the heterojunction [12], [13]. This positive charge is believed to draw up mobile negative charge carriers from the n-type GaN region, resulting in the formation of the 2DEG [13]. The Schrödinger equation and Poisson equation can be used self-consistently to study the details of 2DEG channel formation as well as current flow mechanisms in these MODFETs [21]. The details of

this method are beyond the scope of this thesis. However, this method has been documented by Morkoc, Di Carlo, and Cingolani and the basics of their model, as reported in the literature, will be described [21].

Using effective mass theory (EMA), the Schrödinger equation takes the form

$$-\frac{h^2}{2}\frac{d}{dz}\left(\frac{1}{m(z)}\frac{d}{dz}\right)\varphi + eV(z)\varphi = F\varphi \tag{2}$$

where $m(z)$ is the position-dependent effective mass, $V(z)$ is the position-dependent electrostatic potential, φ is the electron wave function, and F is the energy level [21]. Taking into account the effects of spontaneous and piezoelectric polarization, the Poisson equation is solved for the displacement field, $D(z)$

$$\frac{d}{dz}D(z) = \frac{d}{dz}\left(-\varepsilon(z)\frac{d}{dz}V(z) + P(z)\right) = e\left(p(z) - n(z) + N_D^+ - N_A^-\right) \tag{3}$$

where $\varepsilon(z)$ is the position-dependent dielectric constant, P the total polarization (as described by Equation (1), $p(z)$ the hole charge concentration, $n(z)$ the electron charge concentration, and N_D^+ and N_A^- the ionized donor and acceptor densities (respectively) [21]. Equation (3) is then solved for V(z), which can be inserted into Equation (2), the Schrödinger equation [21]. Equation (2) is subsequently solved to yield the energy levels and wave functions of the system [21]. By applying Fermi statistics, the electron charge density at the interface is obtained

$$n_{2D}(z) = \frac{m(z)k_B T}{\pi\hbar^2}\sum_i \left|\varphi_i(z)\right|^2 \ln\left[1 + e^{(E_F - E_i)/k_B T}\right] \tag{4}$$

where E_F is the Fermi level, E_i is the energy of the ith-quantized level, T the temperature and k_B the Boltzman constant [21]. The calculated electron density from Equation (4) is placed back into Equation (3) (the Poisson equation), and the iteration is repeated until convergence is achieved [21]. Additionally, the Morkoc, *et. al*. model states that the channel charge density is controlled by two factors: (i) the gate bias and (ii) the Al content in the $Al_xGa_{1-x}N$ layer, which tailors the polarization field [21].

The development above leads directly toward a drain current model that is also proposed by Morkoc, Di Carlo, and Cingolani [21]. Their model is based on the FET layout displayed in Figure 10. As Figure 10 shows, their model takes into account the presence of drain (R_D) and source (R_S) resistance. Their model considers the drain-source potential as gradually varying along the channel (2DEG) from the source bias, V_S, to the

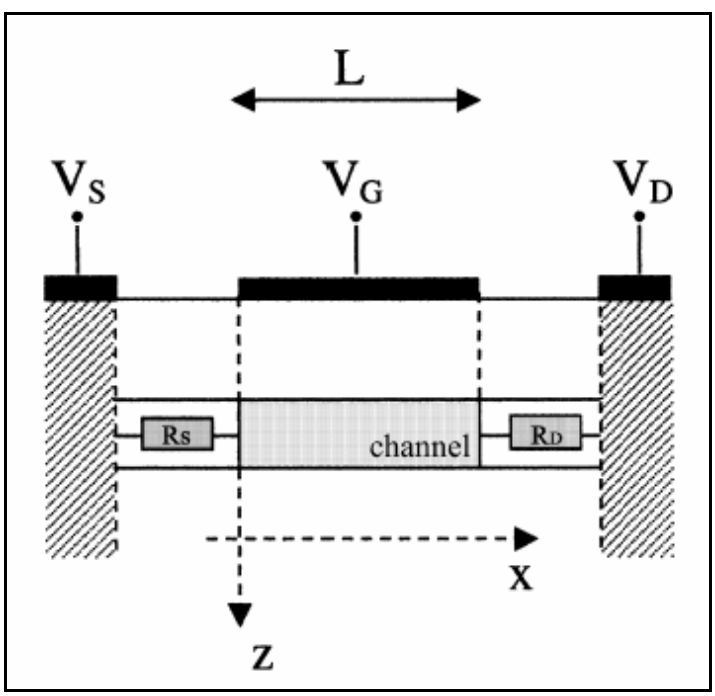

Figure 10. Schematic Representation of the FET Model Used for Drain Current Derivation [21]

drain bias, V_D [21]. Thus, it is possible to calculate the sheet charge density, n_s, at an infinite number of points along the channel, provided that the potential on the top surface, $V(x)$, is considered for each point along the channel [21]. For the n-channel devices used in this research, V_S is zero and V_D is positive, therefore $V(x)$ contributes to channel depletion. The resulting sheet charge density as a function of x is

$$n_s(x) = n_s\left(V_G - V(x)\right) \text{ [21].} \tag{5}$$

Neglecting diffusion contributions yields the following source-to-drain current, I_{DS},

$$I_{DS} = -qWv(x)n_s(x) \tag{6}$$

where W is the gate width and $v(x)$ the electron mean velocity [21]. The electron mean velocity is given empirically as

$$v(x) = \frac{\mu_0 E(x)}{1 + \frac{E(x)}{E_C}} \tag{7}$$

where $E(x)$ is the electric field (-d$V(x)$/dx), μ_0 is the low field mobility, and E_C is the electric field at saturation (v_{sat}/μ_0) [21]. The parasitic drain and source resistances are included explicitly using

$$\begin{aligned} V_S^e &= V_S + I_{DS}R_S \\ V_D^e &= V_D - I_{DS}R_D \end{aligned} \tag{8}$$

where V_D^e and V_S^e represent the potentials at the drain-channel and source-channel boundaries [21]. Substituting Equation (5) and Equation (7) into Equation (6) yields an explicit equation for the drain-to-source current:

$$I_{DS} = -qW \frac{\mu_0 E(x)}{1 + \frac{E(x)}{E_C}} n\left(V_G - V(x)\right) \text{ [21].} \tag{9}$$

It should be noted that at least one additional $Al_xGa_{1-x}N$/GaN FET model has been developed by Albrecht, Ruden, Binari, and Ancona [23].

Taking a step back from the theory, a summary of the basic characteristics and operation of these transistors will now be provided. The polar nature of $Al_xGa_{1-x}N$ is the key ingredient to the operation of these devices. This intrinsic property produces both a spontaneous polarization and piezoelectric effect. The piezoelectric effect is made active by the tensile strain caused by the growth of $Al_xGa_{1-x}N$ on GaN [12]. The spontaneous polarization and strain-activated piezoelectric effect combine to yield a net electric field in the $Al_xGa_{1-x}N$ layer. This field (directed into the GaN layer) is indicative of the net positive charge that has collected at the $Al_xGa_{1-x}N$/GaN interface. This net positive charge in turn draws up mobile electrons out of the n-type GaN region thus providing the interfacial quantum well with a high number of carriers to populate its energy states; these carriers constitute the 2DEG.

The 2DEG carrier concentration established by the positive stationary charge in the $Al_xGa_{1-x}N$ layer is dependent on two important factors: (i) Al concentration in the $Al_xGa_{1-x}N$ layer and (ii) applied gate voltage. The former is a device design property,

while the latter is an operation-dependent property. Thus, for any working $Al_xGa_{1-x}N$/GaN MODFET, the former is essentially a fixed parameter while the latter is a controllable variable. Consequently, the gate voltage can be used to vary the population of the 2DEG and this is the mechanism that results in the "transistor" nature of the device. For positive gate voltages ($V_G > 0$), the net electric field in the GaN layer will be increased proportionally to the magnitude of V_G, resulting in an increase in carrier concentration in the 2DEG. For negative gate voltages ($V_G < 0$), the net electric field in the GaN layer will be decreased proportionally to the magnitude of V_G, resulting in a reduction in carrier concentration in the 2DEG. This explains the transistor action observed in the *I-V* curves for these devices (See Figure 6 for example of *I-V* curves). There are several additional properties involved in the operation of $Al_xGa_{1-x}N$/GaN MODFETs including the Schottky barrier gate contact, ohmic source/drain contacts, and 2DEG transport properties. Details of these and other properties can be found in [21].

Finally, an additional, consistently observed effect in the operation of these devices involving the screening of the electric field in the $Al_xGa_{1-x}N$ layer is described in numerous sources [12], [24], [25], [26]. This electric field screening is believed to be responsible for the compression of the DC drain current and is also believed to be directly related to electron trapping in the $Al_xGa_{1-x}N$ layer of these transistors [12], [24], [25]. The result of this effect is a decrease in the drain current for devices operated under DC conditions. Figure 11 illustrates one explanation for this effect in which electrons from the gate are injected into empty surface donors resulting in a reduction in 2DEG carrier

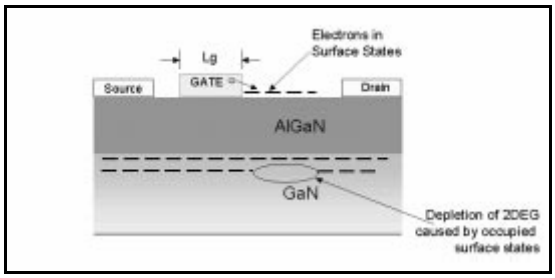

Figure 11. Proposed Mechanism for DC Drain Current Compression [12]

concentration [12]]. SiN passivation (See Figure 7) is known to eliminate this drain current compression although the explanation for this effect is still under debate [12].

Radiation Interactions

A significant number of studies have examined the interactions that electrons have in GaN. A brief discussion of these results will be presented here. It should be noted that there are fewer articles related to electron interactions in $Al_xGa_{1-x}N$. In general, it can be stated that ionizing radiation results in two primary types of effects: transient effects that are dose rate dependent and permanent effects that are total dose dependent [10]. Because this research is concerned with the effects that electrons have on $Al_xGa_{1-x}N$/GaN MODFETs, both transient effects and total dose effects are important. The majority of research in this field has been geared to study the damage that results from electron radiation exposure. This damage is primarily characterized by the displacement of atoms in the material lattice. The following will examine this damage in GaN.

As electrons impact GaN, there are several possible outcomes. One is for the electron to pass completely through the material without imparting any energy, leaving the GaN completely unaffected. This outcome is entirely dependent on the stopping

power of the material and the amount of material through which the electron passes. Stopping power is the average rate at which charged particles lose energy at any point along their tracks [27]. For electrons, stopping power (or total stopping power) is customarily separated into two components: collision stopping power and radiative stopping power [27]. Collision stopping power is the average energy loss per unit pathlength due to elastic collisions as well as inelastic coulombic interactions with bound atomic electrons. Collision stopping power results in atomic displacements (in other words Frenkel pair creation), ionization, and excitation [27]. Because the momentum component associated with mass for energetic electrons is so small, the majority of collision power results in ionization and excitation. Radiative stopping power is the average energy loss per unit pathlength due to the emission of bremsstrahlung radiation in the electric field of the atomic nucleus as well as the atomic electrons [27]. The primary reason total stopping power is separated into these two components relates to the different mechanisms by which incident electron energy is transferred to the target lattice [27]. The energy imparted by incident electrons resulting in ionization and excitation of atoms (Collision stopping power) is absorbed in the medium rather close to the particle track [27]. However, the energy imparted through bremsstrahlung radiation (Radiative stopping power) travels far from the particle track before being absorbed [27].

Figure 12 shows the relationship between stopping power and incident electron energy for both $Al_xGa_{1-x}N$ and GaN (as calculated by the XGEN code, which is part of the TIGER package – See Appendix A). Figure 12 is also a good indicator that the

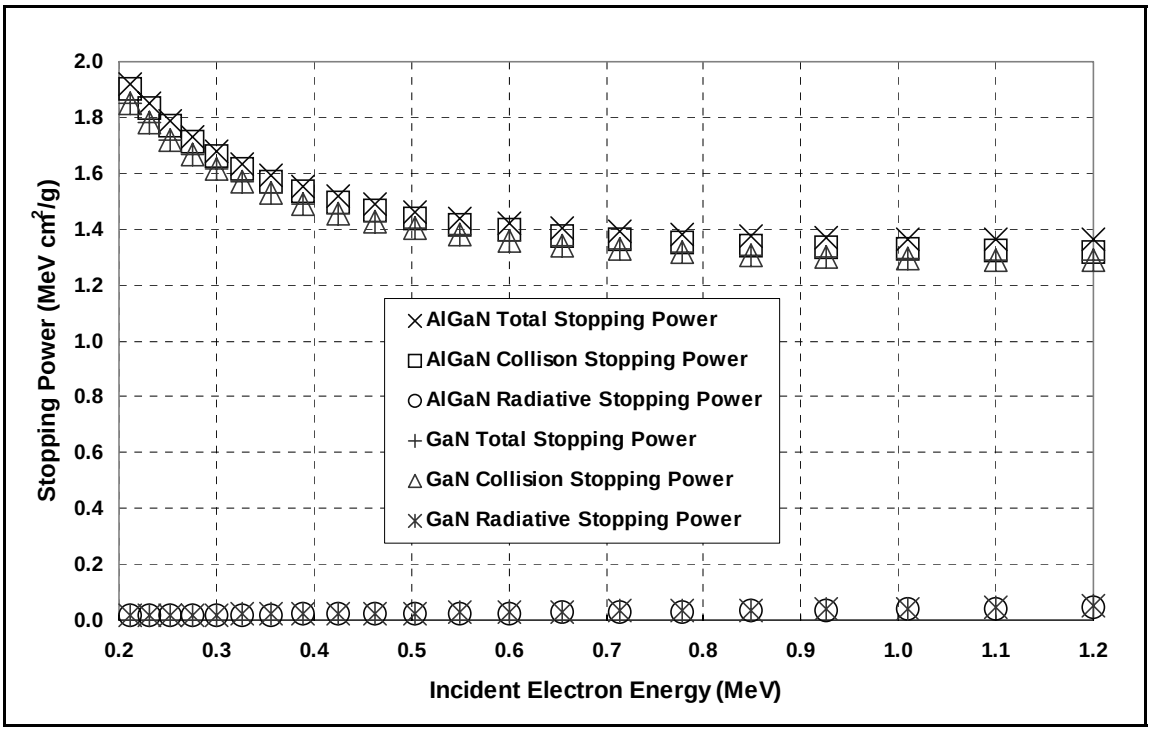

Figure 12. Electron Stopping Power in $Al_xGa_{1-x}N$ and GaN as Calculated by XGEN

radiative stopping power component is almost negligible compared to the collision stopping power. This tells us that the majority of energy deposited in the material will remain close to the incident electron tracks and result in a large amount of ionization and excitation.

Another important metric related to stopping power is range. Range is defined to be the thickness of a material that is penetrated by the incident particle before the incident particle loses all of its energy [9]. Figure 13 shows the relationship between range and incident electron energy for both $Al_xGa_{1-x}N$ and GaN (as calculated by the XGEN code). A physically more understandable version of range in units of distance (cm) can be determined by dividing the ranges given in Figure 13 by the density of the material. The

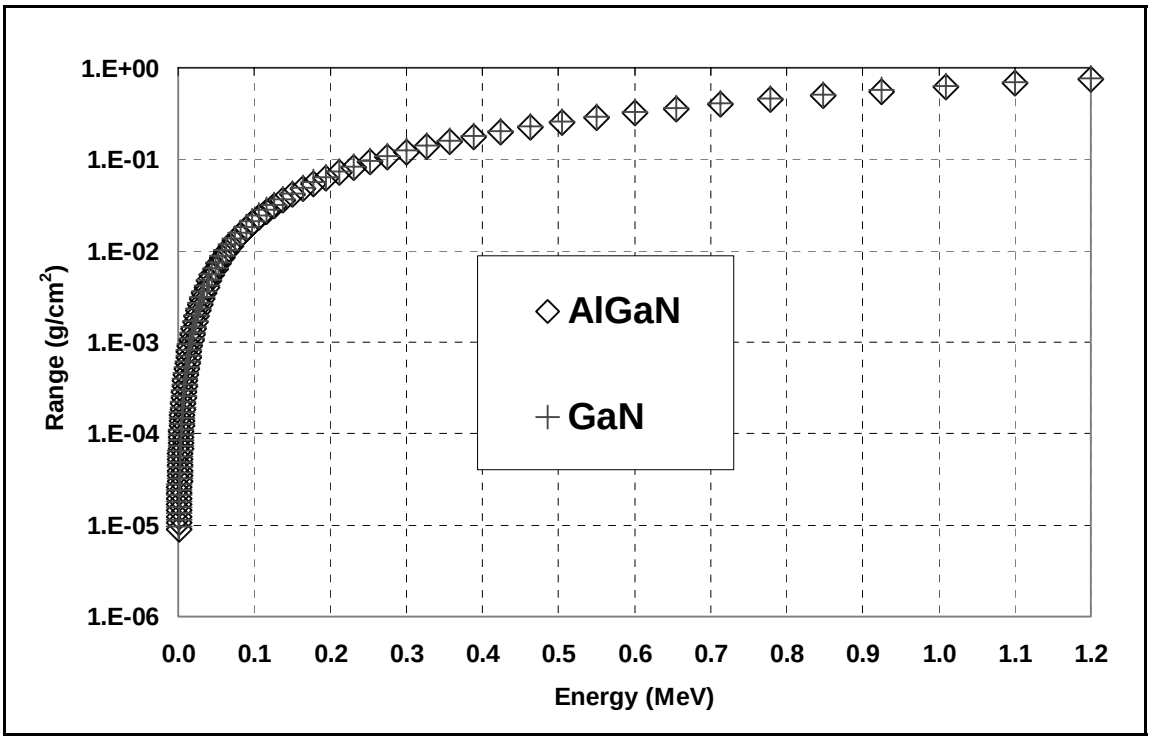

Figure 13. Electron Range in $Al_xGa_{1-x}N$ and GaN as Calculated by XGEN

bottom line for $Al_xGa_{1-x}N$ and GaN is that higher energy electrons penetrate deeper into the material. A detailed presentation of the methods used to determine stopping power and range is beyond the scope of this thesis, however, [27] provides an in-depth development of such theory.

As electrons enter $Al_xGa_{1-x}N$ and GaN materials, they release much of their energy through elastic collisions with lattice atoms (Ga, N, or Al). These collisions can result in displacement damage whereby individual atoms of the lattice are knocked out of their natural position in the lattice. Little is known about the interactions that electrons have in $Al_xGa_{1-x}N$ so this discussion will be primarily focused on GaN. The rates at which displacement damage occurs for Ga and N atoms are functions of both atomic binding energy and collisional energy transfer [10]. Atomic binding energies are

generally intrinsic to a material; in general, Ga atoms are bound less tightly than N atoms in GaN [10]. Collisional energy transfer is heavily dependent on the lattice atom's mass; this means that more energy can be transferred to the less massive nitrogen atoms [10].

The minimum displacement energies in GaN have been determined through theoretical calculations [10]. Taken from the data for all collision angles, gallium has a minimum displacement energy of 22 ± 1 e*V* while nitrogen has a minimum displacement energy of 25 ± 1 e*V* [10]. The maximum energy that can be transferred to an individual lattice atom by an incident electron via coulomb scattering is

$$E_{trans}^{\max} = 2\frac{\left(E_{e^-} + 2m_{e^-}c^2\right)}{m_{atom}c^2}E_{e^-} \tag{10}$$

where E_{e^-} is the incident electron energy, m_{e^-} is the electron mass, m_{atom} is the mass of the target atom, and c is the speed of light [10]. Using Equation 10, one can calculate the maximum energy transferred to a lattice atom from an incident electron. The results of this calculation for incident electron energies of interest are summarized in Table 4. Of the four incident energies listed in Table 4 only the 0.45 MeV energy would not cause Ga displacements. Furthermore, Table 4 suggests that higher incident electron energies (~1 MeV) might be able to produce displacement atoms of sufficient kinetic energy to create knock-on damage resulting in line defects. However, Greene points out that large damage cascades (line defects) are not expected from the primary knock-on atoms because they are limited to ~290 eV for N atoms and 41 eV for Ga atoms [10].

Table 4. Maximum Energy Transferred to Gallium and Nitrogen Lattice Atoms for Given Incident Electron Energies

Incident Energy (MeV)	Max Energy Transferred to Ga Atom (eV)	Max Energy Transferred to N Atom (eV)
0.45	20.27	100.86
0.7	36.87	183.45
0.8	44.58	221.86
1.2	81.53	405.73

In addition to radiation interaction theory, modeling and simulations can be used to determine the effects that radiation has on a material. This aspect of the thesis was accomplished through the TIGER codes software package. The results of these radiation simulations are provided along with a brief discussion in Appendix A.

IV. Experimental Procedures

Transistor Fabrication

This research endeavor began with three 90° pie-shaped Cree wafer pieces of SiC with GaN and $Al_xGa_{1-x}N$ layers deposited on top. In total, the three pieces constituted 75% of a complete two-inch Cree wafer that was grown using metal-organic vapor-phase epitaxy (MOVPE). The SiC substrate thickness was 413 μm; the GaN layer (grown on top of the SiC) was 2μm (nominal thickness); the $Al_xGa_{1-x}N$ layer (grown on top of the GaN layer) was 25 nm (nominal thickness). The $Al_xGa_{1-x}N$ layer was grown with 27% AlN and 73% GaN resulting in a $Al_{0.27}Ga_{0.73}N$ layer. The room temperature carrier concentration was measured to be 1.3×10^{13} cm^{-2} and the mobility was measured to be 1300 $cm^2/V\cdot s$ (measured by Cree).

Transistor fabrication was carried out at AFRL SNDD. The process took advantage of AFRL/SNDD's GaN baseline process that produces $Al_xGa_{1-x}N$/GaN MODFETs. These MODFETs are fabricated in a collection of reticles, with each reticle containing a variety of test structures as well as varying designs of MODFETs. Figure 14 shows a picture of a single reticle (the last column of transistors is only partially shown). The lower left side of each reticle contains a variety of test structures used to test the quality of the reticle. The upper left side contains a single C-V ring and FatFET, which is a single gate 50 μm transistor. The majority of the remaining real estate is occupied by double gate transistors that have varying width-to-length ratios (See Figure 14). A single

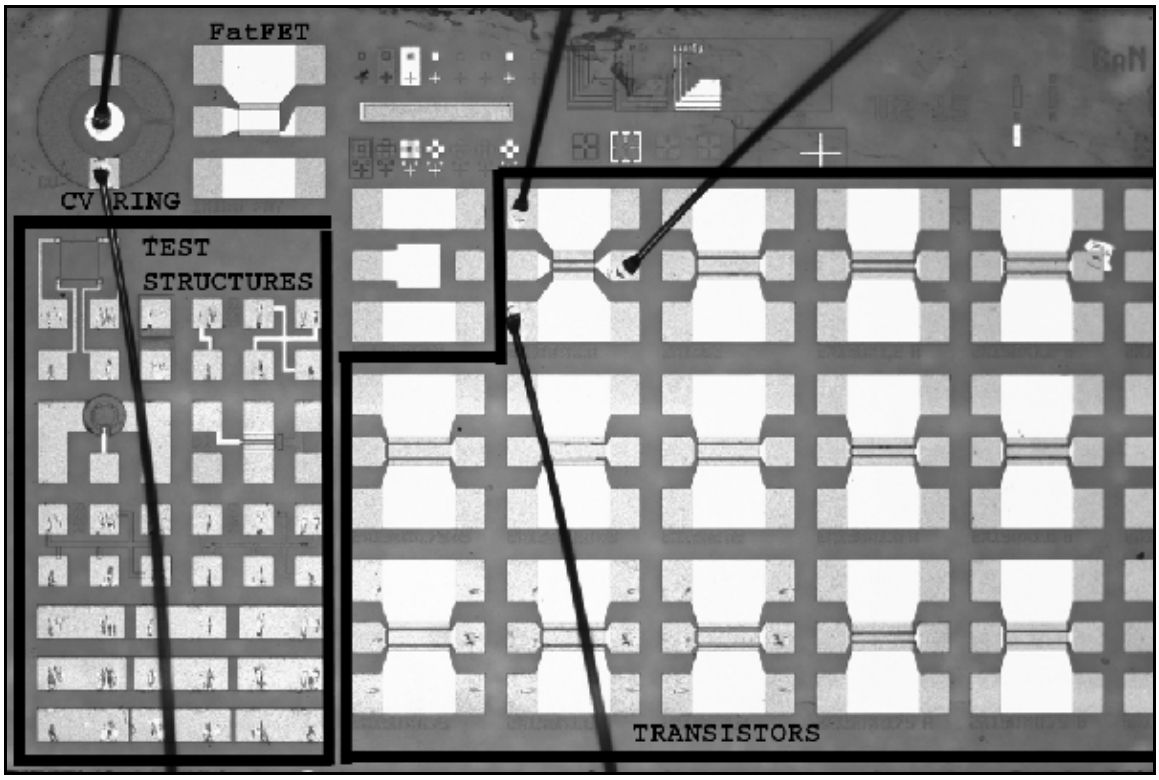

Figure 14. Single Reticle Layout

two-inch wafer can be processed in automated fashion at AFRL/SNDD yielding 244 reticles. However, this process requires a complete two-inch wafer, which was unavailable. Therefore, device fabrication was completed by hand following the same procedures as the automated process.

The fabrication process involved three main steps. The first step, called Mesa Isolation, involved the use of photolithography and etching to produce mesas with a height of ~1200 Å. Figure 15 shows the ultraviolet (UV) exposure system used for photolithography (One of the transparent wafer pieces is sitting on the withdrawn developer platform). Once completed, the mesas are the only regions of the wafer where

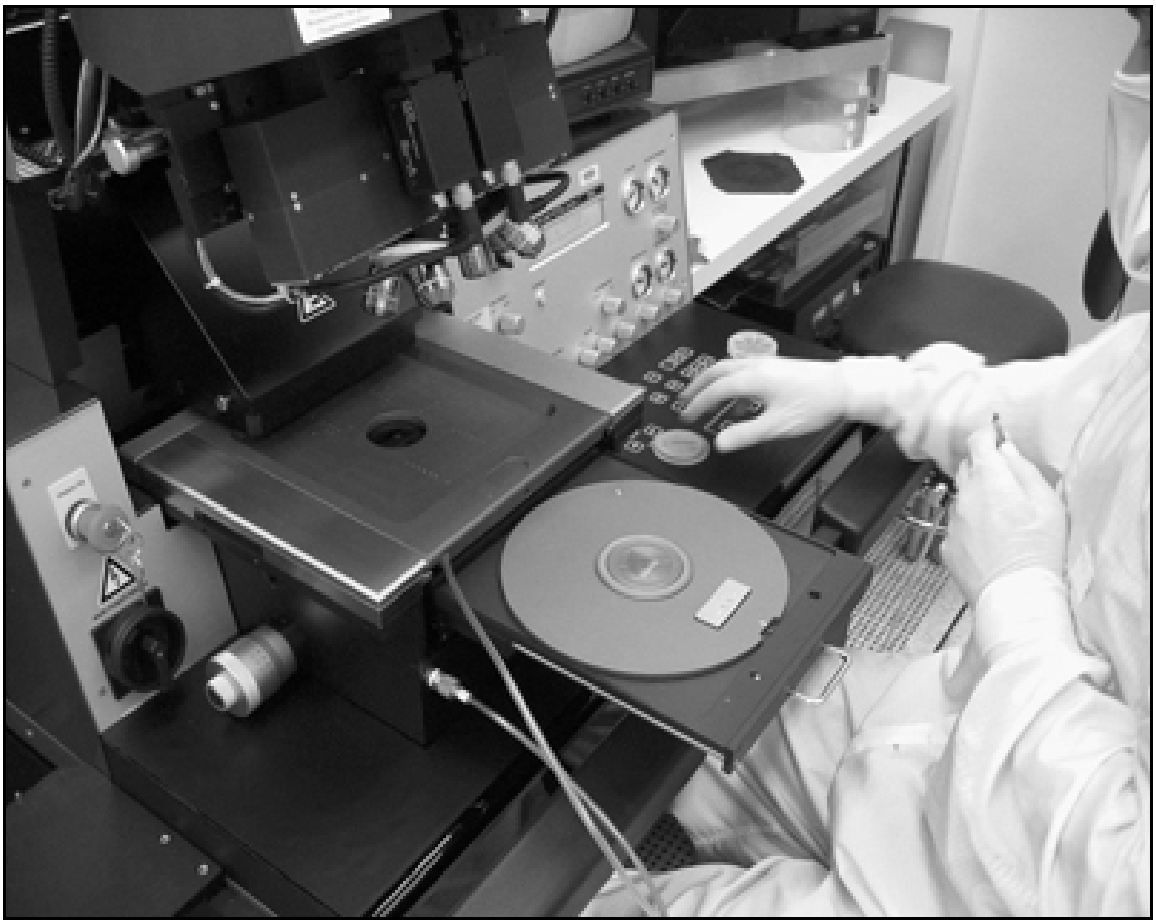

Figure 15. AFRL/SNDD UV Exposure System Used for Photolithography

the $Al_{0.27}Ga_{0.73}N$ layer still exists; this is because the 1200 Å etch depth penetrates completely through the 250 Å $Al_{0.27}Ga_{0.73}N$ layer. These mesas are necessary because they isolate the gate regions from the conductive 2DEG region.

The second processing step, called Ohmic, involved the use of photolithography and metal deposition to perform an ohmic metal liftoff. This liftoff yielded the foundation for source and drain ohmic contact pads that sit on exposed GaN as well as source and drain transistor contacts that lie on the mesas. The ohmic metal consisted of four individual layers: 350 Å titanium, 2300 Å aluminum, 500 Å nickel, and 200 Å gold.

The final processing step, called Optical Gate, involved photolithography and metal deposition to again perform a metal liftoff. This liftoff deposited gate metal on top of the previously deposited ohmic metal, thus completing construction of the ohmic contacts. Additionally, this liftoff deposited gate metal between the mesa and the contact pads. Finally, and most importantly, this liftoff deposited gate metal on the mesas forming the gates themselves. The gate metal consisted of 200 Å nickel and 2800 Å gold. Figure 16 shows the layout for the FatFET, which was the specific transistor used in this research. The name FatFET is given because the transistor's gate length of 50 μm is much larger than the ~1.2 μm gate lengths that exist on all the other transistors on the reticle (See Figure 14 for location of FatFET on the reticle and for comparison purposes). Figure 17 shows a cross section of FatFET (taken along the line illustrated in Figure 16) and helps to correlate the layout of the FatFET to the layout of the MODFET used in drain current model presented by Morkoc *et. al*. (See Figure 10).

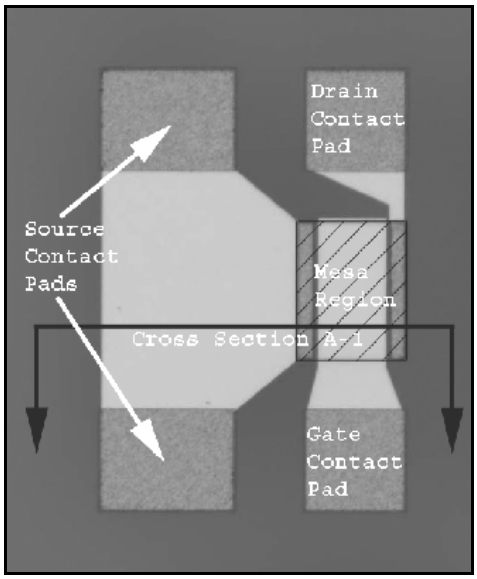

Figure 16. FatFET Layout

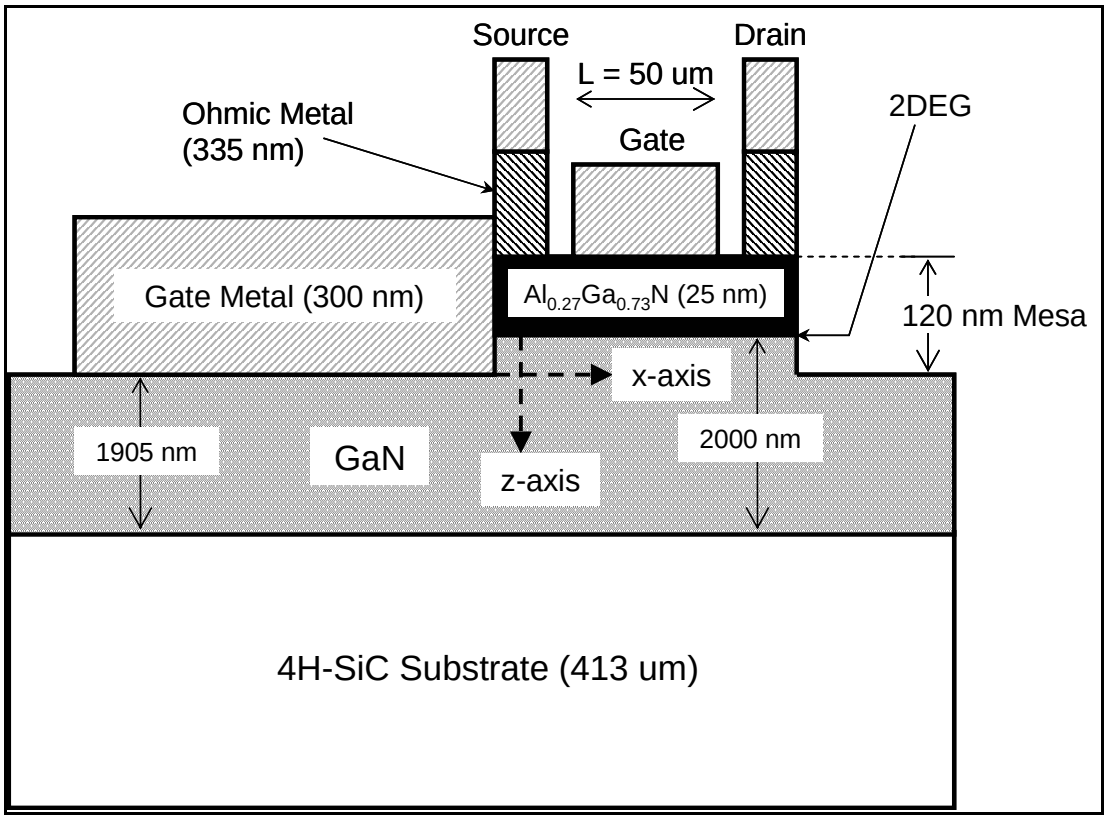

Figure 17. Cross Section A-1 (Not to Scale)

Once the fabrication was completed, the transistors were tested using AFRL/SNDD's DC/RF Tester (See Figure 18). This tester systematically evaluated the performance of the test structures and three of the transistors on each reticle (DC/RF Tester probe tip scratches are visible in Figure 14). Although not every transistor on every reticle checked out, the yield was sufficiently high (~75%) to meet the needs of this research effort. It is worth mentioning that the three 90° pie-shaped wafer pieces were labeled JS01A, JS01B, and JS01C. JS01A and JS01B were completed following the Optical Gate process and DC/RF testing. However, after DC/RF testing, JS01C was submitted for SiN passivation, a fourth, optional process step. Only transistors from JS01A were used in this research leaving JS01B and JS01C for follow-on work.

Figure 18. AFRL/SNDD DC/RF Transistor Tester

Packaging

Following fabrication and testing, several of the reticles on JS01A and JS01C were diced and packaged by Mr. Larry Callaghan of AFRL/SN. Figure 19 shows a picture of JS01A following fabrication. Careful inspection of Figure 19 will reveal the layout of the individual reticles on the wafer piece (small rectangles in Figure 19). Reticles were individually identifiable by a two-dimensional labeling system that gave each reticle a vertical and horizontal address; the horizontal address listed first, the vertical address listed second (See Figure 20). The packaging process involved physically bonding the reticle to the package bottom and wire-bonding the desired transistors such

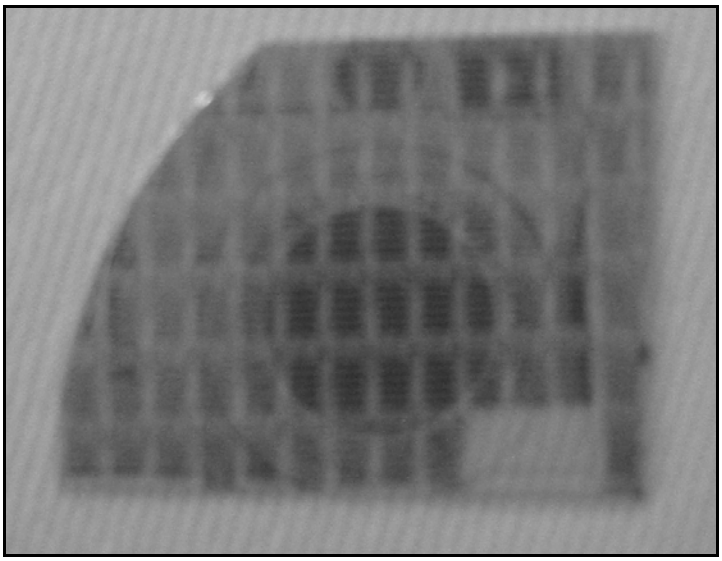

Figure 19. Unpackaged Reticles from JS01A

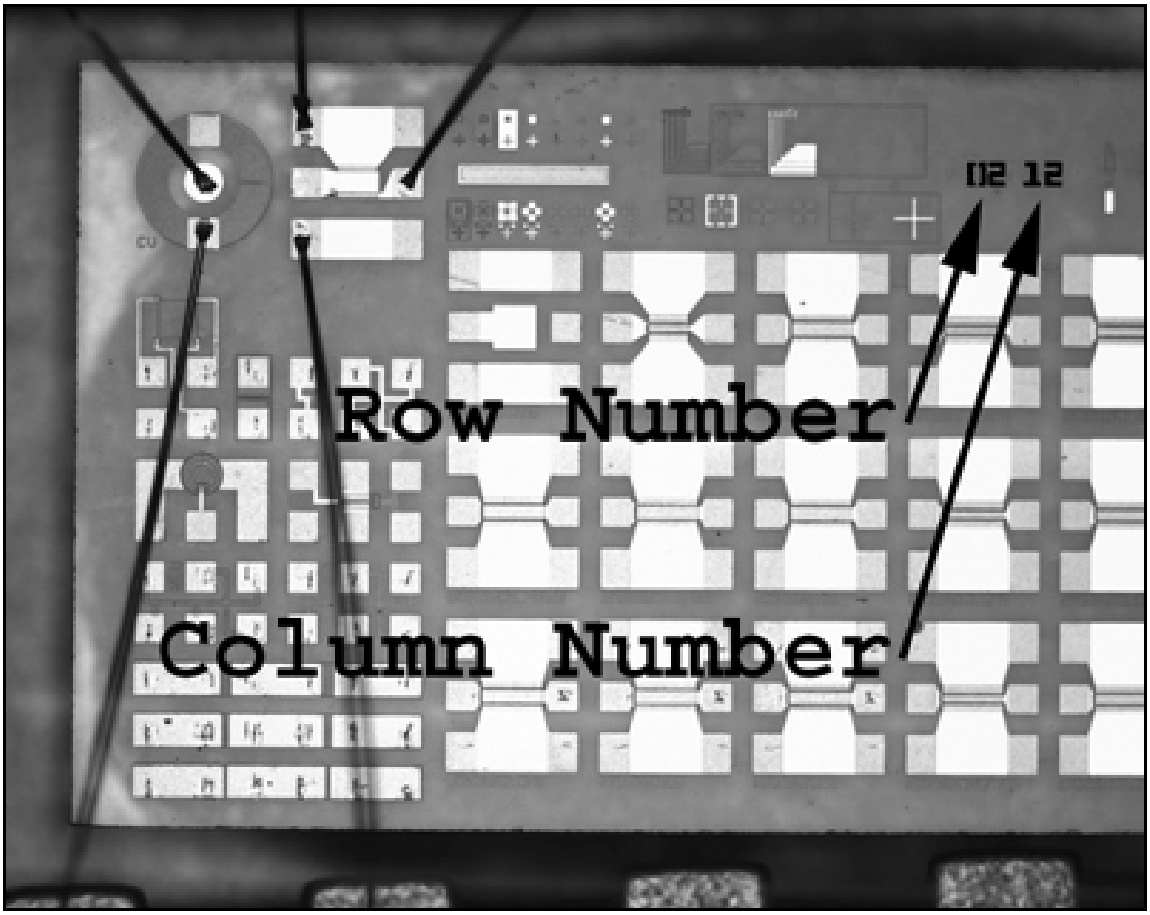

Figure 20. Reticle Labeling System

that they were appropriately connected to the package pins. For the irradiation experiments conducted in this research, the FatFET was the transistor used for testing and thus was always wire-bonded. The choice of the FatFET was made for two important reasons. First, the irradiation experiments involved cryogenic temperatures at which, transistor operation improves dramatically due to increased carrier mobilities. At these temperatures, every transistor on the reticles, with the exception of the FatFET, produces *I-V* curves beyond the measurement capabilities of the *I-V* equipment. However, the FatFET, due to its smaller width-to-length ratio, produces *I-V* curves that work perfectly for the measurement equipment at these temperatures. The second reason for choosing the FatFET was the larger mesa area needed by the FatFET. This larger mesa area was viewed as the best way to observe radiation effects on the 2DEG, which only exists beneath the mesa areas.

Figure 21 shows two examples of packaged reticles ready to be tested. Although the wire bonds cannot be seen in Figure 21 they are visible in Figure 20. As Figure 21 shows, the topsides of the reticles were left uncovered. This was done to allow electron radiation unabated access to the transistors. The first of the samples to be packaged were labeled A0211, A0212, A0213, A0214, A0215, and A0216; these samples were primarily used to verify the capabilities of the data acquisition program and equipment. After verifying the integrity of the data acquisition program and equipment, six samples were diced and packaged to be used for the radiation experiments. These samples were labeled A0313, A0314, A0315, A0316, A0408, and A0409. As indicated above, the labels themselves provide the exact location on the exact wafer piece from which the samples

were taken. Figure 22 shows the exact wafer locations occupied by all six irradiated reticles during the fabrication process (A0313, A0314, A0315, and A0316 were irradiated in the first experiment; A0408 and A0409 were irradiated in the last experiment).

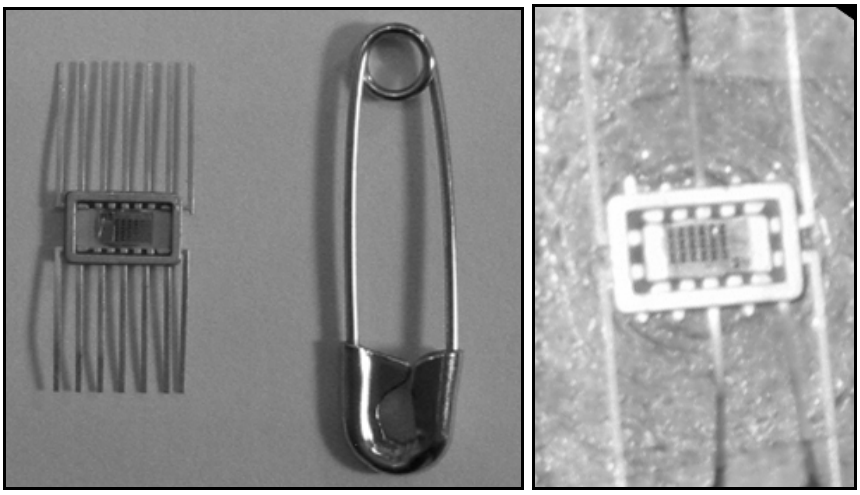

Figure 21. Packaged Reticles

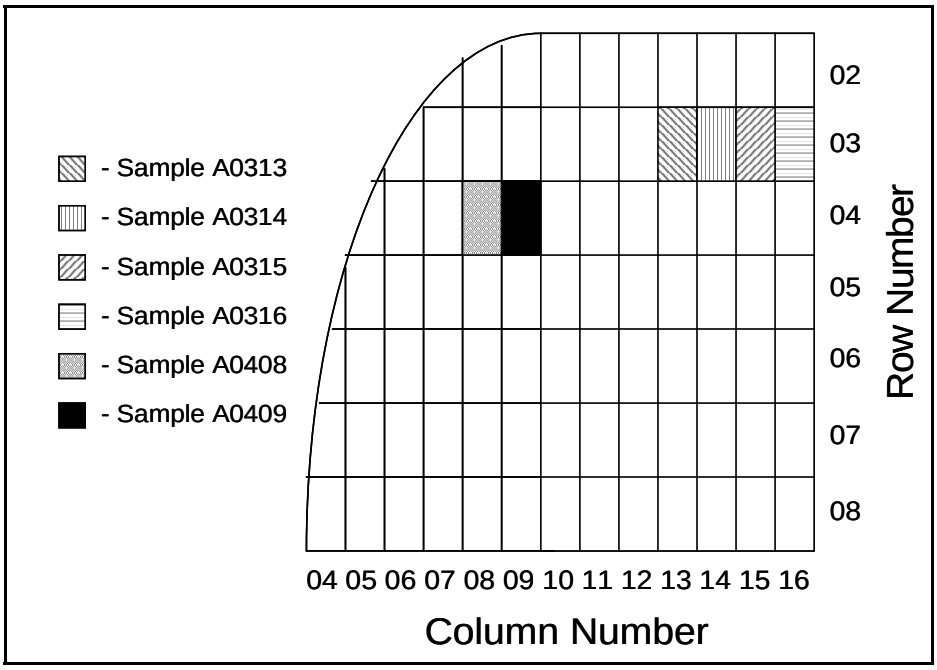

Figure 22. JS01A Reticle Identification Map Showing Locations of Irradiated Samples

Pre-Irradiation Characterization

After packaging was completed, the transistors were further tested using two separate methods. The first method used the experimental setup that would eventually be used to carry out the irradiation experiment while the second method involved the use of AFIT's probe-stand. The equipment involved with the first method included two Keithley 237 High Voltage Source Measurement Units (SMUs), a cold head/sample mount assembly, a National Instruments General Purpose Interface Bus (GPIB), and a laptop running a homemade Microsoft Visual Basic program (See Figure 23). The Visual Basic program is presented in its entirety in Appendix B. The cold head/sample mount assembly was machined for previous work [10] by the AFIT model shop (See Figure 24). The cold head is essential for two main reasons: it allows samples to be maintained at LiN temperatures during irradiation and it allows electrical operation and measurement of samples during irradiation as well as real-time temperature monitoring via a Resistive Temperature Device (RTD) embedded in the cold head. The equipment involved with the second method included a Hewlett Packard 41501A SMU and Pulse Generator Expander, a Hewlett Packard 4155A Semiconductor Parameter Analyzer and an Allesi Rel-6100 probe-stand (See Figure 25 and Figure 26). Both methods were used to measure transistor *I-V* curves for 0 V < V_D < 10 V and V_G = -2 V, -3 V, and -4 V; the source was always grounded during measurement. It is worth mentioning that the range of gate voltages over which these transistors can operate is approximately -4 V < V_G < 0.5 V. For V_G < -4 V the transistors enter cutoff (no 2DEG exists) whereas for V_G > 0.5 V the transistors cease to function properly causing the associated *I-V* curves to experience large distortions.

Figure 23. Building 470 Experimental Setup for Pre-Irradiation *I-V* Characterization

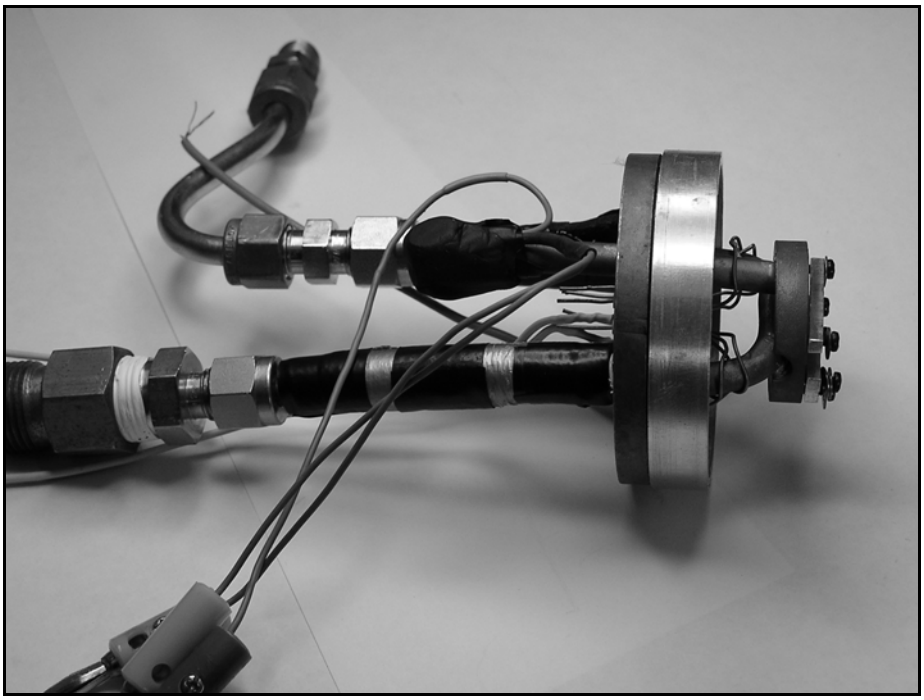

Figure 24. Cold Head and Sample Mount Assembly [10]

Figure 25. AFIT Probe-Stand Used for Pre- and Post-Irradiation *I-V* Characterization

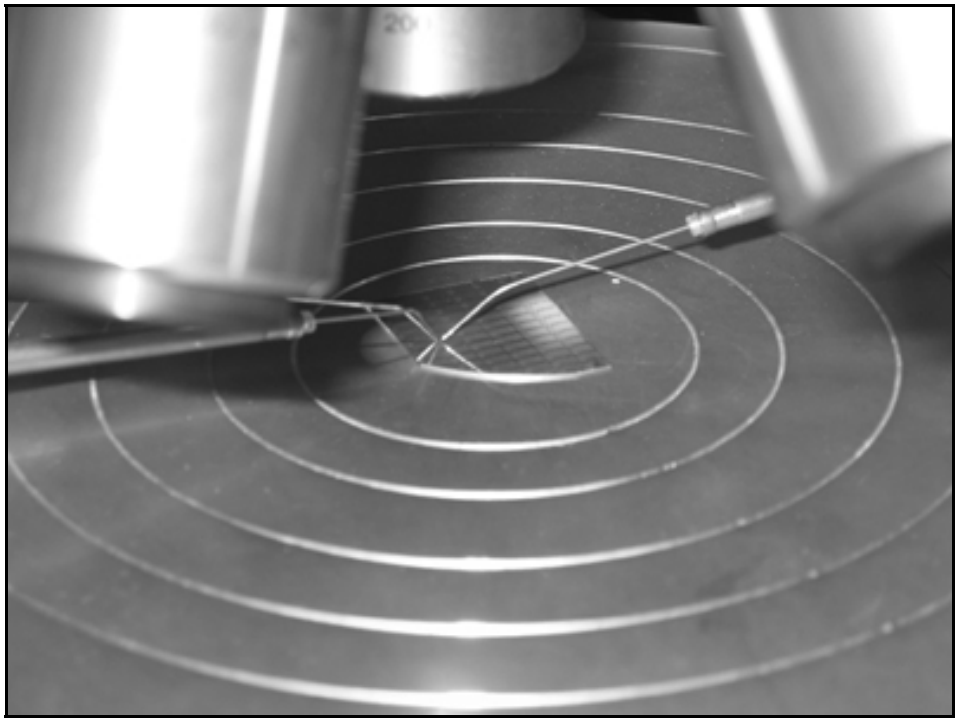

Figure 26. AFIT Probe-Stand Testing of JS01A

Irradiation Experiments

Two different irradiation experiments were conducted; the first experiment was performed over two days (09-10 December 2003) and the second experiment over one day (28 January 2004). Both experiments were conducted under the supervision of Dr. Gary Farlow who operated the electron VDG generator. Figure 27 shows a picture of the WSU VDG generator. The VDG at WSU is capable of producing low- to mid energy electrons routinely in the range of 500 keV to 1.8 MeV with beam currents less the 30 μA. The electron beam aperture area is 3.3 cm^2 and the beam is directed through an evacuated aluminum chamber held below 9×10^{-6} torr. The VDG produces a fairly uniform beam of monoenergetic electrons. Temporal current deviation is estimated at ± 3%; temporal energy deviation is estimated at ± 5% [10]. Spatial beam uniformity is estimated by the WSU VDG facility staff to be ± 2-3% as observed over a 2 cm by 2 cm square during optical measurements of irradiated plastics [10]. The beam current is used to control dose rate and was set as high as 6.0 μA and as low as 0.13 μA. The electron beam chamber is equipped with magnetic beam steering and an aperture for control of secondary emissions [10]. The electron beam chamber is capped at the end opposite the aperture with a cryogenically cooled vacuum flange that is part of the cold head and sample mount assembly (The plume of smoke in Figure 27 is nitrogen gas expanding as it changes phase from a liquid to a gas upon exiting the cold head). Total dose is determined using a current integrator that measures the beam current imparted onto the cold head.

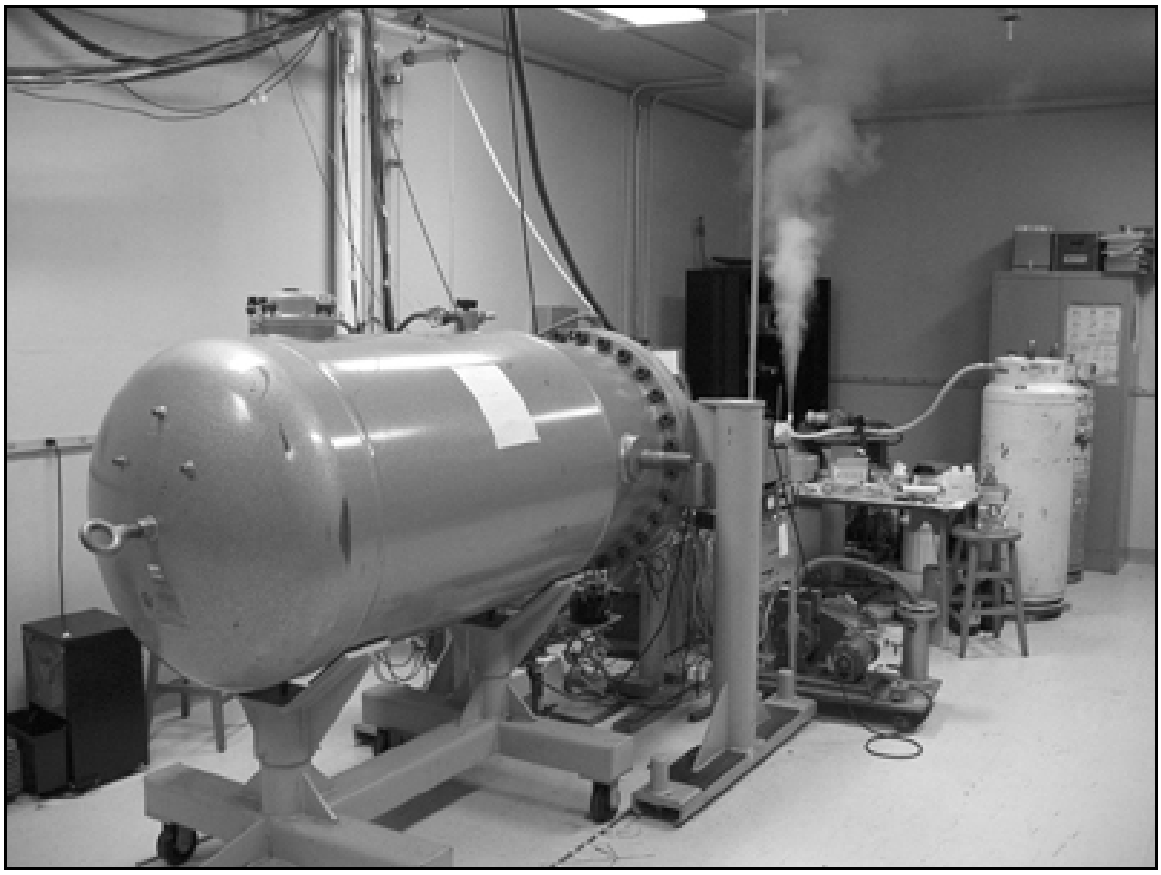

Figure 27. Wright State University Van de Graff Generator

At this point, it is important to mention that the capabilities of the WSU VDG system are well suited for this research effort based on two parameters: energy and dose. Both parameters can be varied over practical values (0.45 MeV < Energy < 1.8 MeV; 10^{12} e^-/cm^2 < Dose < 10^{18} e^-/cm^2) corresponding to the energies and doses that a satellite system might encounter in orbit. This is extremely important because this research effort is primarily focused on determining the radiation effects that would be experienced by an $Al_xGa_{1-x}N$/GaN MODFET integrated into a satellite-based system. As Figure 2 showed (see page 5), satellites operating in LEO, MEO, or GEO orbits could be exposed to electron fluxes upwards of 3×10^6 $e^-/cm^2\cdot s$ which corresponds to an annual dose of

9.46×10^{13} e^-/cm^2. Furthermore, the energies of the electron fluxes in Figure 2 are for energies greater than 1 MeV. Electrons with energies of a few hundred keV are present in even greater concentrations. Thus, although the energies and doses were partly chosen for practical, equipment related reasons, their values (shown below) are directly related to doses and energies that a satellite system could reasonably encounter in orbit.

The first experiment can be further subdivided into four different sub-experiments, each involving a single reticle: A0313, A0314, A0315, and A0316. All sub-experiments began with device mounting and testing in an attempt to pre-characterize the sample one final time using the exact experimental setup that would be used during irradiation. Sample mounting was achieved through careful placement of the individual samples on the cold head using thermally conductive grease to act as not only an adhesive between the sample and cold head, but also to ensure the sample was thermally connected to the cold head. The grease also served as an electrical insulator between the cold head and the sample's metal package. However, it is important to note that the electrical insulation provided by the grease is reduced during cryogenic and radiation exposures. For the 09-10 December experiments, the sample was further electrically isolated by placing scotch tape between the sample package and the cold head. The extra leads on a sample's package were taped down to the cold head leaving loose only the three package leads connected to the FatFET. The reason the extra leads were taped down to the cold head was to provide a conductive path that would allow any beam-deposited charge to dissipate through the cold head and the VDG current integrator.

After mechanical mounting was completed, electrical connections were made by soldering the three untapped sample leads (corresponding to the FatFET) to the electrical feed-through lines on the cold head. This allowed electrical connections to be made from the FatFET to the external banana plug connectors on the cold head (See Figure 28 and Figure 29). These banana plug connectors were then connected to coaxial lines, which ran approximately 18 meters before reaching the Keithley SMUs. Two coaxial lines were used for drain/gate voltage sourcing and drain/gate current measurements. The transistor source contact was connected to the shield of the coax lines, which was in turn connected to the common ground shared by the SMUs. Two additional coax lines were used to monitor the temperature through the RTD embedded in the cold head. Figure 30 shows a schematic of the experimental equipment.

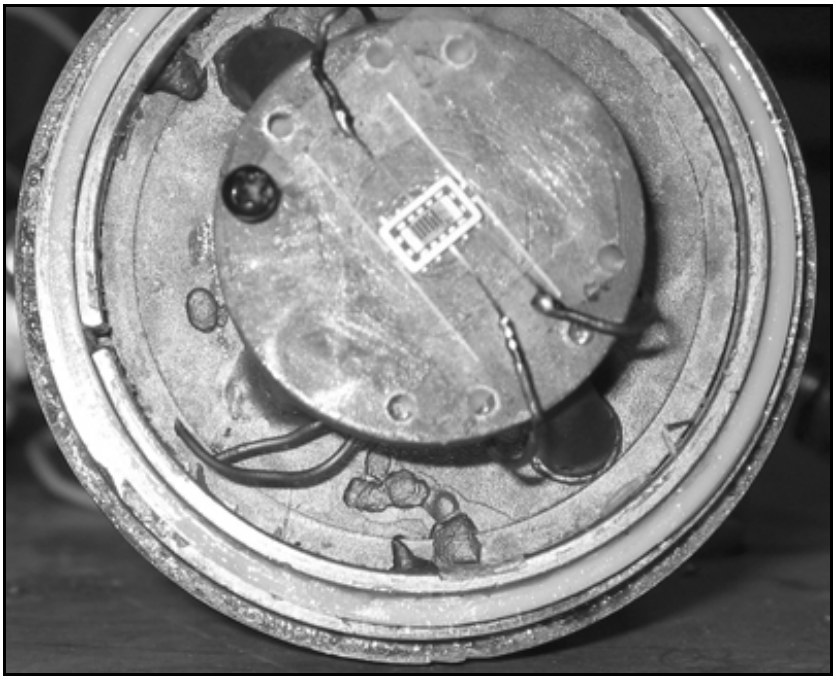

Figure 28. Cold Head/Sample Mount with Sample Showing Internal Feed-Through Lines Soldered to Sample Leads

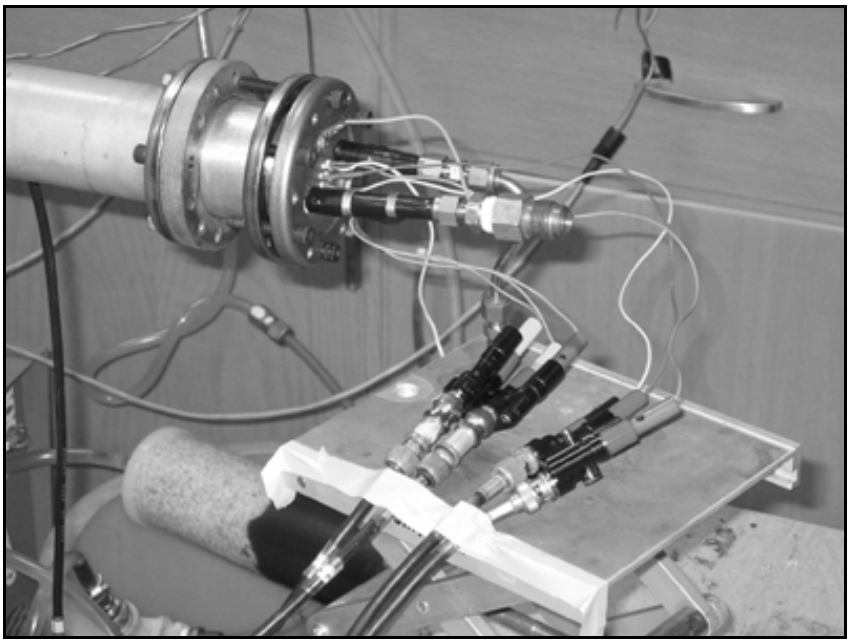

Figure 29. Cold Head Mounted to VDG Beam Chamber Showing External Feed-Through Lines Connected to Instrumentation Lines

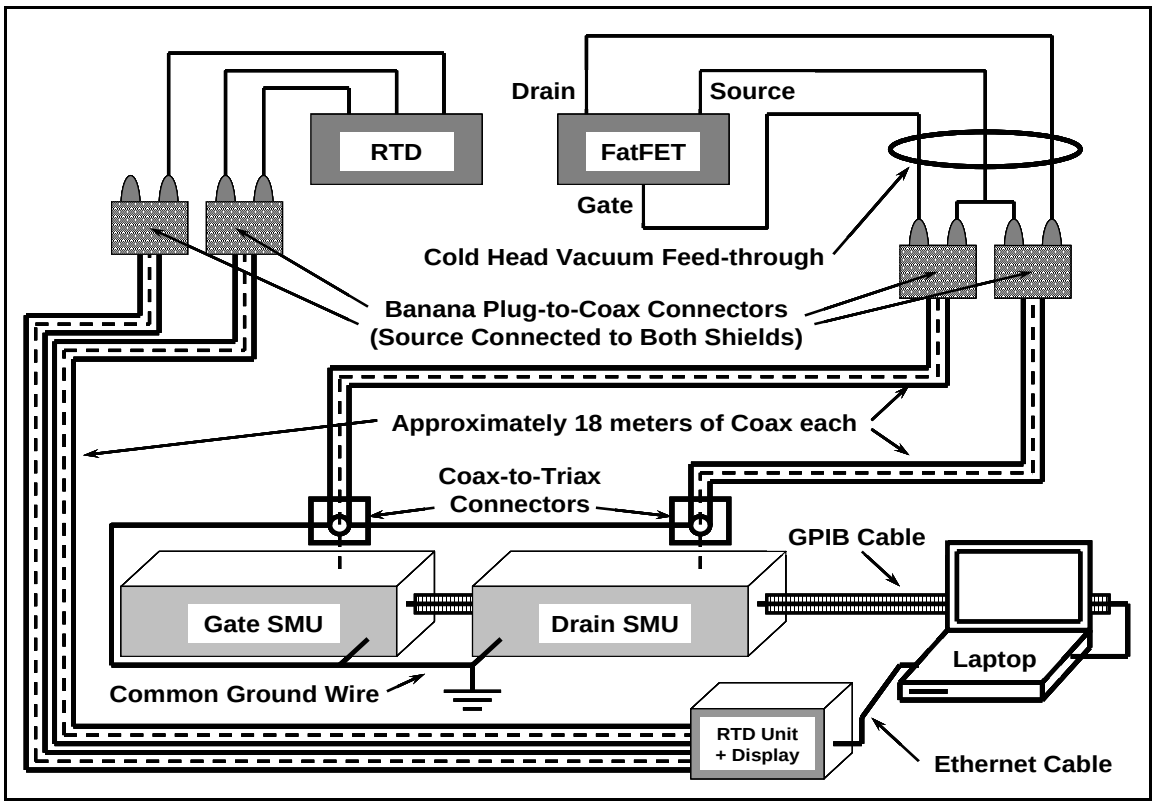

Figure 30. Schematic of WSU VDG Experimental Setup

Figure 31 shows a picture of the cold head operating under cryogenic conditions. A major concern under the conditions depicted in Figure 31, was the possibility for electrical shorts to develop between various external electrical lines caused by condensation collecting on the electrical connections. This problem was mitigated by stuffing tissue paper around the electrical lines in the immediate vicinity of the cold head and sealing the lines off with simple wax paper and masking tape. This would help to prevent much of the condensation collection that results when cold bodies are placed in moisture-filled air.

Figure 31. Cold Head Operation Under Cryogenic Conditions

Once the sample was mounted and operating properly the beam chamber would be pumped out below 9×10^{-6} torr. The data acquisition program would then begin to record data continuously as the LiN was turned on and the cold head cooled to below 90 K. After a steady state LiN temperature was reached (typically around 85 K), the VDG would be turned on. At this point in the experiment, the procedures carried out for Sample A0316 diverge from those carried out for the first three sub-experiments. The first three sub-experiments involved recording *in-situ* measurements of the FatFET's gate and drain currents during irradiation. However, each time a sample was irradiated, the FatFET *I-V* curves would instantly and drastically change from their ideal transistor-like appearance to incoherent noise. It was quickly theorized that the problem was related to current leaking from the electron beam current integrator circuit into the operated FatFET. Following three unsuccessful attempts to perform *in-situ* measurements, it was decided to abandon the *in-situ* measurement concept.

The fourth sample, A0316, was irradiated with the FatFET unpowered; this was accomplished by disconnecting the coax cables from the Keithley SMUs. Following low temperature irradiation, the VDG was turned off, the coax cables were reconnected to the Keithley SMUs, and the data acquired. However, this experiment yielded no results because it too rendered incoherent noise. As a result, Experiment 1 appeared to be a failure. However, post-irradiation visual inspections of the transistors, along with post-irradiation *I-V* measurements of the other, unconnected transistors on the three reticles, yielded several important results. The visual inspections, showing consistent and violent damage to the drain contacts, provided a better understanding of how the FatFETs, which

Table 5. First Irradiation Experiment Summary (09-10 December 2003)

Sample	Energy (MeV)	Beam Current (μA)	Total Dose (e^-/cm^2)	Irradiation Time (minutes)
A0313	1.2	6.0	6×10^{16}	80
A0314	0.8	1.0	6.5×10^{14}	6
A0315	0.8	1.0	7.88×10^{14}	7
A0316	0.7	1.0	1×10^{15}	9

were operated during irradiation, were rendered permanently unusable. The *I-V* measurements of the other, unconnected transistors indicated that the transistors experienced no permanent degradation following a room temperature anneal. Table 5 shows a summary of important information relating to the four sub-experiments conducted during the first main experiment.

The second experiment can be subdivided into two different sub-experiments, each involving a single reticle sample: A0408 and A0409. These experiments used an approach similar to that, which was used for the irradiation of sample A0316. Thus, the measurements would not be taken while the beam was operating so that the current integrator's current would not leak into the transistor circuit. However, because of the previous failure, we made one additional adjustment to the process. After discussing the issue with Dr. Farlow, it was proposed that disconnecting the current integrator (following irradiation) and shorting the cold head metal to the ground of the SMU circuitry would provide an ample current path to evacuate the excess electrons deposited by the beam on to the cold head. It was hoped that this procedure would prevent the previously reported occurrence of drain contact damage. The electron beam energy was another experimental parameter that was changed for this experiment; it was reduced to

450 keV. This reduction was implemented in an effort to limit the beam energy during the VDG's first few irradiations following recently conducted VDG repairs.

After irradiating the first sample (A0408) to a total dose of 1×10^{14} e^{-}/cm^{2} while the FatFET was left unpowered (the coax lines running to the Keithley SMUs were left connected but the SMUs were placed in standby mode), the VDG was turned off and the current integrator disconnected from the cold head metal. The cold head metal was then shorted to the Keithley system ground and *I-V* measurements were taken. Upon examining the *I-V* data, this methodology proved appropriate. The experiment continued by powering down the FatFET, turning the VDG on, and irradiating the sample to a dose two times the initial dose, yielding a total dose of three times the initial dose. Following irradiation, the VDG was turned off, the current integrator disconnected, and the cold head shorted to the Keithley ground. Throughout this process, the device maintained transistor behavior. The procedure was repeated a third time delivering a total dose equivalent to nine times the original dose. This time the newly measured transistor curves did not exhibit transistor behavior and it was concluded that the transistor was destroyed, perhaps by a static discharge through the unit, in a similar fashion as believed to have occurred during the previous experiments.

After removing sample A0408 from the cold head and mounting sample A0409, the second phase of experiment two was started. Except for the radiation dose intervals, the procedure for A0409 was carried out in the same manner as the procedure used for sample A0408. Due to a lack of time, higher beam currents were used to yield higher dose intervals that allowed a higher total dose to be achieved. Table 6 shows a summary

of important information related to the two sub-experiments conducted during the second main experiment. It is worth mentioning that the average time between VDG shutdown and data acquisition startup was approximately two minutes. The most important result concerning experimental procedures, was that A0409 never failed after four separate doses up to a total dose of 3.67×10^{15} e^-/cm^2. This fact serves to validate the experimental method applied during the second experiment.

Table 6. Second Irradiation Experiment Summary (28 January 2004)

Sample	Energy (MeV)	Beam Current (μA)*	Relative Dose (e^-/cm^2)	Relative Irradiation Time (min)	Total Dose (e^-/cm^2)	Total Irradiation Time (min)
A0408	0.45	0.13	1×10^{14}	7	1×10^{14}	7
A0408	0.45	0.13	2×10^{14}	13	3×10^{14}	20
A0408	0.45	0.13	6×10^{14}	39	9×10^{14}	59
A0409	0.45	0.3	3×10^{14}	8	3×10^{14}	8
A0409	0.45	0.3	6.7×10^{14}	13	9.7×10^{14}	21
A0409	0.45	0.3	9×10^{14}	18	1.87×10^{15}	39
A0409	0.45	0.3	1.8×10^{15}	50	3.67×10^{15}	89

*Beam current fluctuations were more pronounced throughout this entire experiment.

V. Experimental Results

First Experiment I-V Measurements

As previously reported, the failure of all four irradiation samples during the first experiment prevented data collection after irradiation. A discussion of these transistor failures is provided in Appendix C. In addition, the only transistor that was pre-characterized was the FatFET, which was permanently destroyed by the experiment. However, three transistors on each reticle were tested using the AFRL/SNDD DC/RF tester. These transistors were dual gate transistors with gate lengths of 0.75, 1.0, and 1.2 μm (They are the three transistors with scratch marks on the contact pads seen in Figure 14). The rightmost of these transistors (1.2 μm gate length) was retested following the first irradiation experiment using the AFIT probe-stand. The one important difference between *I-V* measurements made using the AFRL/SNDD DC/RF tester and the AFIT probe-stand is that only half of the transistor (one gate) could be operated using the AFIT probe-stand whereas both gates were operated in the DC/RF tester. This distinction should result in a 50% reduction in drain currents measured by the AFIT probe-stand. In other words, the drain currents measured by the DC/RF tester should be exactly twice as large as the drain currents measured by the AFIT probe-stand. To account for this difference, all DC/RF measured drain currents were divided by 2 to yield drain currents that were directly comparable to the AFIT probe-stand measured drain currents. Because these two measurement processes were different for several reasons (different equipment, different testing processes, etc.), several control measurements were taken of unirradiated

samples to see how well the measurements compared. Ideally, the measurements would be identical. Figure 32 and Figure 33 show one example of this comparison. Additional examples can be found in Appendix D: Figure 69 through Figure 76. These comparisons clearly indicate that the AFIT probe-stand consistently measures drain currents lower than those measured by the DC/RF tester. Quantifying this measurement change is somewhat difficult due to the varying amounts of reduction; however, a good estimate is 10-20% reduction in drain current.

Figure 34 and Figure 35 show the pre- and post-irradiation *I-V* curves for Sample A0313. This sample was given the highest dose (6×10^{16} e^-/cm^2) of any sample irradiated in either experiment and involved the most energetic electrons (1.2 MeV) of any experiment. Based on the 10-20% reduction in drain current shown in Figure 35, it was concluded that the appearance of radiation-induced drain current degradation shown in Figure 34 was accountable through the difference in measurement processes as stated above. Additional pre- and post-irradiation *I-V* curves can be found in Appendix D: Figure 77 through Figure 80. From the evidence shown in Figure 32 through Figure 35 along with the additional relevant figures in Appendix D, it was concluded that no permanent radiation effects remained following room temperature annealing.

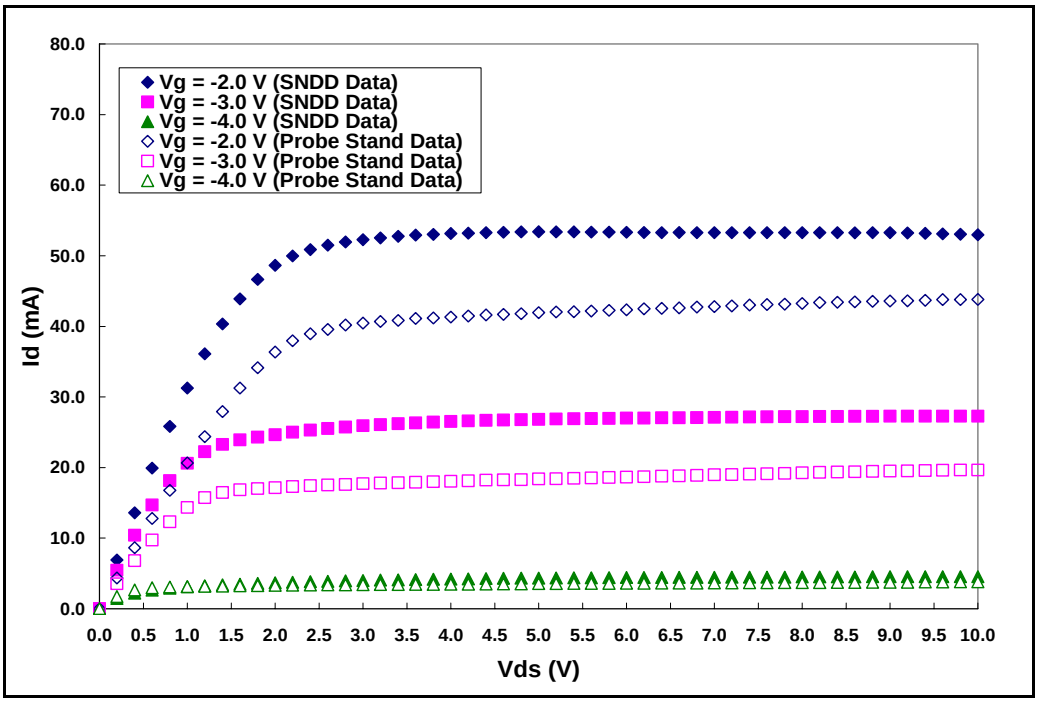

Figure 32. Sample A0410 2X150X1.2 Transistor, SNDD vs. AFIT Room Temperature *I-V* Curves

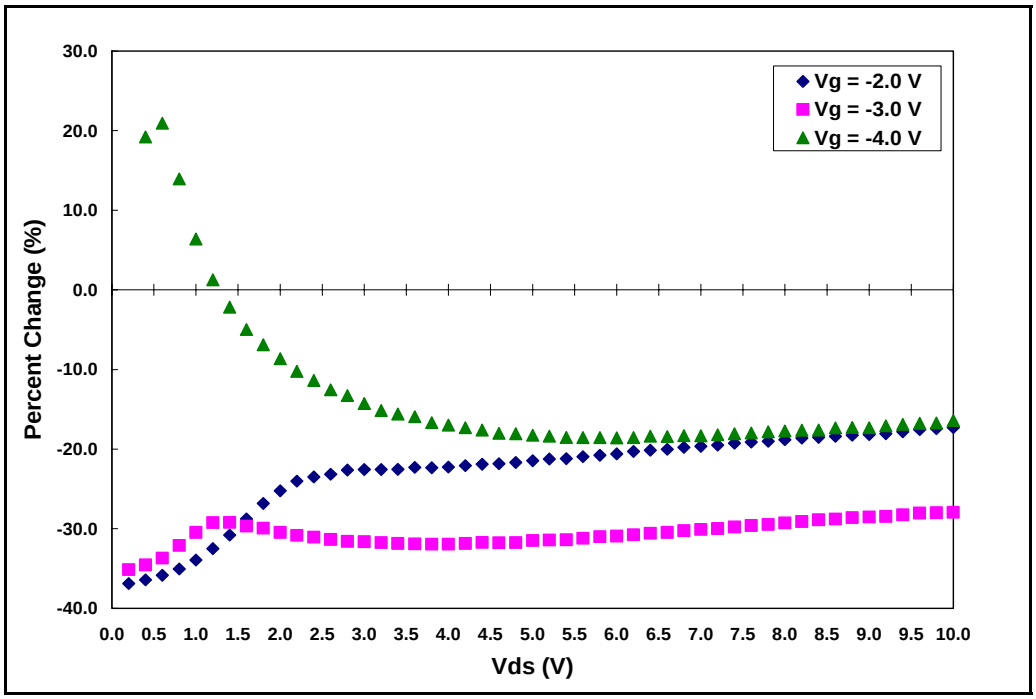

Figure 33. Sample A0410 2X150X1.2 Transistor, Percent Change from SNDD to AFIT Room Temperature *I-V* Curves

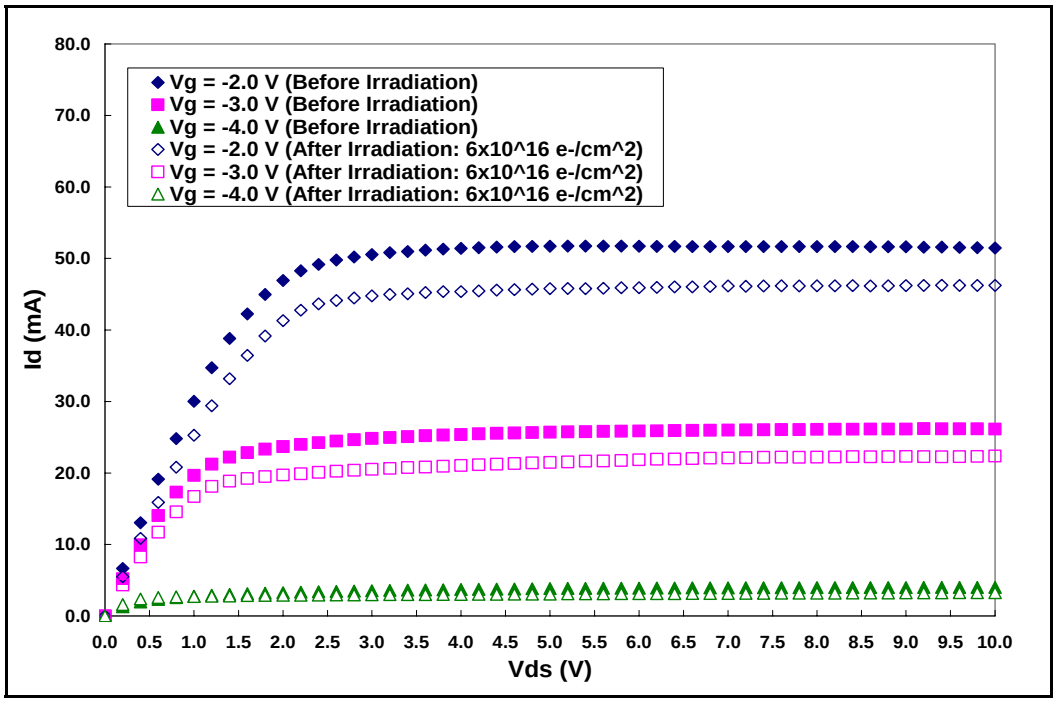

Figure 34. Sample A0313 2X150X1.2 Transistor Pre- and Post-Irradiation Room Temperature *I-V* Curves (1.2 MeV Electrons)

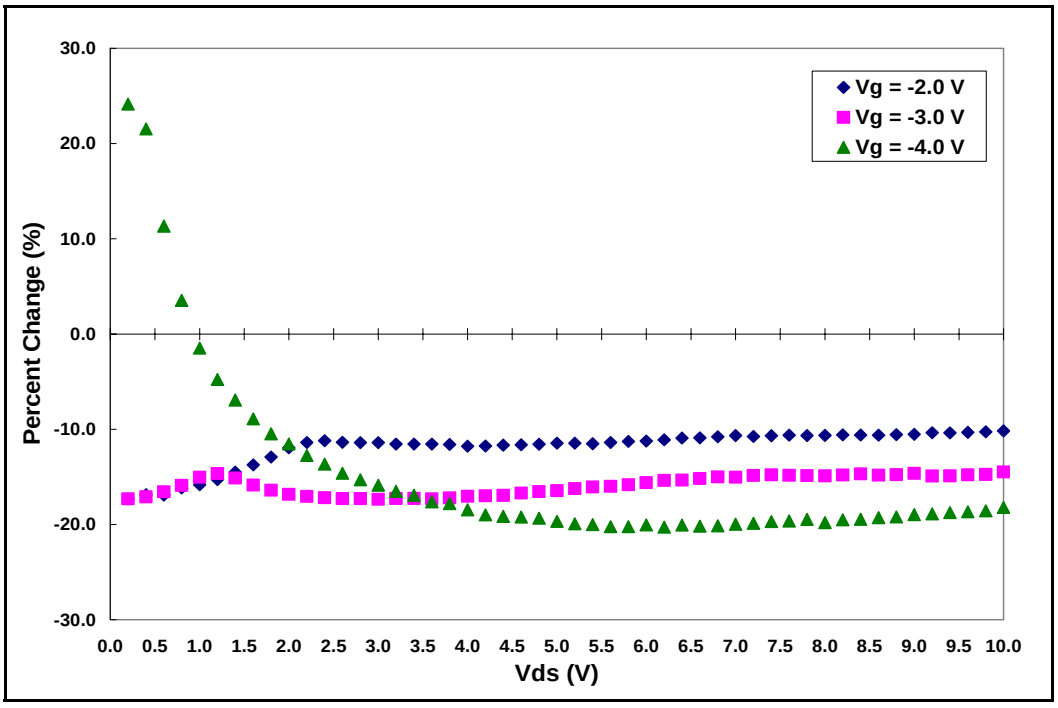

Figure 35. Sample A0313 2X150X1.2 Transistor Percent Change from Pre- to Post-Irradiation Room Temperature *I-V* Plots (1.2 MeV Electrons)

Second Experiment I-V Measurements

As reported earlier, the second irradiation experiment was successful in producing post-irradiation *I-V* curves at LiN temperatures. These post-irradiation curves provided invaluable data allowing for a more detailed examination of the radiation effects on these transistors. Figure 36 and Figure 37 show the changes in sample A0408 FatFET drain and gate currents caused by the initial irradiation of 10^{14} e^-/cm^2. The data displayed in these figures was collected at LiN temperature over several minutes both before and after irradiation. Five sets of data were averaged to yield the pre-irradiation plots, and four sets of data were averaged to yield the post-irradiation (10^{14} e^-/cm^2) plots. The changes evident in Figure 37 indicate a clear increase in gate leakage current. More surprising were the changes appearing in Figure 36, which show large increases in the drain currents following irradiation. This effect stands in sharp contrast to the effect observed by White, *et. al*. who reported that the drain currents decreased in magnitude following various proton irradiations (See Figure 6). Furthermore, Figure 36 indicates that the increases in drain current are not related to the applied gate voltage, which also stands in opposition to the results presented by White, *et. al*.

Figure 38 and Figure 39 show the changes in the same sample's drain and gate currents caused by the second irradiation of 2×10^{14} e^-/cm^2. The data displayed in these figures includes the same 10^{14} e^-/cm^2 dose curves presented in Figure 36 and Figure 37 along with a new set of curves taken from an average of three sets of data collected following the second irradiation. Figure 38 clearly indicates that only extremely small

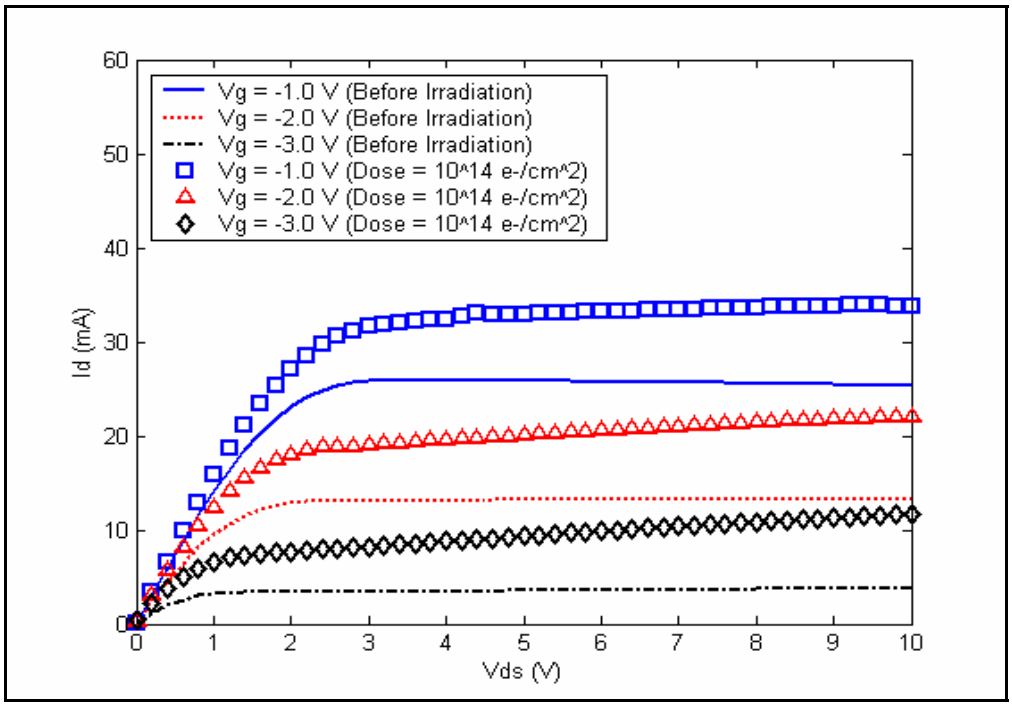

Figure 36. Sample A0408 FatFET First Irradiation: Change in *I-V* Curves at LiN Temperature (0.45 MeV Electrons)

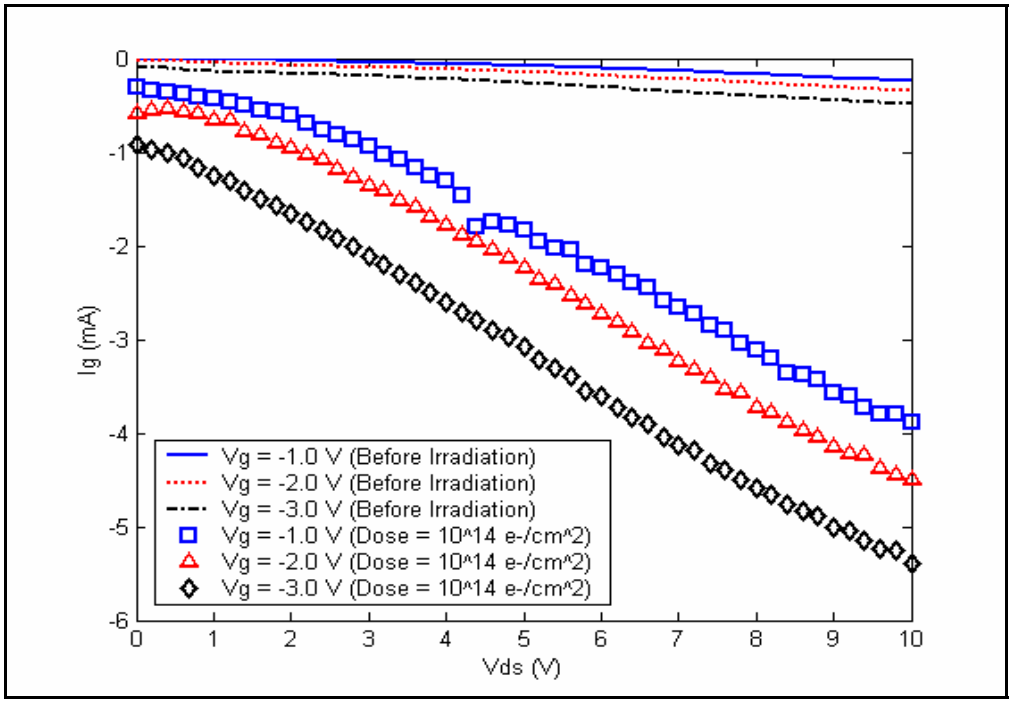

Figure 37. Sample A0408 FatFET First Irradiation: Change in Gate Leakage Currents at LiN Temperature (0.45 MeV Electrons)

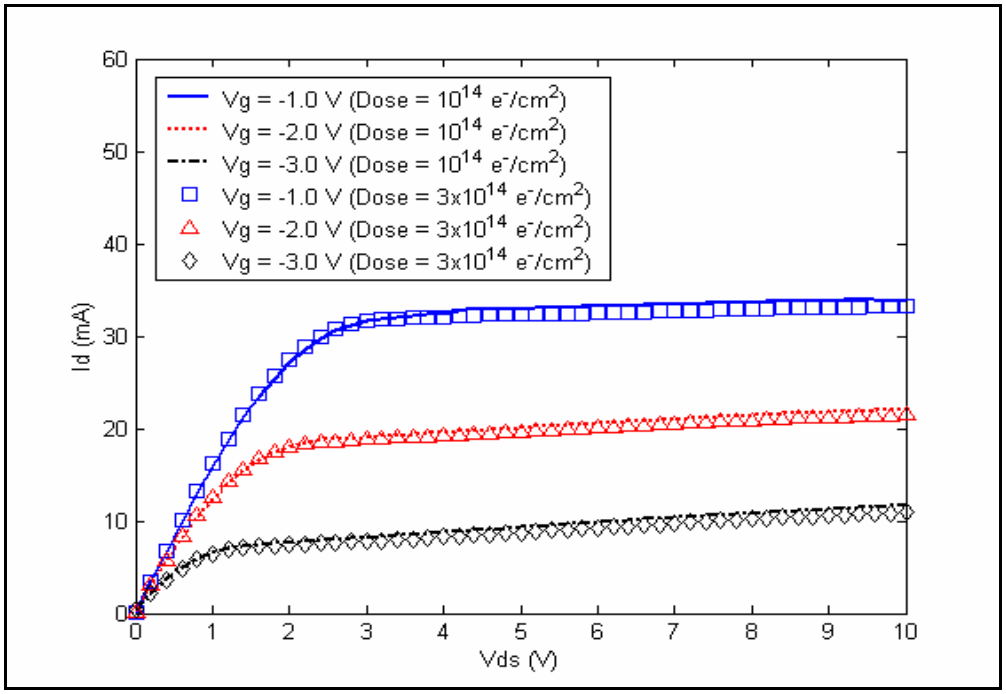

Figure 38. Sample A0408 FatFET Second Irradiation: Change in *I-V* Curves at LiN Temperature (0.45 MeV Electrons)

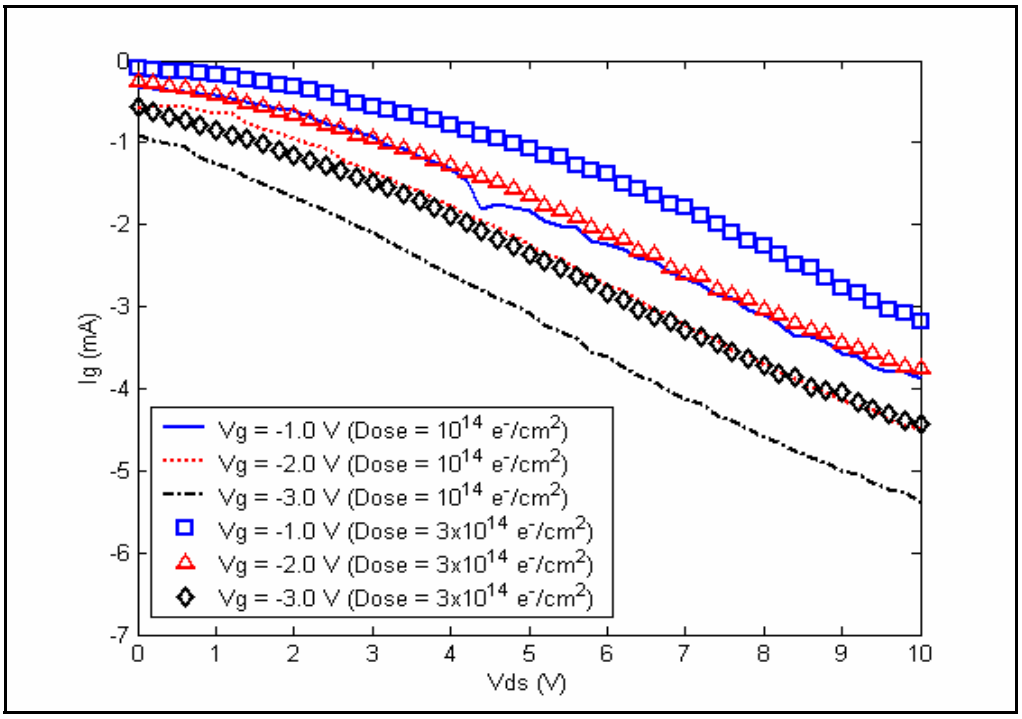

Figure 39. Sample A0408 FatFET Second Irradiation: Change in Gate Leakage Currents at LiN Temperature (0.45 MeV Electrons)

changes took place in the drain current even though the device was subjected to twice the initial dose! This fact indicates that the transistor's changes were not related to the total dose but rather to the initial radiation exposure. Furthermore, the extremely small drain current changes are directly correlated to the gate leakage changes and are so small they are attributed to measurement error. (The magnitude of both drain and gate currents increased by approximately 0.5 to 1 mA from the second irradiation.)

Figure 40 and Figure 41 show the changes in sample A0409 FatFET drain and gate currents caused by the initial irradiation of 3×10^{14} e^-/cm^2. The data displayed in these figures was collected at LiN temperature over several minutes before and after irradiation, similar to the manner used in the A0408 experiments presented above. Seven sets of data were averaged to yield the pre-irradiation plots, while four sets of data were averaged to yield the post-irradiation (3×10^{14} e^-/cm^2) plots. Similar to the initial radiation data for sample A0408's FatFET, Figure 41 indicates a rather large increase in gate leakage current for sample A0409's FatFET. Additionally, the increases in drain currents evident from Figure 40 show striking resemblance to the drain current increases previously reported for sample A0408 (See Figure 36).

Figure 42 and Figure 43 show the changes in the drain and gate currents for the same sample (A0409) caused by the second irradiation of 6.7×10^{14} e^-/cm^2. The data displayed in these figures includes the same 3×10^{14} e^-/cm^2 dose curves presented in Figure 40 and Figure 41 along with the new set of curves taken from an average of four sets of data collected after the second irradiation. Once again, a clear correlation is

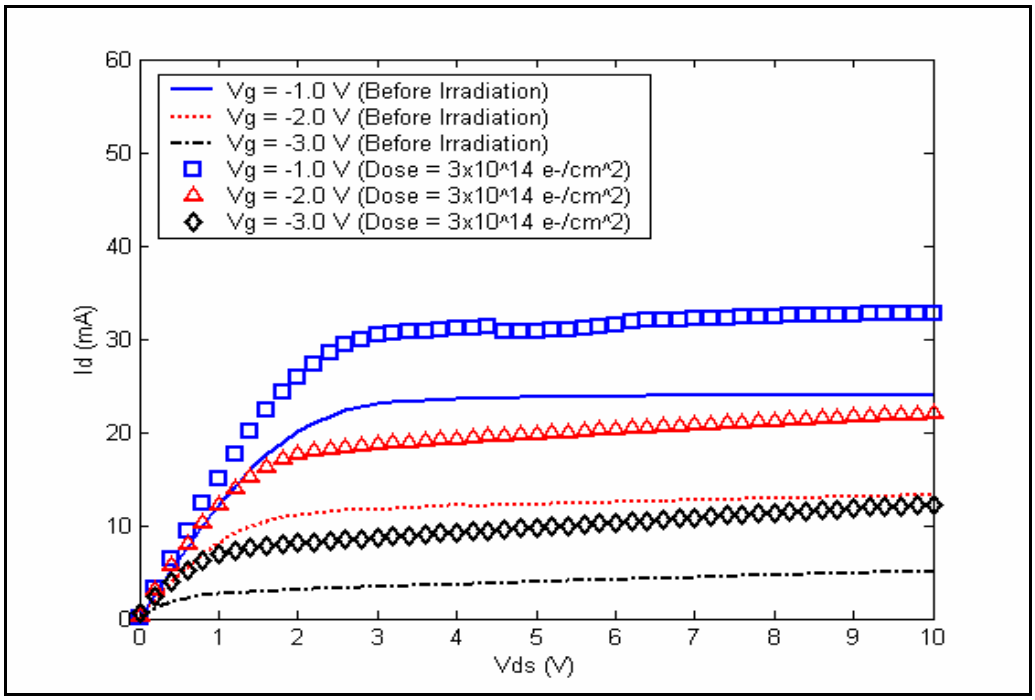

Figure 40. Sample A0409 FatFET First Irradiation: Change in *I-V* Curves at LiN Temperature (0.45 MeV Electrons)

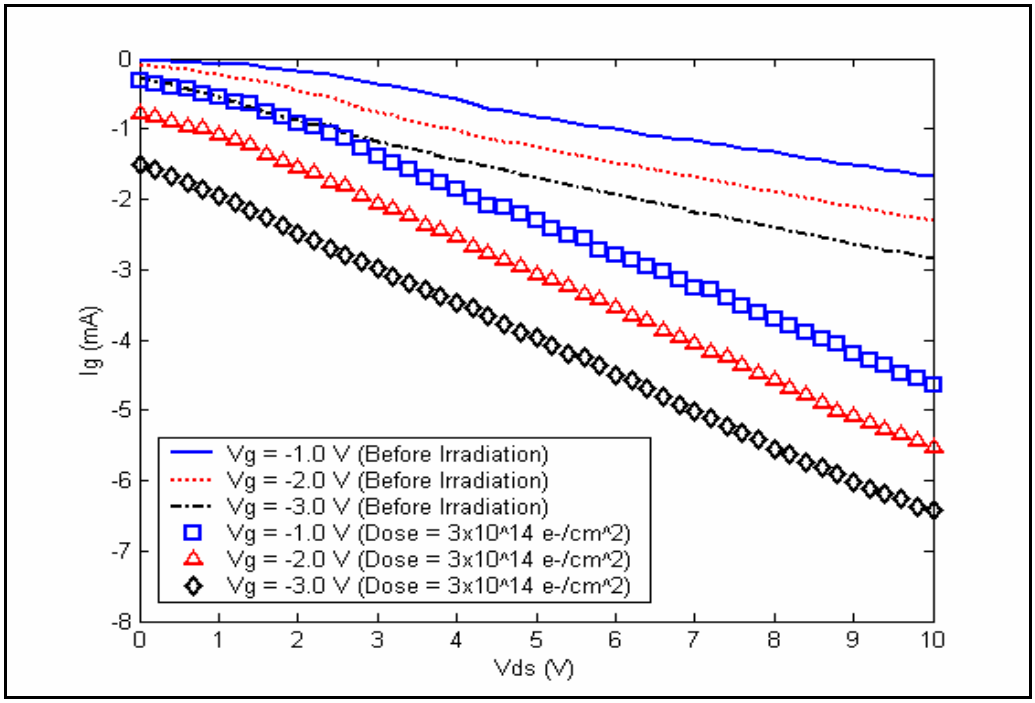

Figure 41. Sample A0409 FatFET First Irradiation: Change in Gate Leakage Currents at LiN Temperature (0.45 MeV Electrons)

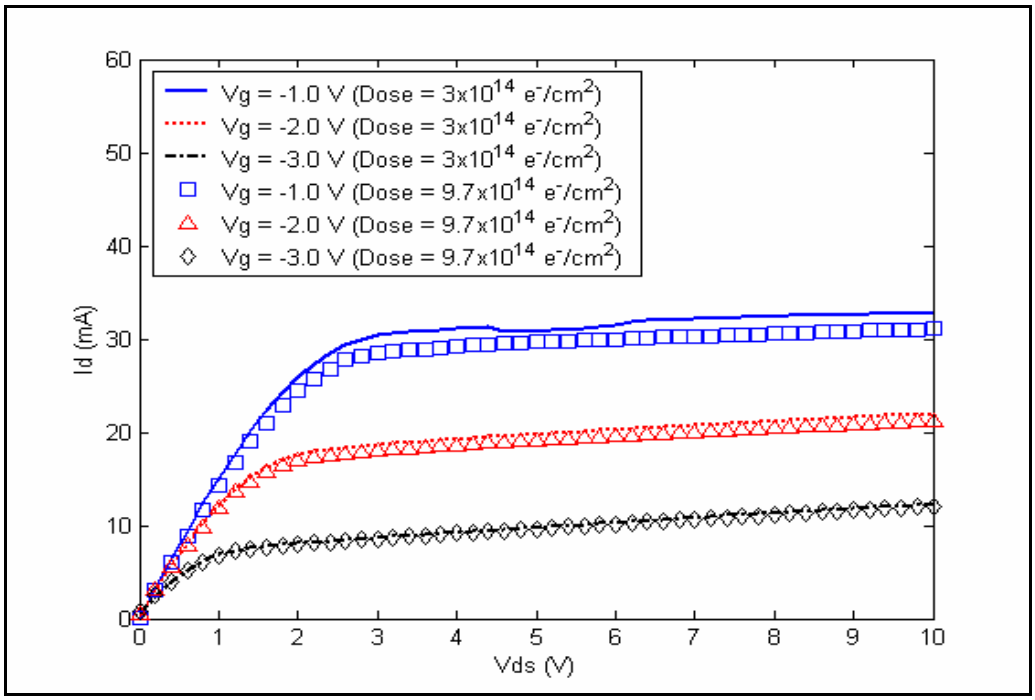

Figure 42. Sample A0409 FatFET Second Irradiation: Change in *I-V* Curves at LiN Temperature (0.45 MeV Electrons)

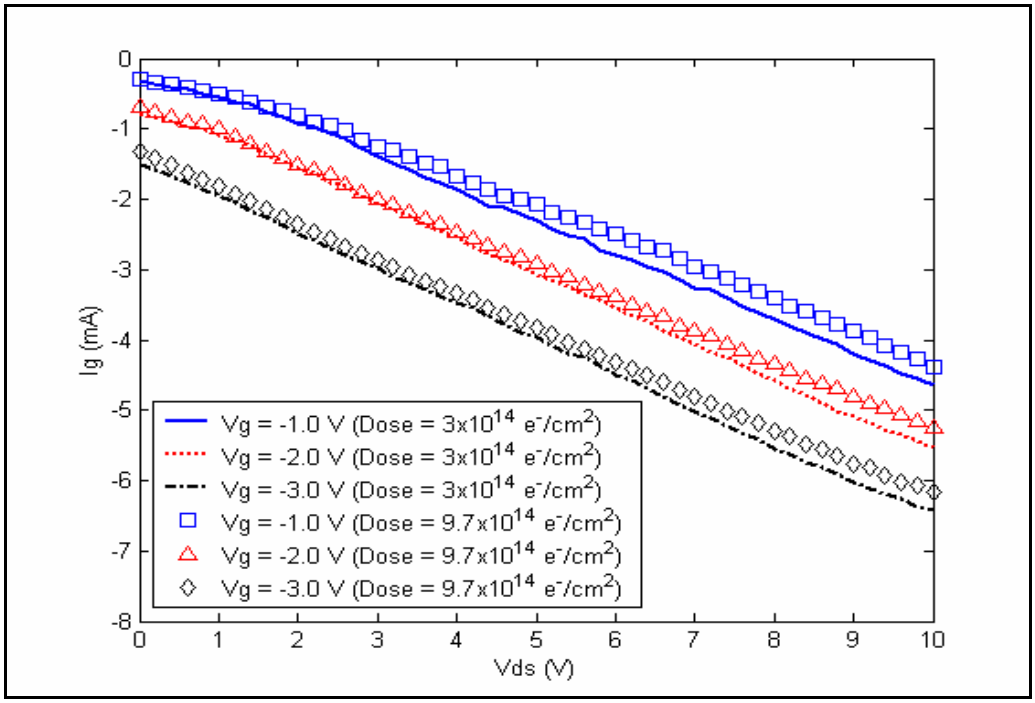

Figure 43. Sample A0409 FatFET Second Irradiation: Change in Gate Leakage Currents at LiN Temperature (0.45 MeV Electrons)

observed between sample A0408 experimental data and sample A0409 experimental data. Figure 42 indicates that extremely small changes took place in the drain currents following the second irradiation, which only adds credence to the results presented in Figure 38. However, the first irradiation for sample A0409 involved a dose three times higher than the dose received in sample A0408's first irradiation. The second irradiation for sample A0409 involved a dose 3.35 times higher than the dose received in sample A0408's second irradiation. The differences in doses together with the similarities in drain and gate current changes provide additional evidence for the notion that the transistor's changes were not related to the total dose but rather to the initial radiation exposure. More evidence supporting this theory can be found in Appendix D: Figure 81 through Figure 84. Another important conclusion can be reached by noting the fact that the dose rates during both the A0408 and A0409 experiments were maintained relatively constant (See Table 6). This fact, combined with the fact that second, third, fourth, and fifth irradiations do not change the gate/drain currents (See Figure 38, Figure 39, Figure 42, Figure 43, and Figure 81 through Figure 84) leads to a conclusion that the gate/drain current increases are not dose rate-dependent effects.

Close examination of the currents in Figure 36 and Figure 37 reveals an interesting but sensible characteristic. For drain-source voltages greater than the saturation voltage (also known as the pinch-off voltage), the pre-irradiation curves maintain a constant magnitude of current. However, over the same range of drain-source voltages, the post-irradiation curves clearly show a small but steady increase. The magnitude of this drain current increase is identical to the magnitude of gate current

increase over the same range of V_{DS}. In other words, the increasing gate leakage has a one-to-one relationship with the increasing drain current in the saturation region. To better illustrate this point, Figure 44 and Figure 45 were created. These figures show what the drain currents from Figure 36 and Figure 40 would look like if the associated gate current magnitudes from Figure 37 and Figure 41 were subtracted. The results of this subtraction (Figure 44 and Figure 45) clearly indicate that gate leakage plays a small role in the overall drain current increase but does not account for the majority of the radiation-induced drain current increase. Furthermore, once the gate leakage has been subtracted, the remaining increase in drain current is constant throughout the *I-V* curve saturation region (the pre- and post-irradiation curves are parallel).

Figure 46 shows the magnitude of the differences in the drain current curves from Figure 36 and the gate current curves from Figure 37. Figure 47 shows the magnitude of the differences in the drain current curves from and Figure 40 and the gate current curves from Figure 41. The plots in Figure 46 and Figure 47 are provided to further show correlation between the radiation effects observed in the sample A0408 experiment and the sample A0409 experiment.

Finally, Figure 48 and Figure 49 show the room temperature pre- and post-irradiation pictures for the A0409 experiment. (This measurement was not possible for A0408 because it broke during the third irradiation.) Although the curves shown in Figure 48 and Figure 49 are not identical, they are extremely close in both magnitude and shape. Thus, these plots further support the argument that no permanent radiation effects remain following room temperature annealing.

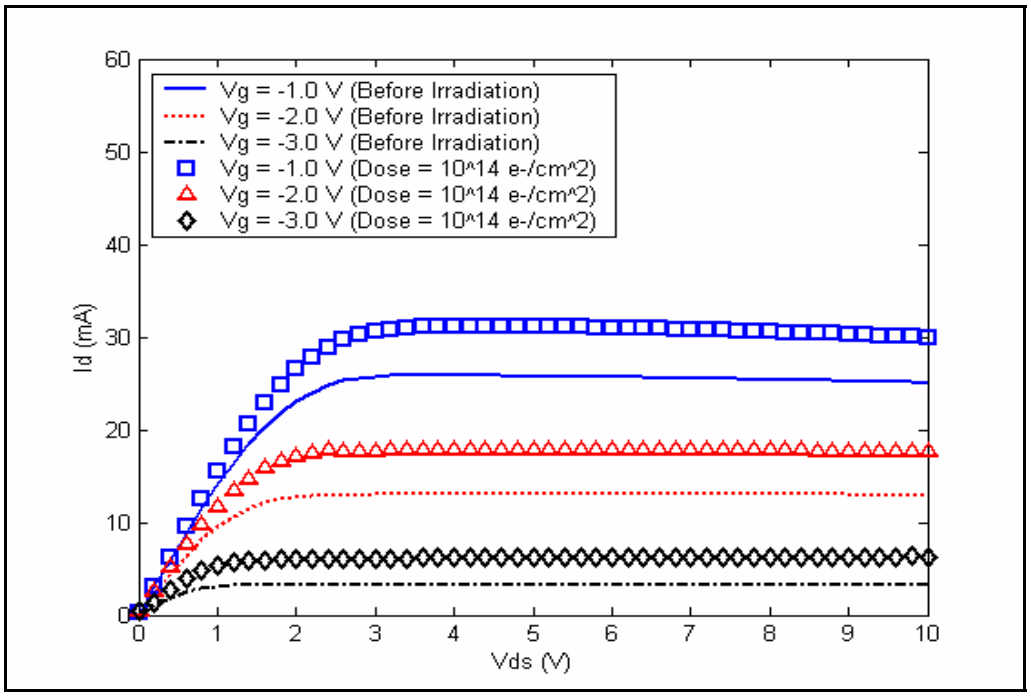

Figure 44. Sample A0408 FatFET First Irradiation, LiN Temperature I-V Curves Minus Gate Leakage

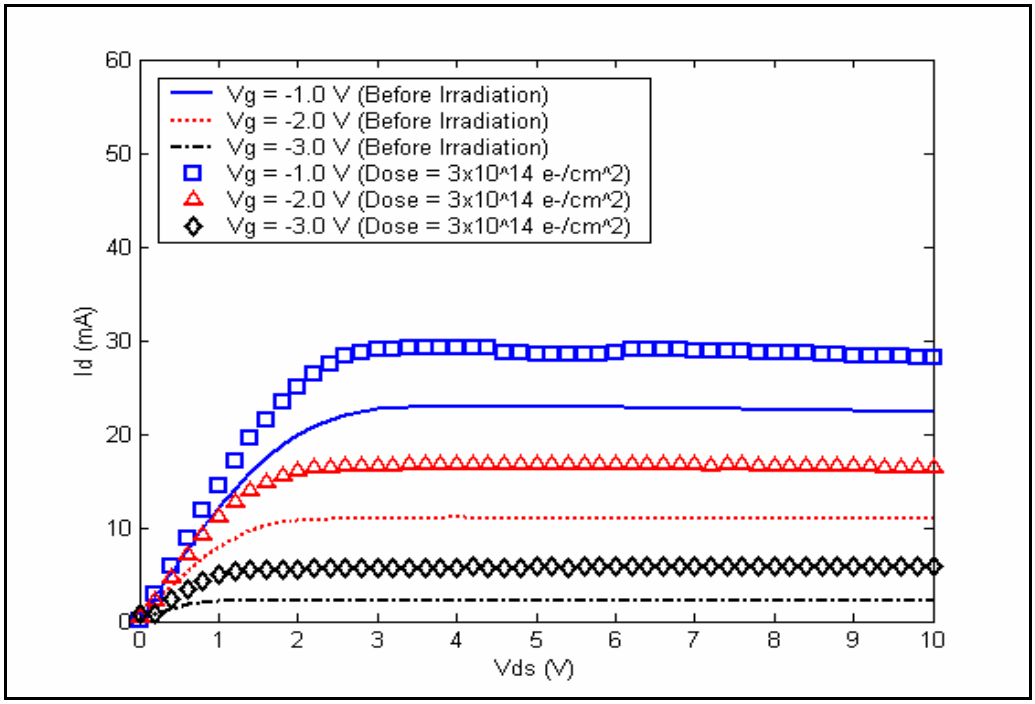

Figure 45. Sample A0409 FatFET First Irradiation, LiN Temperature I-V Curves Minus Gate Leakage

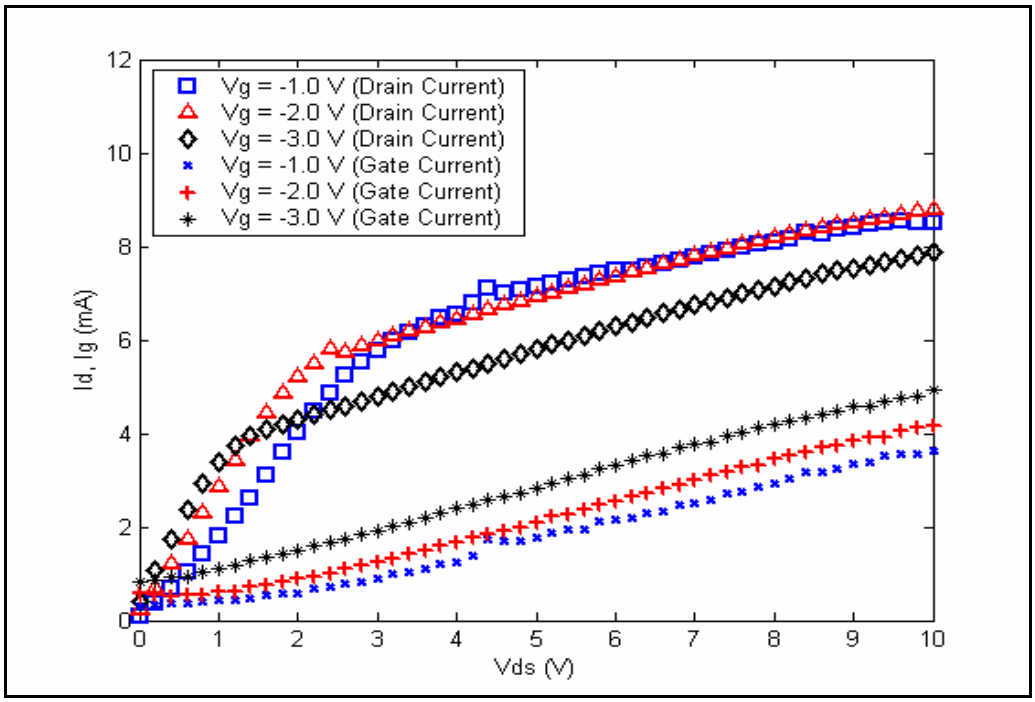

Figure 46. Sample A0408: Magnitude of Change in Drain and Gate Currents for First Irradiation (1×10^{14} e^-/cm^2 at 0.45 MeV)

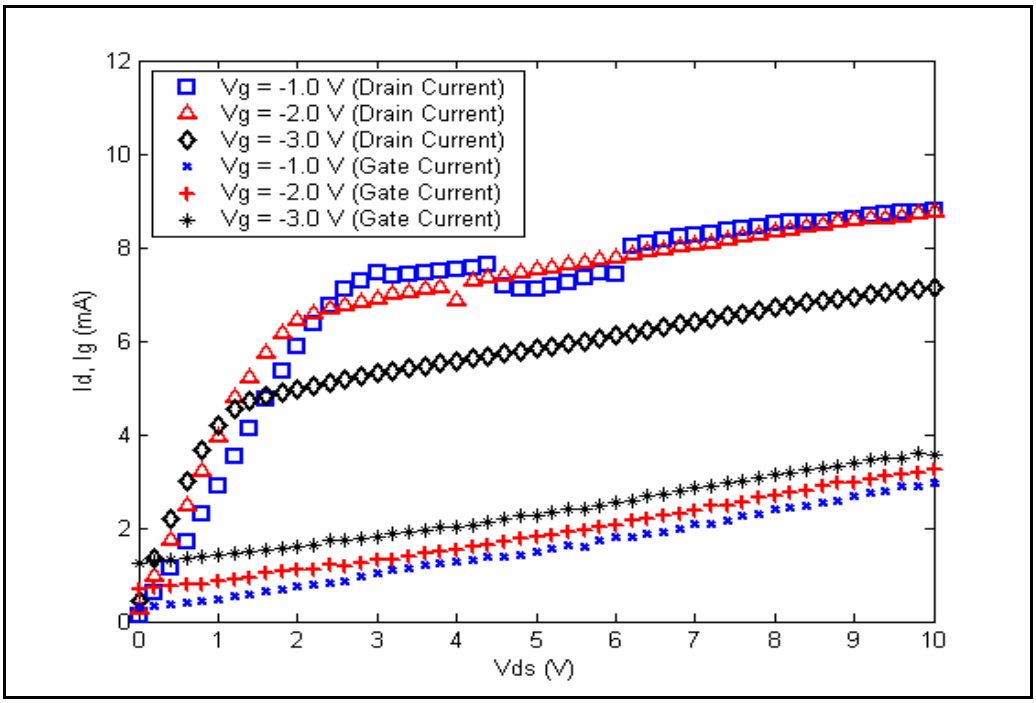

Figure 47. Sample A0409: Magnitude of Change in Drain and Gate Currents for First Irradiation (3×10^{14} e^-/cm^2 at 0.45 MeV)

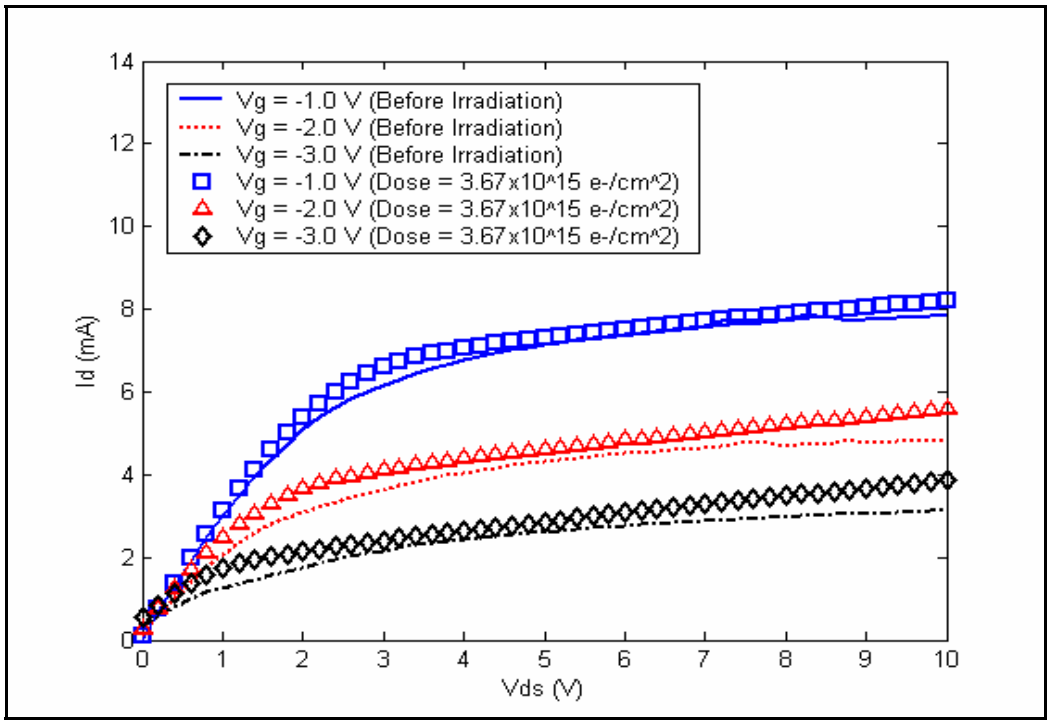

Figure 48. Sample A0409 FatFET Room Temperature Pre- and Post-Irradiation *I-V* Curves

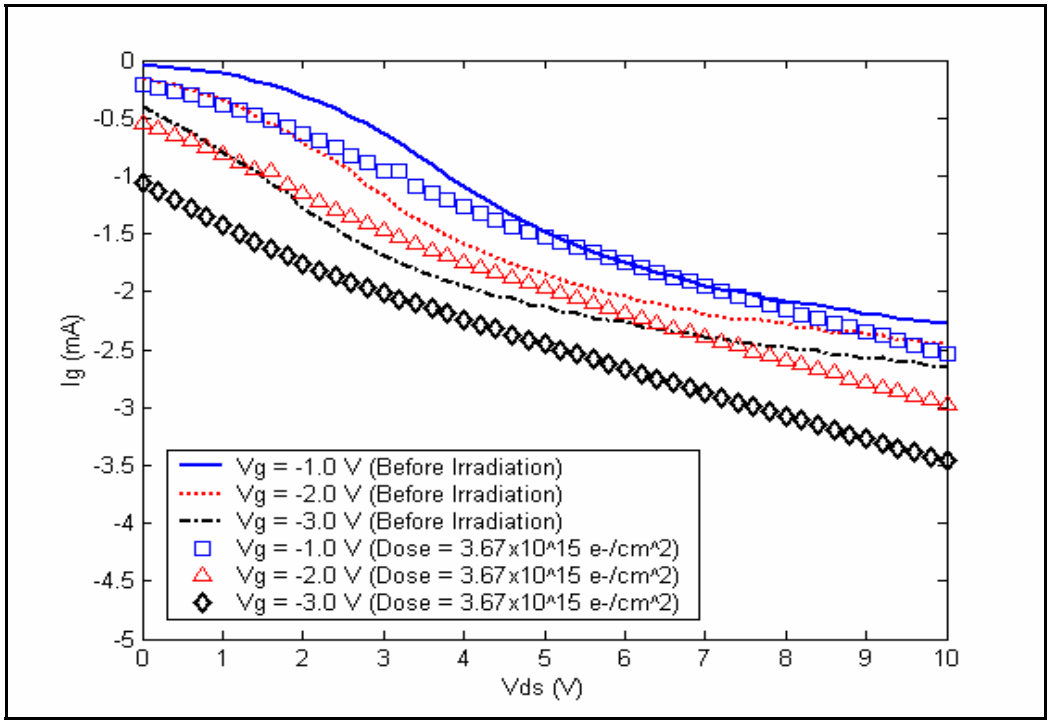

Figure 49. Sample A0409 FatFET Pre- and Post-Irradiation Gate Leakage Currents

Analysis and Discussion

The first major radiation effect observed was the large increase in gate leakage current. This effect could be evident from either of two explanations. One explanation relates to the Schottky barrier gate contacts, which the electron radiation could have damaged resulting in a contact becoming more ohmic in nature. However, if this were the case, the damage would be expected to be permanent even after a room temperature anneal. Previously presented measurements clearly indicate that this is not the case. Another explanation relates to the mechanisms by which carriers can transport through the insulating $Al_{0.27}Ga_{0.73}N$ region.

Karmalkar, Sathaiya, and Shur report that the gate leakage mechanism consists of two parallel electron transport processes: trap-assisted tunneling and direct tunneling [28]. Thermionic emission should also be considered but only at sufficiently high temperatures - which are not the case in this study [28]. They go on to report that the trap-assisted tunneling component is dominant at low temperatures (T < 500K) [28]. An assumption made stated that traps are distributed throughout the $Al_xGa_{1-x}N$ layer and spread over an energy band located within the barrier height [28]. Additionally, Qiao, *et. al*. performing studies on ohmic contacts to $Al_xGa_{1-x}N$/GaN heterostructures, found that carrier transport across the $Al_xGa_{1-x}N$ barrier layer is dominated by the tunneling of electrons that originate from the 2DEG [29]. Finally, Khan, *et. al*. studying metal-oxide-semiconductor heterostructure field-effect transistors (MOS-HFETs), reports a six order of magnitude reduction in gate leakage resulting from the integration of an oxide region between the gate contact and the $Al_xGa_{1-x}N$ layer [30]. This gate leakage reduction

provides additional evidence to support the theory that the $Al_xGa_{1-x}N$ layer is susceptible to carrier transport.

These findings point toward a conclusion that the large increase in gate leakage was caused by electron radiation-induced trap creation. Although the nature of these traps is unknown, it can be surmised from the results that 0.45 MeV electron radiation creates a large increase in the trap concentration throughout the $Al_xGa_{1-x}N$ layer. Furthermore, because electrons have an extremely low non-ionizing energy loss (NIEL) it can be assumed that the activation energy of these traps is low. Using DLTS Nozaki, Feick, and Weber report discovering $Al_xGa_{1-x}N$ traps with activation energy of 0.28 eV [24]. It is therefore speculated that either this trap or a similar trap is created in $Al_xGa_{1-x}N$ layer by low energy electron radiation, resulting in large increases the gate current. Although the nature of these traps remains unknown, their ability to affect device performance has clearly been demonstrated.

The second major radiation effect observed was the large increase in drain current. From Equation (6) on page 29, it is known that I_{DS} is directly related to four variables: the charge of an electron, the width of the gate, the electron mean velocity in the channel, and the channel sheet charge density. Since both the charge of an electron and the gate width are constants, we know that any change in drain current must be caused by either a change in the channel sheet charge density (in other words, the 2DEG carrier concentration) or a change in the electron mean velocity in the channel. Thus, an explanation for the drain current increase will stem from one of two possibilities: (a) the current increase was caused by a direct increase in carrier concentration in the 2DEG; (b)

the 2DEG population remained unchanged and the increase was caused by an increase in the electron mean velocity in the 2DEG. One of these possibilities can easily be proven over the other through simple dose-dependent C-V measurements, which can be used to calculate 2DEG carrier concentrations. However, since the results of these measurements are not available, some basic theories will be presented that serve to explain the experimental results.

The first possibility leads to an explanation for the drain current increase that is based on a trapped charge collection process in the $Al_xGa_{1-x}N$ layer. Throughout the literature, there is much debate over the mechanism(s) that causes DC drain current compression [12], [24], [31]. These debates revolve around the existence, and effects that surface states in the $Al_xGa_{1-x}N$ layer have on the 2DEG. One of the most important issues involved in this debate is the nature of the surface states, "Are they acceptor states or donor states?" Morkoc, Di Carlo, and Cingolani propose that the states are actually amphoteric (i.e. they can act as either acceptors or donors) [11]. The importance of the debates over these surface states relates directly to the fact that the $Al_xGa_{1-x}N$ layer is extremely thin (25 nm). Consequently, any charge trapped in the $Al_xGa_{1-x}N$ layer would have enormous consequences on the fields seen by potential 2DEG carriers residing in the GaN layer [32]. Essentially, such trapped charge would act like a virtual gate voltage similar to the effects of ionizing radiation on metal oxide semiconductor field-effect transistors (MOSFETs). The result of a virtual gate voltage would be made evident through a vertical shift (either up or down depending on the type of charge) in the *I-V*

curves. For these n-channel transistors, a net positive charge would have to be trapped in the $Al_xGa_{1-x}N$ layer to produce the positive vertical shift in *I-V* curves that was measured.

Applying the assumption that the 2DEG carrier concentration is changed, the following process is proposed. Electron radiation, interacting with atoms in the $Al_xGa_{1-x}N$ layer, ionizes a plethora of electrons. The large amounts of ionization involved with this theory are supported by the previously reported fact that Collisional Stopping Power, which results in ionization and excitation, accounts for the overwhelming majority of energy deposited in $Al_xGa_{1-x}N$ (See Figure 12). Furthermore, the large amounts of ionization involved with this theory are produced by relatively low doses (10^{14} e^-/cm^2 and possibly lower). The ionized electrons would then be subject to one of two possibilities. The first possibility involves the majority of the ionized electrons to be temporarily trapped in energy states near the conduction band of $Al_xGa_{1-x}N$. For these trapped electrons to be swept out of the $Al_xGa_{1-x}N$ layer a sufficiently high electric field must exist which could only be created through an applied gate bias. Thus, once the transistor is operated following irradiation, the electrons are released from their high-energy traps and cleared out of the $Al_xGa_{1-x}N$ region. The second possibility involves the majority of the ionized electrons to be immediately made mobile by the intrinsic electric fields associated with the highly polarized $Al_xGa_{1-x}N$ layer. This would result in charge collection at the $Al_xGa_{1-x}N$/GaN heterointerface, which would be dumped into the 2DEG.

Either possibility would result in the removal of numerous electrons from the $Al_xGa_{1-x}N$ layer, leaving behind a net stationary positive charge. This new stationary positive charge would add to the overall net positive charge in the $Al_xGa_{1-x}N$ layer

(created by polarization fields) resulting in an increase in the electric field seen by the potential 2DEG carriers in the GaN layer. The increased electric field (directed into the GaN layer) would draw an increased number of mobile electrons out of the GaN layer and deposit them into the 2DEG, yielding higher 2DEG carrier concentrations. As previously indicated, this proposed process essentially involves the creation of a virtual gate voltage similar to the threshold voltage shifting effect that occurs in electron irradiated MOSFETs. This proposed explanation is bolstered by the observation that the saturation voltages shown in Figure 44 and Figure 45 increase directly as the drain current curves increase. In other words, if one did not know they were looking at pre- and post-irradiation curves in these figures, they would assume that the six curves shown differ only in their applied gate voltage. This effect is well known for silicon MOSFETs where an increase in the number of carriers present at the inversion layer (the channel), results in a higher drain voltage needed to achieve saturation (V_{Dsat} increases with increasing V_{G}) [1].

An alternative to the process presented above can be formulated by assuming that the second possibility occurred, which says the post-irradiation 2DEG population remained unchanged and the drain current increase was caused by an increase in the electron mean velocity in the 2DEG. This proposed process relies on an excellent understanding of 2DEG properties and theory. Unfortunately, this understanding has yet to be developed. However, a general process can still be presented based on previously reported $Al_xGa_{1-x}N$/GaN MODFET theory, radiation interaction theory, and experimental data.

From Equation (7) on page 29, the electron mean velocity in the channel is known to be related to several factors including the low-field mobility, μ_o, the position-dependent electric field above the channel, $E(x)$, and the electron velocity under saturation conditions, v_{sat}. Equation (7) indicates for large $E(x)$, any change in $E(x)$ would be balanced by its presence in both the numerator and denominator. For the FatFET, the drain-source distance is approximately 78 μm, which results in an average drain-source electric field, of 128 V/cm for V_{DS} = 1 V. Because this large value of $E(x)$ is produced for small values of V_{DS}, $E(x)$ can be mathematically eliminated as the possible cause of the drain current increase. Additionally, Equation (7) indicates for large μ_o, any change in μ_o would be balanced by its presence in both the numerator and denominator. As reported by Cree, the channel mobility is 1300 $cm^2/V{\cdot}s$. This value of mobility is sufficiently large to mathematically eliminate μ_o as the possible cause of the drain current increase.

This leaves v_{sat} as the only possible source to explain the drain current increase. From Equation (7), we know that v_{sat} is directly proportional to the electron mean velocity and thus directly proportional to the drain current. Consequently, any increase in v_{sat} could directly explain an increase in drain current. If we assume that incident electron radiation created a sufficiently high enough number of states that are located immediately below the 2DEG, it is possible for the quantum well to expand deeper into the GaN layer. This assumption is supported by the data presented in Appendix A, which shows that large amounts of incident electron energy are imparted in the GaN region of the transistors. The new, wider quantum well would effectively increase electron mobility in the quantum well. Although this increased mobility would not result in large drain current

increases at lower drain-source voltages, it would increase v_{sat} since mobility and carrier velocity are directly proportional. The new, larger value of v_{sat} would shift the non-linear and saturation portions of the *I-V* curves higher as shown in Figure 44 and Figure 45.

An alternative to both the above theories involves a reduction in the resistivity of the drain and source ohmic contacts. Reducing the resistivity in these contacts would directly explain the drain current increase. However, any contact resistivity change is expected to be permanent. Thus, the application of this theory would result in permanent increases in drain current. However, the room temperature annealing data recorded in the second experiment, along with the room temperature measurements made in the first experiment indicate that no such permanent increases exist.

A final theory can be postulated based on the possibility that persistent photocurrents were created during irradiation. Dirtrich, *et. al*. has demonstrated that $Al_xGa_{1-x}N$/GaN FETs show pronounced persistent photoconductivity (PPC) and that the drain current is sensitive to illumination [31]. They further show that the drain currents affected by PPC, were also dependent on drain and gate bias history and that the drain current recovery is temperature dependent [31]. However, they conclude by adding that the physical origins for their observations are not yet understood [31]. Consequently, it is unknown whether this theory would involve an increase in 2DEG carrier concentration. It is worth noting that, although the increase in drain current is surprising (almost to the extent of being unbelievable), it is not an unheard of occurrence. The University of Florida has shown variations in drain currents for similar $Al_xGa_{1-x}N$/GaN MODFETs that extend upwards of ± 10% in work that has yet to be published [32]. Although, their

changes were caused by variations in the mechanical strain experienced by the $Al_xGa_{1-x}N$ layer and not by irradiation, their work does help to alleviate fears that the consistently measured drain current increases presented in this research were a fluke.

The final major radiation effect observed was the complete removal of radiation-induced current changes through room temperature annealing. This effect was observed by the room temperature measurements recorded before and after the first experiment (Figure 34, Figure 35 and Figure 77 through Figure 80) as well as the room temperature measurements recorded during the second experiment (Figure 48 and Figure 49). This very broad radiation effect indicates that any electron radiation-induced damage that affects transistor performance must have a low activation energy associated with it causing it to anneal at temperatures below 300 K.

VI. Conclusions and Recommendations

Conclusions

Irradiation of $Al_xGa_{1-x}N$/GaN MODFETs using low energy electrons creates temperature-dependent damage that greatly affects transistor operation. These effects are observed in transistor operation via the following two manners:

- Gate leakage currents are increased up to one order of magnitude
- Drain currents are increased 5 to7 mA independent of the applied gate voltage

The damage that causes these effects anneals out between 77 K and 300K. The mechanism that causes the first effect is an increase in electron traps throughout the $Al_xGa_{1-x}N$ layer caused by the incident electron radiation. These traps support an increase in trap-assisted tunneling which manifests itself as an increase in gate current. The mechanism that causes the second effect is unknown. Three possibilities explaining this effect are presented, the most likely of which involves the creation of additional positive space charge in the $Al_xGa_{1-x}N$ layer induced by the ionization of electrons spurred from incident electron radiation. This new positive space charge adds to the positive space charge created by the polarization fields present in the $Al_xGa_{1-x}N$, to yield a higher net positive space charge. This increased space charge draws more potential carriers out of the GaN layer yielding higher 2DEG carrier concentrations that are responsible for the increased drain currents. Finally, although the originally hypothesized drain current degradation was never shown to occur, it is still possible that higher doses and/or higher

energies of electron radiation create 2DEG scattering centers of sufficient quantity to reduce 2DEG carrier mobility and lifetime resulting in a counteraction of the drain current increases observed in these experiments. Consequently, either a specific dose or a specific energy may exist that results in identical in pre- and post-irradiation *I-V* curves measured at LiN temperature.

Recommendations for Further Work

The previously presented results not only raise additional questions but also require additional research to be validated. The increase in gate leakage is presented with high confidence but could be further supported by a study that examines the temperature-dependence of gate leakage currents in these devices. By demonstrating that gate leakage decreases with increasing temperature, for T < 357K, a study could prove that the gate leakage was caused via trap-assisted tunneling. This proof stems from the fact that the trap concentrations decrease with increasing temperature (they anneal) causing a reduction in trap-assisted tunneling current. For temperatures greater than 357K, it is known that temperature-assisted tunneling becomes the dominant leakage mechanism causing the total gate leakage current to increase [33].

The opposition between the two possibilities that relate to the explanation of the second radiation effect (labeled (a) and (b) above) can be resolved through simple pre- and post-irradiation, low-temperature, C-V measurements. These measurements would show either an increase in 2DEG concentration or no change at all. Additionally, an experiment that monitors a wider range of gate voltage *I-V* curves (including a cut-off curve and maximum curve without distortion) would most certainly shed some light onto

the mechanism that causes the drain current increase. For example, if post-irradiation, LiN temperature data of the highest pre-irradiation non-distorted *I-V* curve (the *I-V* curve that is associated with the transistor's maximum gate voltage without distortion - see discussion at bottom of page 45) is plotted and shows a new, higher, non-distorted *I-V* curve, the explanation involving an increase in the 2DEG carrier concentration caused by a virtual gate voltage would be invalidated. This is because it is known that *I-V* curves for these transistors with $V_G > 0.5$ V become distorted. Thus, if a transistor was operated at LiN temperatures following irradiation and electron irradiation caused a virtual gate effect which increased the total gate voltage, the *I-V* curve for $V_G = 0.5$ V would have to become distorted because the total gate voltage would be greater than 0.5 V.

Another important question that was not answered relates to the long-term stability of the radiation effects at low temperatures. An experiment in which a transistor was irradiated (at LiN temperatures) and then operated periodically (remaining at LiN temperatures) over several hours (constant operation is discouraged because it would inherently alter device operation) might show a slow degradation of these effects.

Finally, it was never determined in the course of this effort, the radiation dose that causes the initial increase in the gate and drain currents. A dose sensitivity study would be extremely useful for determining this dose. Furthermore, such a study could be extended to pursue an upper dose level that causes drain current reduction for the device. Both low and high dose information would prove extremely insightful as research on the nature of these transistors continues. This specific research effort could be further enhanced by energy-dependent measurements over the range 0.4 – 1.8 MeV.

Appendix A – TIGER Code Simulations

The TIGER Code software package includes a host of radiation effects modeling programs. The two components utilized in this research were the XGEN program and the TIGER ITS program. The XGEN program takes a user-defined input deck and returns radiation interaction information on the materials included in the input deck. The following is one example of an input deck used to run the XGEN program for this specific research problem. Part of the information gained from the use of this input deck was plotted in Figure 12 and Figure 13. Notice the correspondence between the layering of the materials and the layout of the transistors as shown in Figure 17.

```
////////////
```

1.2 MEV P-CODE CROSS SECTIONS FOR
Ni/Au/Ti/Al/Ni/Au/Al(0.27)Ga(0.73)N/GaN/SiC

////////////

Because the research consisted of irradiations at different energies, the TIGER ITS codes had to be run more than once. Furthermore, Figure 17 indicates that there are three different paths an electron might take to impact the transistor's conduction channel. One path takes electrons through the Gate and Ohmic Metals (source and drain) and into the $Al_{0.27}Ga_{0.73}N$ region. Another path takes electrons through only the Gate Metal (this is the gate itself) before entering the $Al_{0.27}Ga_{0.73}N$ region. Finally, a third path takes electrons straight into the $Al_{0.27}Ga_{0.73}N$ region (between the source and gate or between the drain and gate). Consequently, the TIGER ITS codes were run a total of nine times in an attempt to paint a complete picture of the radiation interactions. The following graphs (Figure 50 through Figure 58) show the results of these simulations and provide some insight as to where energy is deposited as well as what incident energies deposit the greatest amount of energy. The last two graphs (Figure 59 and Figure 60) are intended to show the dose deposited across the 2DEG.

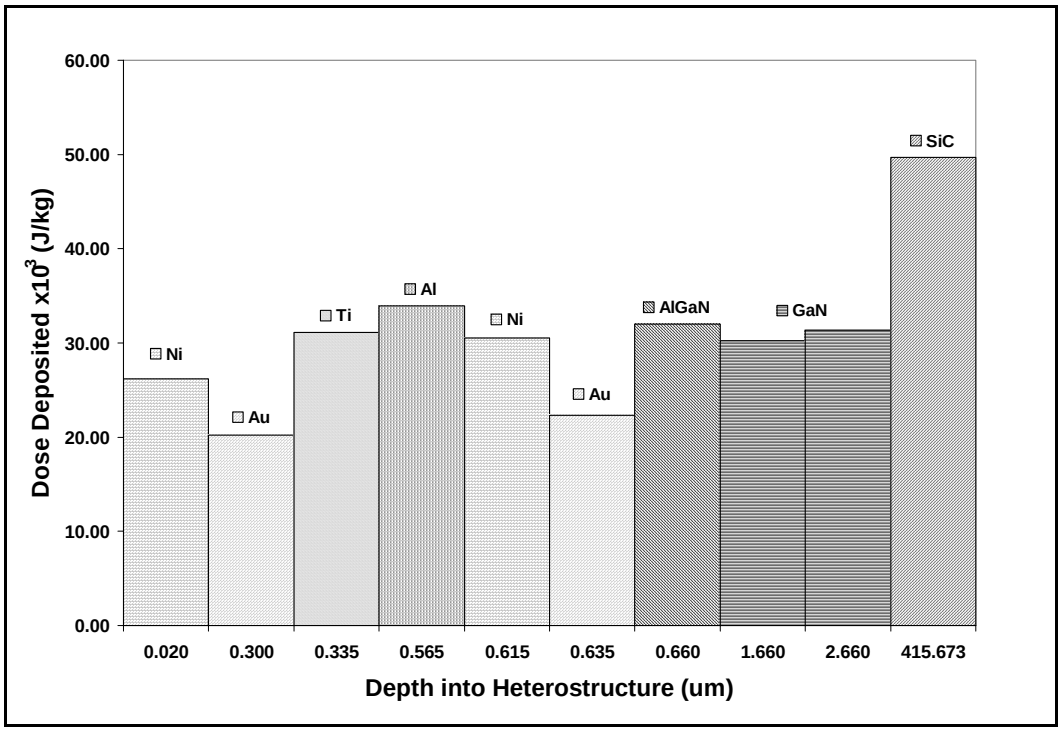

Figure 50. Dose Deposited in Source and Drain Regions by 10^{14} e^-/cm^2 (0.45 MeV)

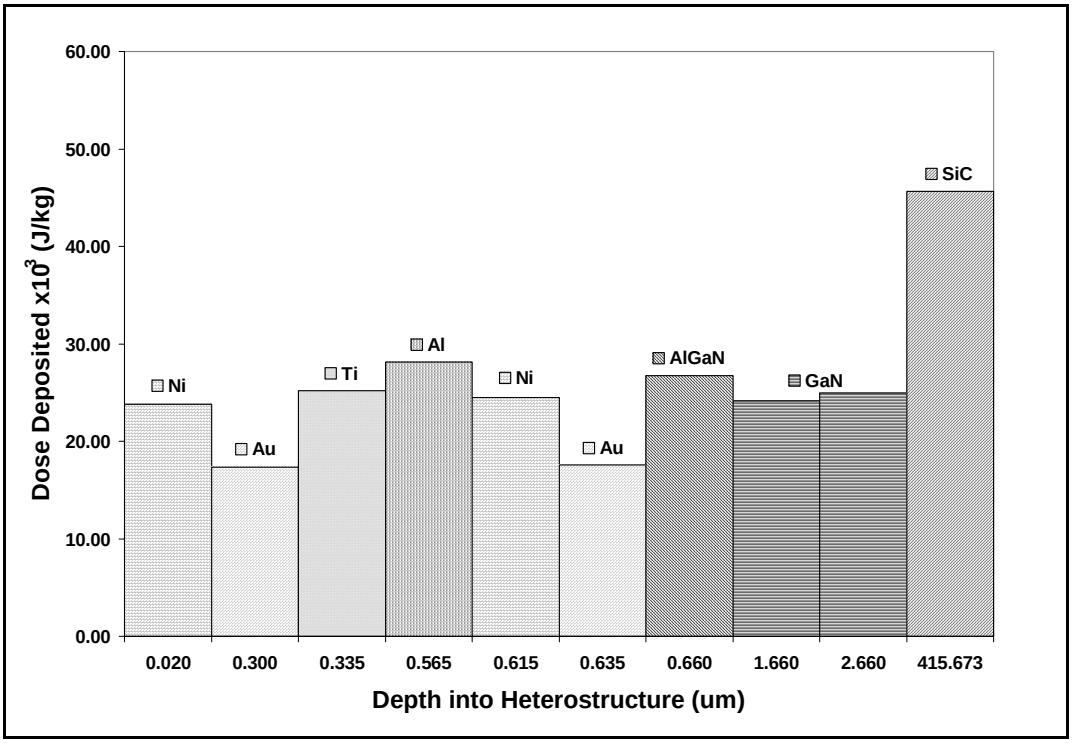

Figure 51. Dose Deposited in Source and Drain Regions by 10^{14} e^-/cm^2 (0.8 MeV)

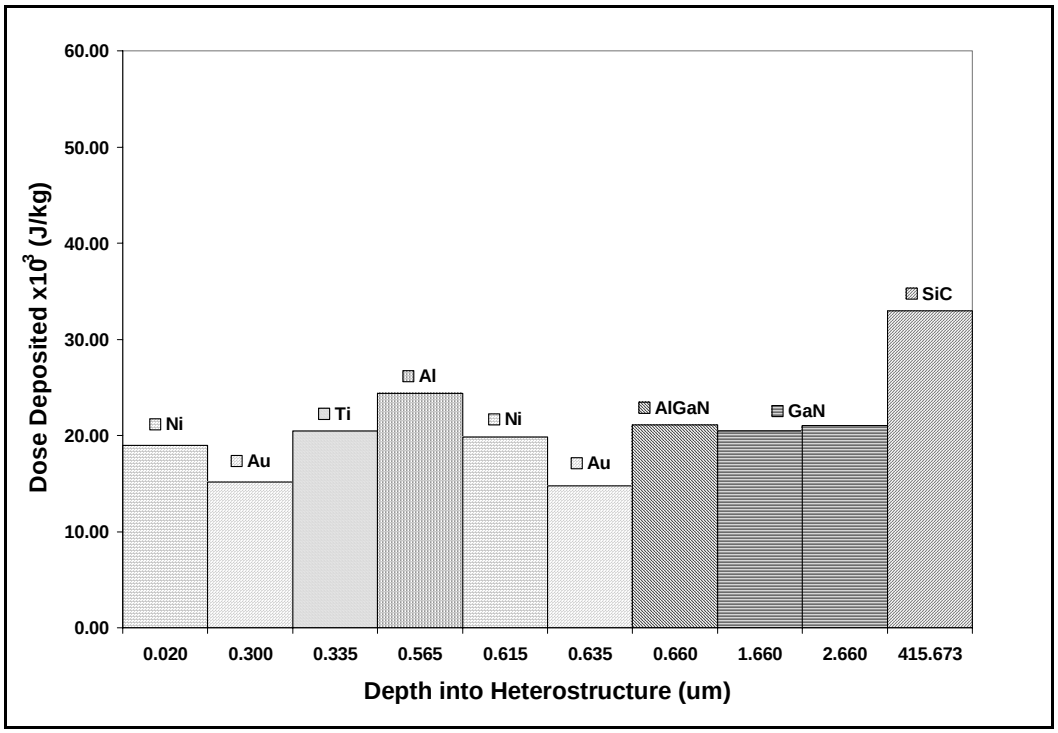

Figure 52. Dose Deposited in Source and Drain Regions by 10^{14} e^-/cm^2 (1.2 MeV)

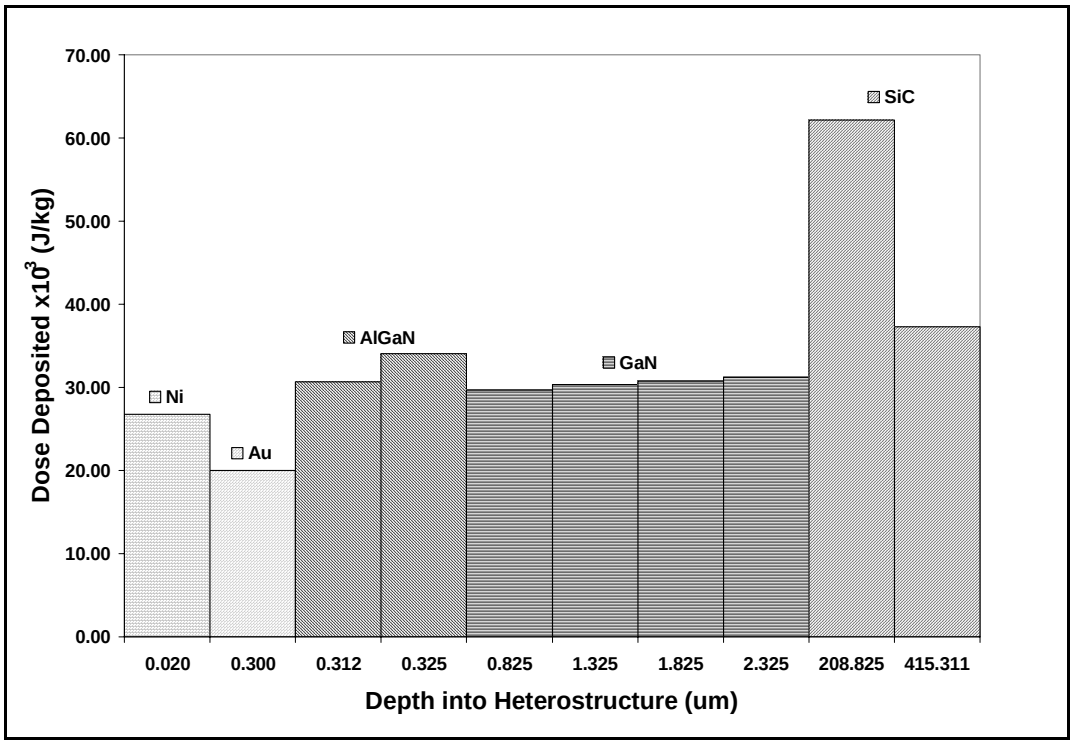

Figure 53. Dose Deposited in Gate Region by 10^{14} e^-/cm^2 (0.45 MeV)

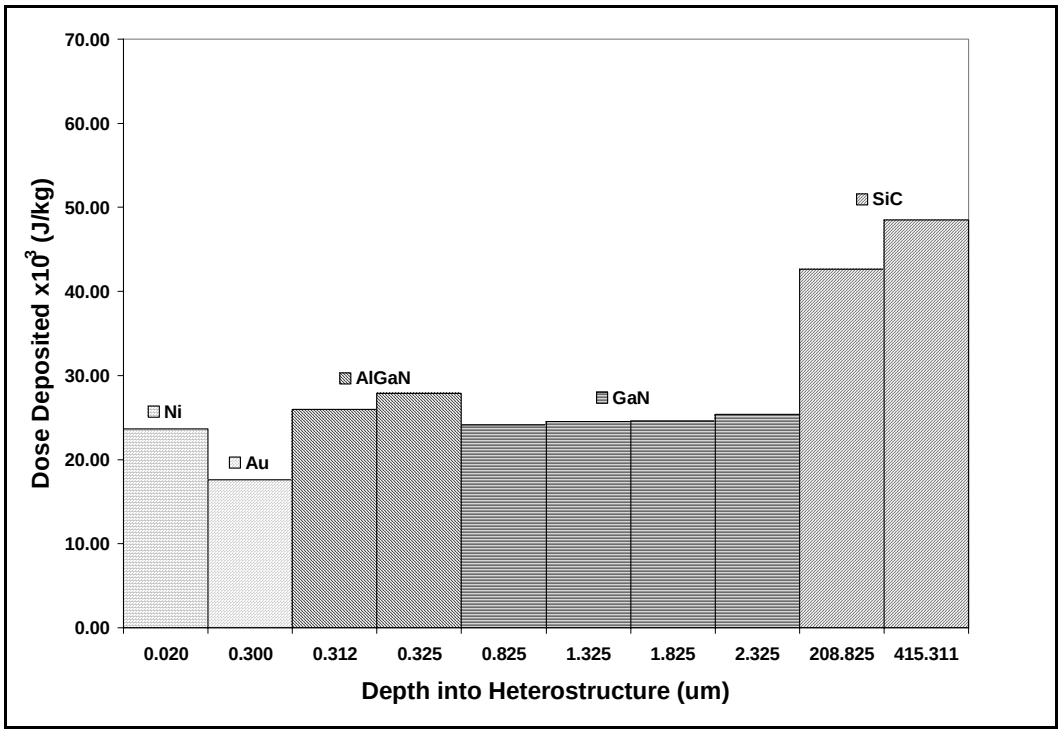

Figure 54. Dose Deposited in Gate Region by 10^{14} e^-/cm^2 (0.8 MeV)

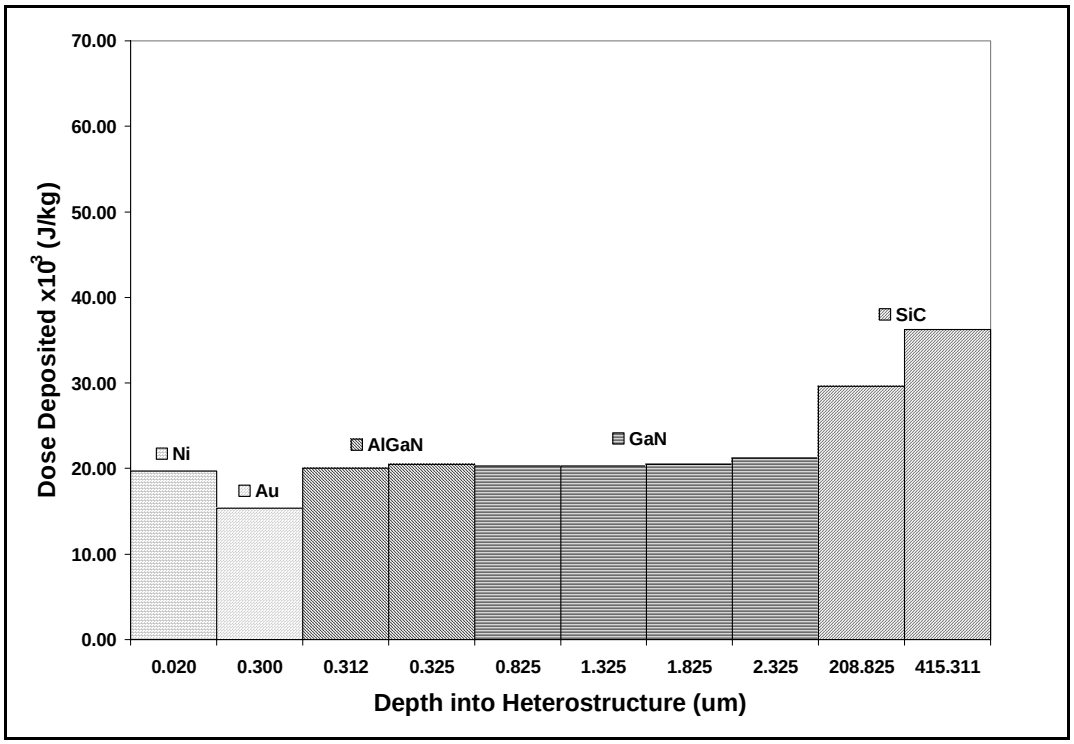

Figure 55. Dose Deposited in Gate Region by 10^{14} e^-/cm^2 (1.2 MeV)

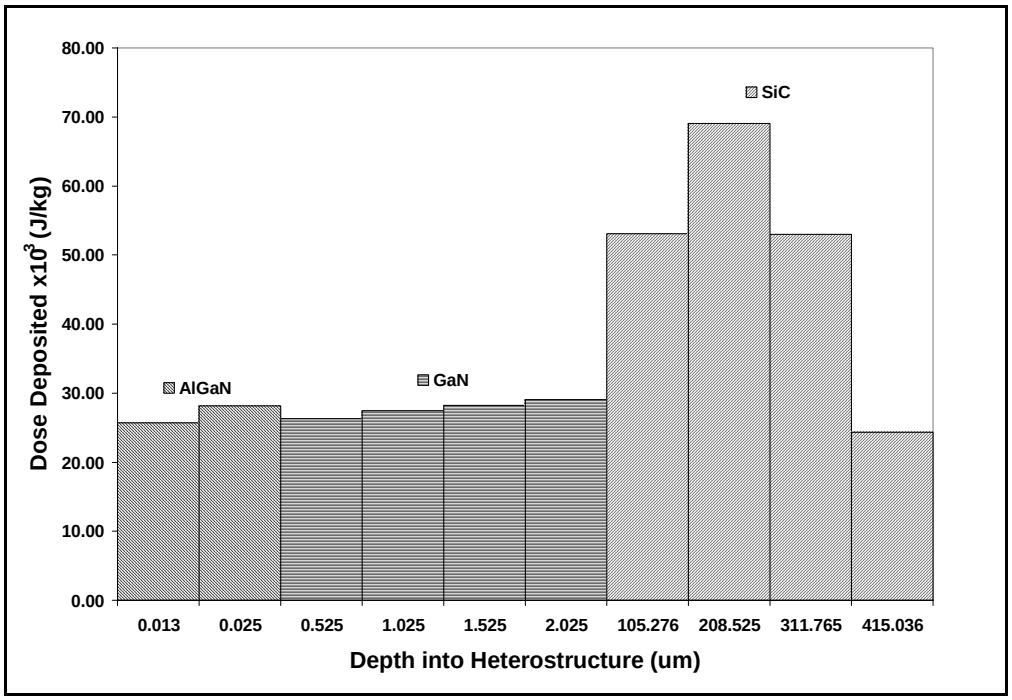

Figure 56. Dose Deposited in Region Between Source and Gate or Drain and Gate by 10^{14} e^-/cm^2 (0.45 MeV)

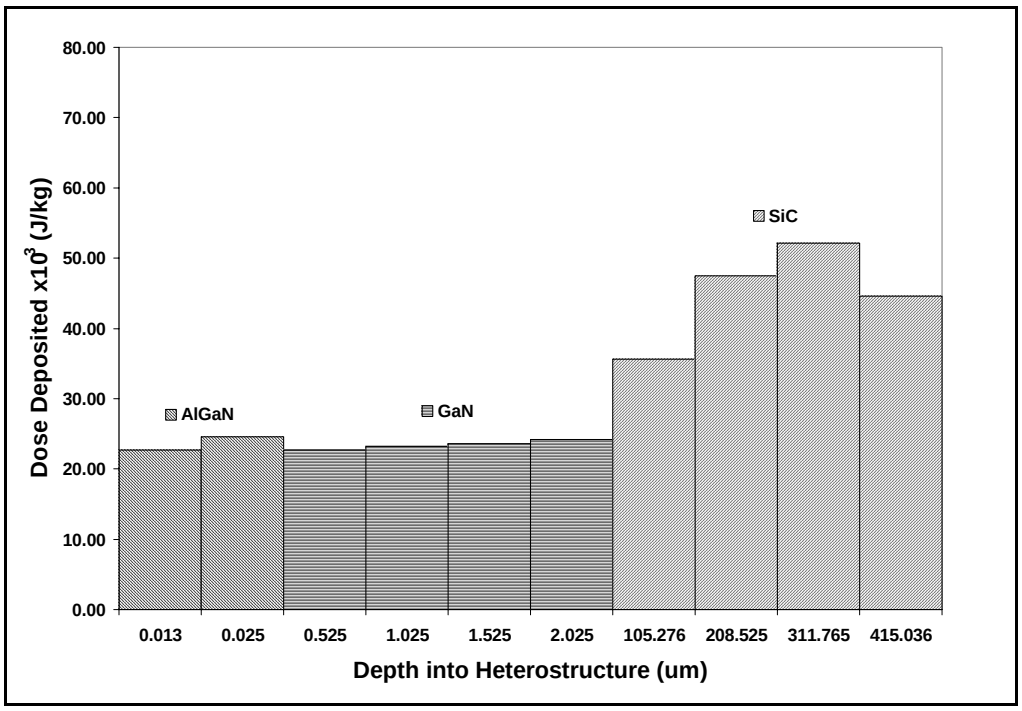

Figure 57. Dose Deposited in Region Between Source and Gate or Drain and Gate by 10^{14} e^-/cm^2 (0.8 MeV)

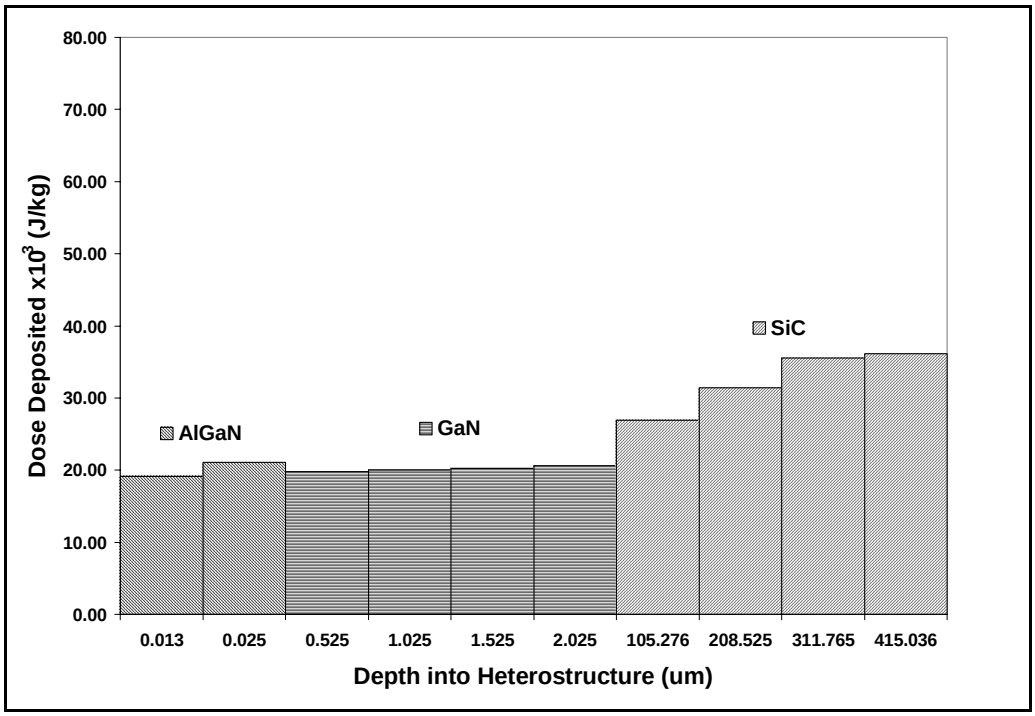

Figure 58. Dose Deposited in Region Between Source and Gate or Drain and Gate by 10^{14} e^-/cm^2 (1.2 MeV)

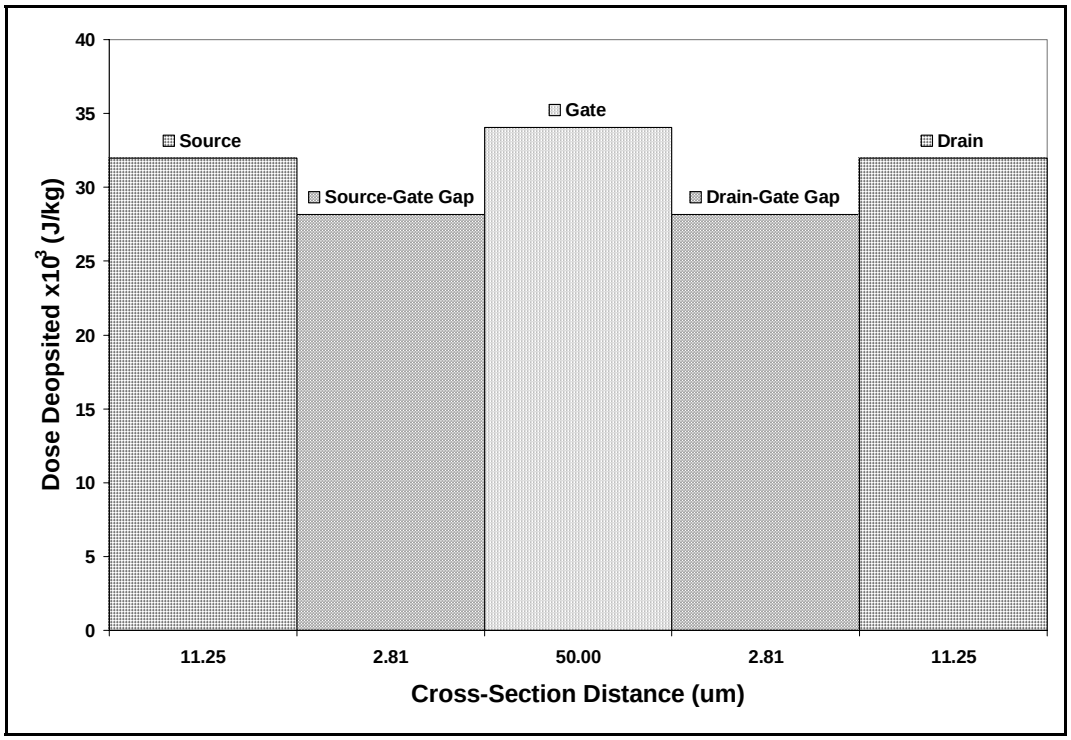

Figure 59. Dose Deposited in $Al_{0.27}Ga_{0.73}N$ Region Along the 2DEG (0.45 MeV)

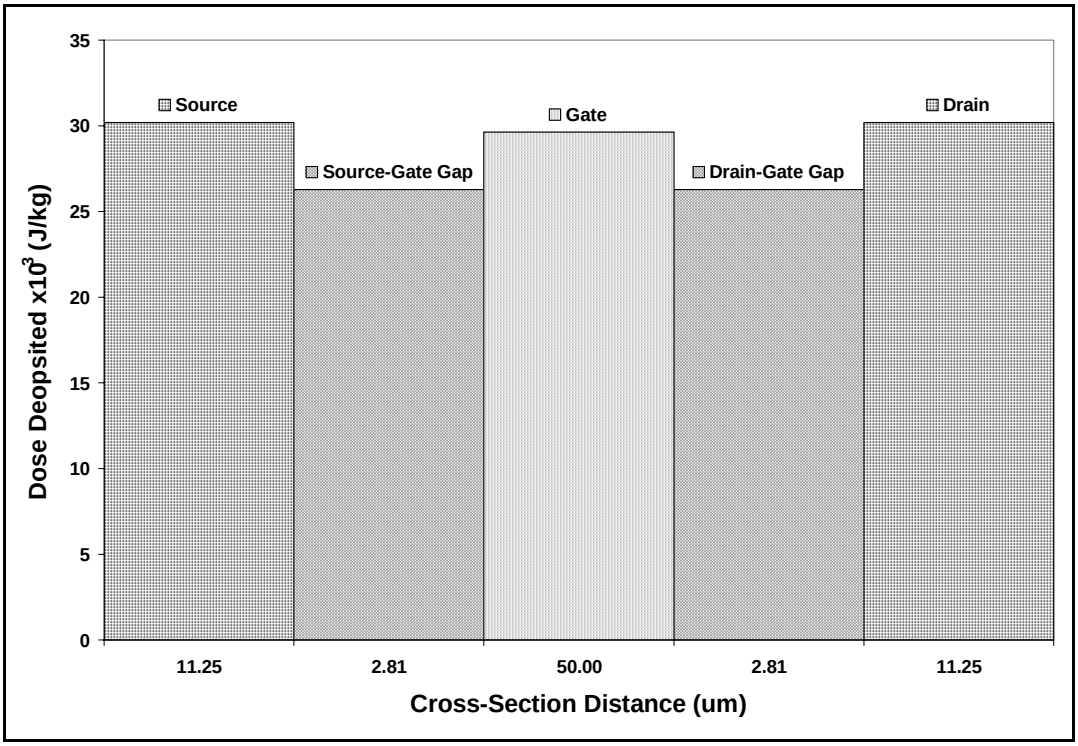

Figure 60. Dose Deposited in GaN Region Along the 2DEG (0.45 MeV)

Appendix B – Visual Basic Data Acquisition Program

The following program was used to characterize and test the transistors in addition to recording drain and gate currents during all six irradiation experiments. It was also used for sample testing and pre-characterization. Underlined text represents program documentation. Entire lines of '/' are provided to distinguish different program modules.

```
Author: James Sattler
Program: Thesis IV
Created: 01 December 2003
Description: Program used to run two Keithley SMUs that in-turn operate a single
transistor. Each Keithley SMUs is responsible for obtaining a current readout
from the transistor. The SMU running the gate voltage reads the gate current;
the SMU running the drain voltage reads the drain current.

////////////
```

```
StopVgBox.Text = "-3.0"
StepVgBox.Text = "-1.0"

Gate/Drain Voltage Label
Vglabel.Caption = "--"
Vdlabel.Caption = "--"
Temperature Label
tempClabel.Caption = "--"
tempKlabel.Caption = "--"
tempFlabel.Caption = "--"

Cycle Label
cyclelabel.Caption = "--"

Time Label
hrslabel.Caption = "--"
minlabel.Caption = "--"
seclabel.Caption = "--"

Comment Box
CommentBox.Text = "No File Comments"

Info Frame
FileLocLbl.Caption = "C:\Documents and
        Settings\user\Desktop\AFIT\Thesis\Data\Keithley Measurments\Raw Data Files"
ChDir FileLocLbl.Caption

Setup GPIB
GPIBDrain.Write ("X")
GPIBGate.Write ("X")
End Sub

////////////
```

```
Private Sub DirSetup()

Dim today As String
Dim dirExist As String
today = Format(Now, "mmddyy")            String of Today's Date
dirExist = Dir(today, vbDirectory)       Check that directory exist

If (Len(dirExist) = 0) Then              If not, create it
   MkDir today
End If

ChDir today
End Sub

////////////
```

```
Record the start time of the experiment
starttime = Format(Now, "hh.mm.ss")
starthrs = Hour(starttime)
startmin = Minute(starttime)
startsec = Second(starttime)
startsumsec = startsec + (60 * startmin) + (60 * 60 * starthrs)

Initialize temperature timer to record temperatures every second
TempTimer.Interval = 1000
TempTimer.Enabled = True

Set up Drain Voltage
GPIBDrain.Write "F0,0X"       DC type measure
GPIBDrain.Write ("P4X")       16 Sample Filter
GPIBDrain.Write ("L100,0X")   Auto Compliance
GPIBDrain.Write "G4,0,0X"     Format Output

Set up Gate Voltage
GPIBGate.Write "F0,0X"       DC type measure
GPIBGate.Write ("P4X")       16 Sample Filter
GPIBGate.Write ("L100,0X")   Auto Compliance
GPIBGate.Write "G4,0,0X"     Format Output

Open I-V Data File
IVFileName = Format(Now, "hh.mm.ss") & "I-V.txt"
Open IVFileName For Output As #1

Write I-V Data File Header
Print #1, IVFileName
Print #1, CommentBox.Text
Print #1,
Print #1, "Cycle Time Temp Vg   Vd   Id       Ig"

Take First Set of Measurements
cycle = 1
Call RecordData
duration = DurationBox.Text

Loop for desired experiment duration
While (elapsedtime < duration)
   cycle = cycle + 1

   Call RecordData           Record!!!

   Close #1
   Open IVFileName For Append As #1

Wend
Panel.Refresh
Close #1
End Sub
```

////////////

```
Private Sub RecordData()

Dim Vg As Single
Dim Vd As Single
Dim Ig As Single
Dim Id As Single
Dim StartVd As Single
Dim StopVd As Single
Dim StepVd As Single
Dim StartVg As Single
Dim StopVg As Single
Dim StepVg As Single
Dim currenttime As String
Dim currenthrs As Long
Dim currentmin As Long
Dim currentsec As Long
Dim currentsumsec As Long
Dim diffsumsec As Integer
Dim totalhrs As Integer
Dim totalmin As Integer
Dim totalsec As Integer
Dim printtime As String


StartVg = StartVgBox.Text
StopVg = StopVgBox.Text
StepVg = StepVgBox.Text
StartVd = StartVdBox.Text
StopVd = StopVdBox.Text
StepVd = StepVdBox.Text


Perform IV Measurements

For Vg = StartVg To StopVg Step StepVg

   GPIBGate.Write ("N1X")       Place Gate SMU in Operate Mode
   GPIBGate.Write ("B" & Vg & ",0,0X")   Turn on Gate Voltage
   GPIBGate.Write "H0X"         Trigger and Execute

   For Vd = StartVd To StopVd Step StepVd

      GPIBDrain.Write ("N1X")       Place Drain SMU in Operate Mode
      GPIBDrain.Write ("B" & Vd & ",0,0X")   Turn on Drain Voltage
      GPIBDrain.Write "H0X"         Trigger and Execute

      printtime = Format(Now, "hh.mm.ss")

      Check the temptimer to read new temperature
      DoEvents

      Id = Mid(GPIBDrain.Read, 6, 12)
      Ig = Mid(GPIBGate.Read, 6, 12)
```

```
        Check the temptimer to read new temperature
        DoEvents

        Print #1, cycle & " " & printtime & " " & FormatNumber(temperature, 1) & " " &
            FormatNumber(Vg, 1) & " " & FormatNumber(Vd, 1) & " " & Id & " " & Ig

        Record current time to determin the total experiment run time
        currenttime = Format(Now, "hh.mm.ss")
        currenthrs = Hour(currenttime)
        currentmin = Minute(currenttime)
        currentsec = Second(currenttime)
        currentsumsec = currentsec + (60 * currentmin) + (60 * 60 * currenthrs)
        diffsumsec = currentsumsec - startsumsec
        totalsec = diffsumsec Mod 60
        totalmin = diffsumsec \ 60
        totalhrs = diffsumsec \ 3600
        elapsedtime = totalmin

        Refresh the Information Panel
        Vglabel.Caption = FormatNumber(Vg, 1)
        Vdlabel.Caption = FormatNumber(Vd, 1)
        cyclelabel.Caption = cycle
        hrslabel.Caption = totalhrs
        minlabel.Caption = totalmin
        seclabel.Caption = totalsec
        Panel.Refresh

    Next Vd

    GPIBGate.Write ("N0X")    Place Gate SMU in Inoperate Mode
    GPIBDrain.Write ("N0X")    Place Drain SMU in Inoperate Mode

Next Vg
End Sub

////////////
```

TempTimer controls how often temperature is updated
It requests an updated temperature from CNi16D Controller, and updates the total amount of elapsed time in seconds of experiment.

```
Private Sub TempTimer_Timer()

   temperature = iDevice.MainReading            Request Temperature Reading

End Sub
```

Appendix C – Experimentally Induced MODFET Damage

As previously indicated, all four FatFETs from the first irradiation experiment were destroyed by the experiments themselves. In addition, a curiously similar effect was observed following the second irradiation experiment involving the same transistor on both A0408 and A0409. The following evidence is presented to better explain these occurrences.

Figure 61 through Figure 64 visually explain why the FatFETs from the first four irradiation experiments broke. All four of these figures show a severed drain contact at approximately the same location on the transistors. Interestingly enough, this location happens to be at the mesa edge of the FatFET. From Figure 16 we know that the mesa edge at the drain contact is a boundary between a Gate Metal region and an Ohmic/Gate Metal region. Furthermore, the gate voltage ranged from -3.5 V to 0.5 V in 0.5 V steps and the drain voltage ranged from 0.0 V to 10.0 V in 1.0 V steps for the first irradiation experiment. This indicates that at one point during each data collection cycle, V_G = -3.5 V and V_D = 10.0 V resulting in a 13.5 V potential difference from gate to drain. Although this difference would be insignificant under normal operating conditions, when combined with large amounts of charge collection, it could produce the physical damage shown in Figure 61 through Figure 64.

With the exception of V_G = 0.0 V, and V_G = 0.5 V, the potential difference between the gate and drain was always the highest across any two transistor contacts. Additionally, large amounts of electrical charge were being deposited to the transistor

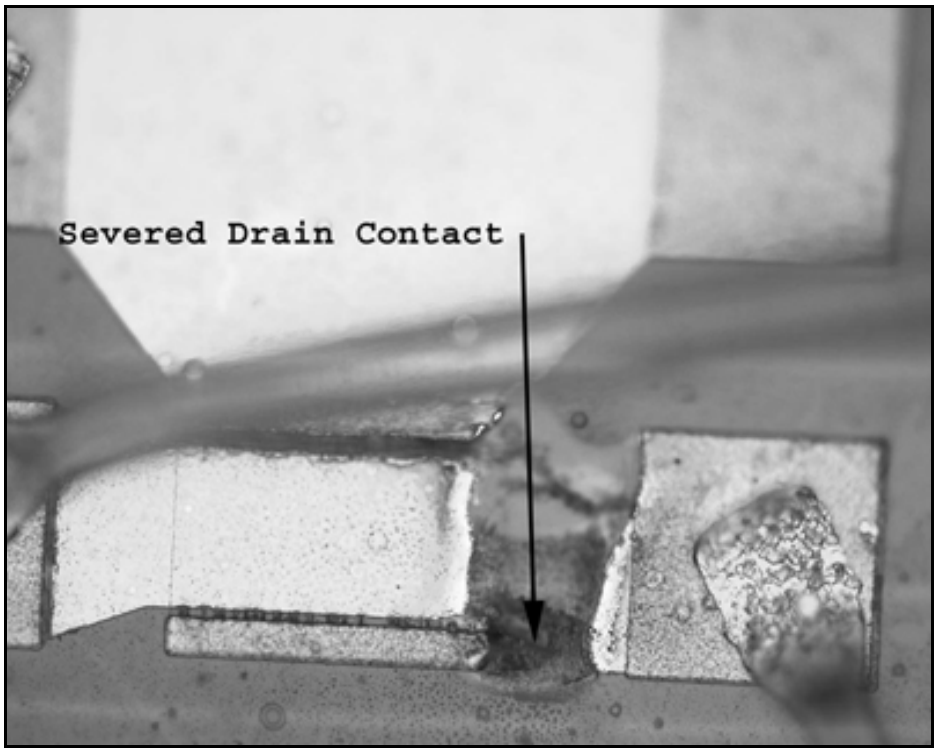

Figure 61. Sample A0313 FatFET Irradiation Experiment Drain Damage

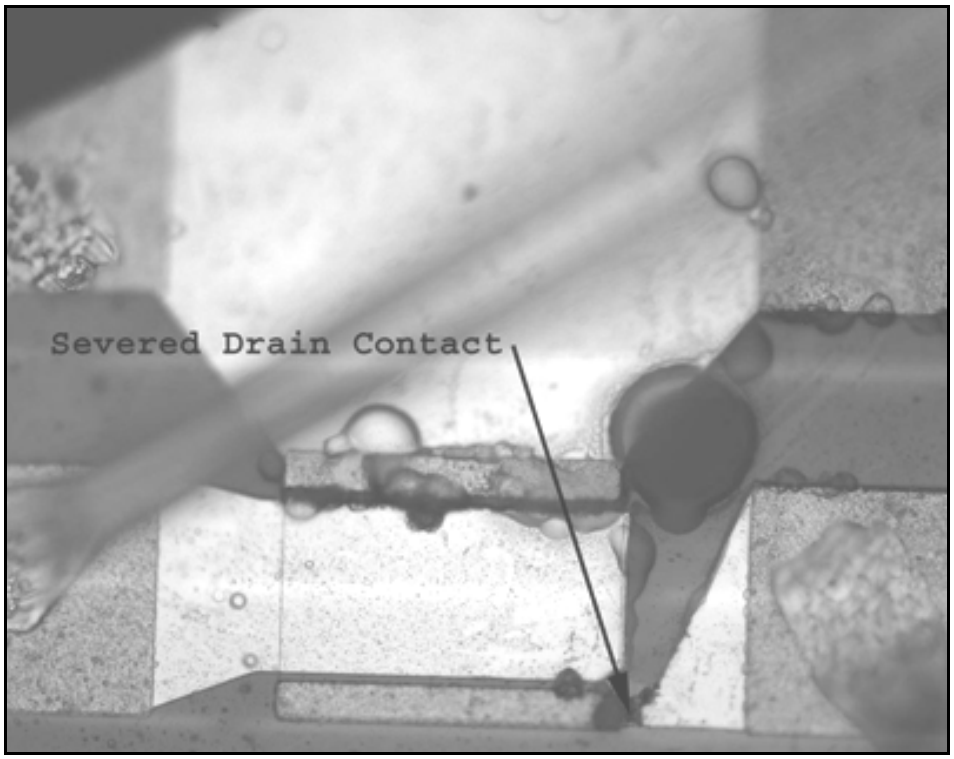

Figure 62. Sample A0314 FatFET Irradiation Experiment Drain Damage

Figure 63. Sample A0315 FatFET Irradiation Experiment Drain Damage

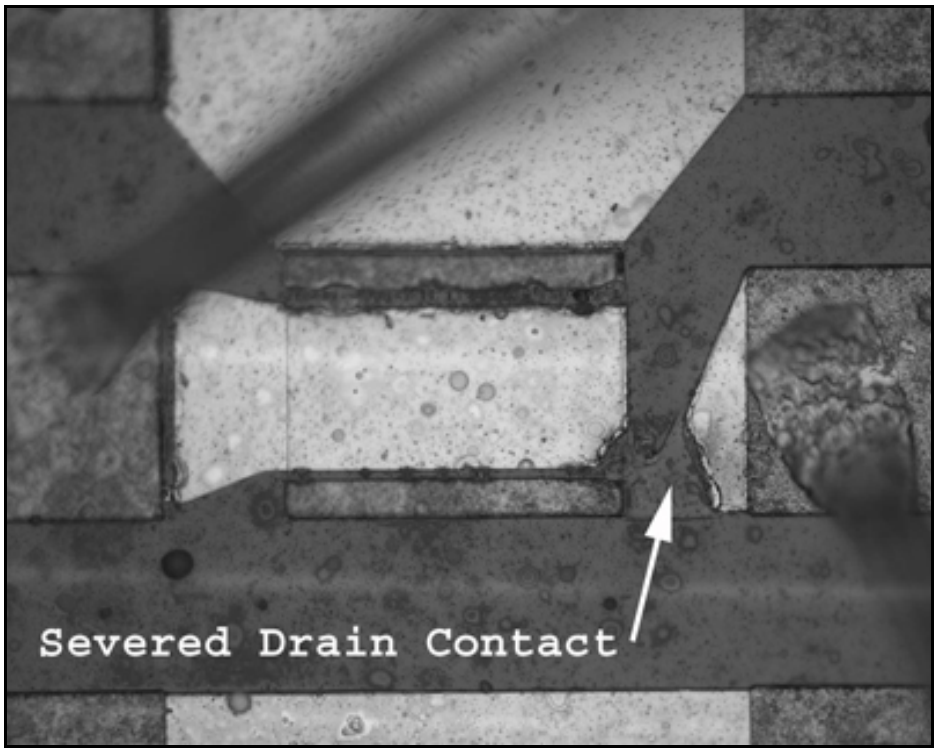

Figure 64. Sample A0316 FatFET Irradiation Experiment Drain Damage

and its leads via the electron beam, throughout the irradiations. Although this charge would be swept out at the source and drain via the large source-drain current, the charge on the gate would be less capable of migrating because the gate is effectively isolated (I_g is small). These two facts lead toward a conclusion that the drain damage was the result of electron beam-induced charge collection on the gate and the resulting discharge from gate to drain. If this discharge delivered a sufficiently high current, the Ohmic or Gate Metals themselves could be subject to damage or even removal from the eptixial layer onto which the metal was deposited.

Immediately following the success of the second irradiation experiment involving samples A0408 and A0409, it was believed that the experiment induced damage seen in the first irradiation experiment was a thing of the past. However, post-irradiation visual inspections of A0408 and A0409 showed two amazingly similar occurrences. Figure 65 shows a picture of the 2X150X1.2A transistor located on sample A0408 prior to irradiation. Figure 66 shows the exact same transistor (as evident by the gate contact scratch imparted by the probe-stand) after irradiation! The destruction imparted this time was not only to the drain contact, but also to both gate contacts. However, once again, the damaged areas are found at the mesa edges indicating a possible structural weakness in the deposited metals near the mesa edges. Most importantly is the fact that, although this transistor was wire-bonded to three pins on the reticle package, those pins were left unconnected during irradiation. Furthermore, Figure 67 and Figure 68 tell the exact same story. Whereas the drain damage involved with the first irradiation experiment could be explained by the operation of the device during irradiation, this new damage to both the

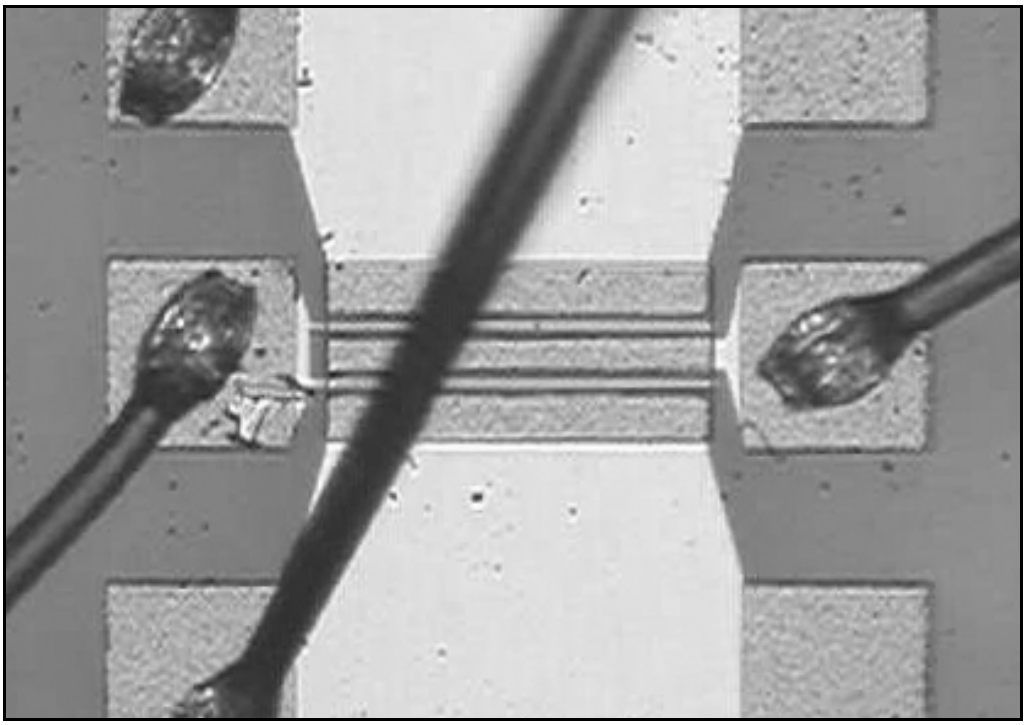

Figure 65. Sample A0408 2X150X1.2A FET Pre-Irradiation Picture

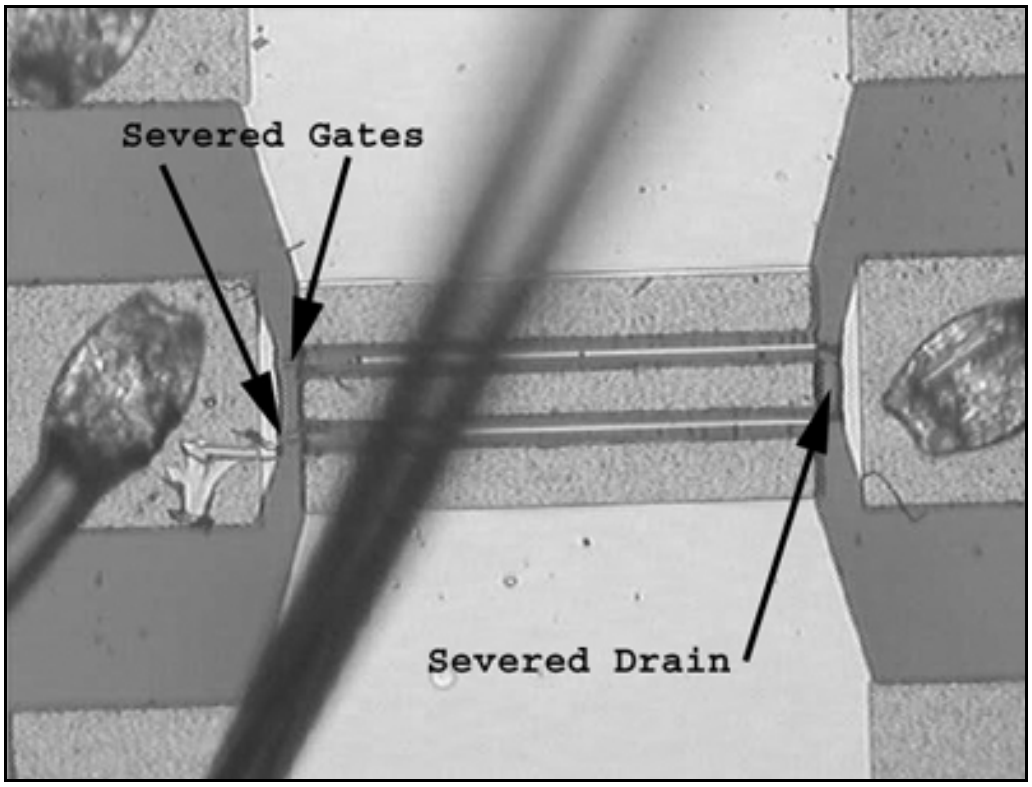

Figure 66. Sample A0408 2X150X1.2A FET Post-Irradiation Experiment Damage

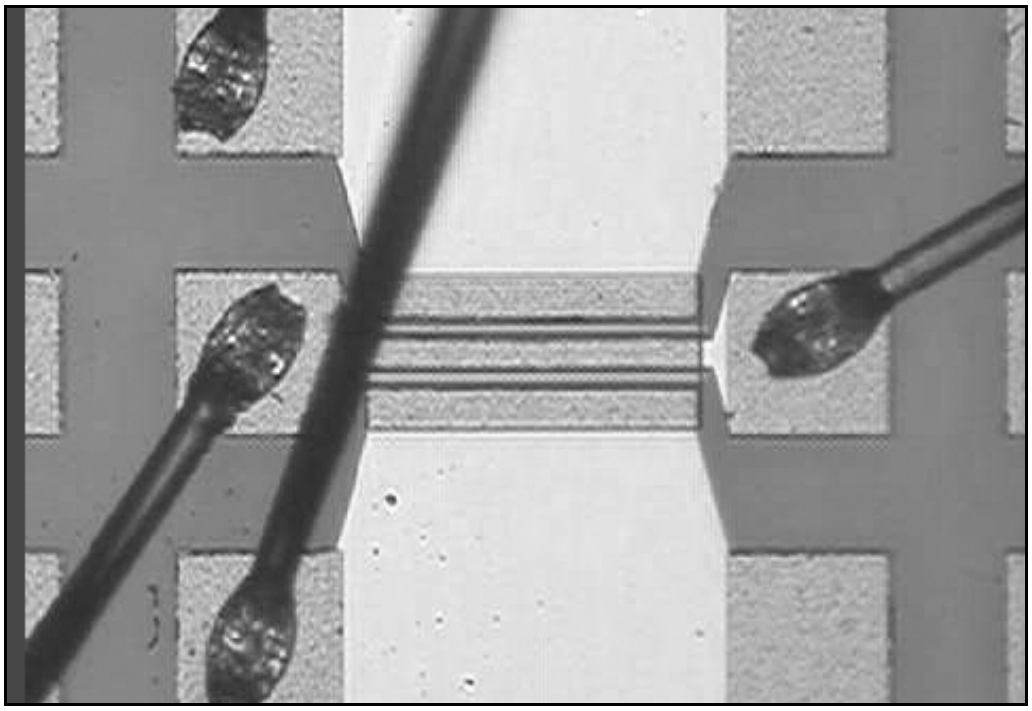

Figure 67. Sample A0409 2X150X1.2A FET Pre-Irradiation Picture

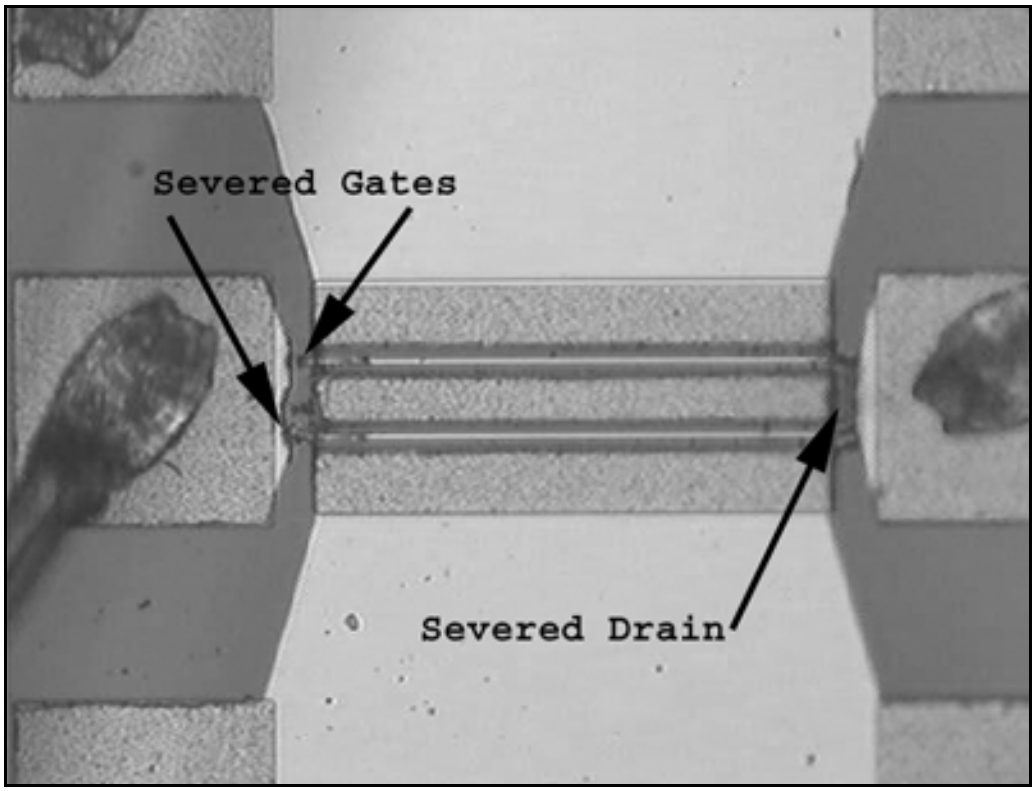

Figure 68. Sample A0409 2X150X1.2A FET Post-Irradiation Experiment Damage

gates and drain must be explained by an alternate theory since these devices were not being operated. Adding to the mystery is the fact that neither FatFET on A0408 or A0409 experienced damage even though they were the only other transistors with wire-bonds.

It would seem safe to conclude that the damage has to be related to these wire-bonds since there was no observable damage imparted to any of the unconnected transistors on all six of the irradiated samples. The only possible theory that might explain the permanent damage observed in all six samples relates to the fact that the package leads connected to the 2X150X1.2A transistors were left floating during irradiation (As stated in the experimental procedures section, the FatFET leads were left connected to the Keithley for Samples A0408 and A0409). It is at least possible that after collecting charge from the electron beam resulting in a potential difference, one of the package leads for the gate or drain came into contact with the cold head metal providing a path through which the drain-gate potential difference could discharge. An instantaneous short between the cold head metal and one of the floating leads is possible because the floating package leads were only a few thousandths of an inch off the metal surface of the cold head. As previously theorized, if the resulting discharge consisted of a sufficiently high current, the Ohmic or Gate Metals could conceivably be damaged or completely removed. One additional experiment that would help to shed some light on this most peculiar of effects, would involve wire-bonding to an assortment of transistors on one reticle and irradiating with the package leads left floating. This experiment would at least help to confirm or deny the appearance that this type of damage is related to wire-bonds.

Appendix D – Additional Experimental Plots

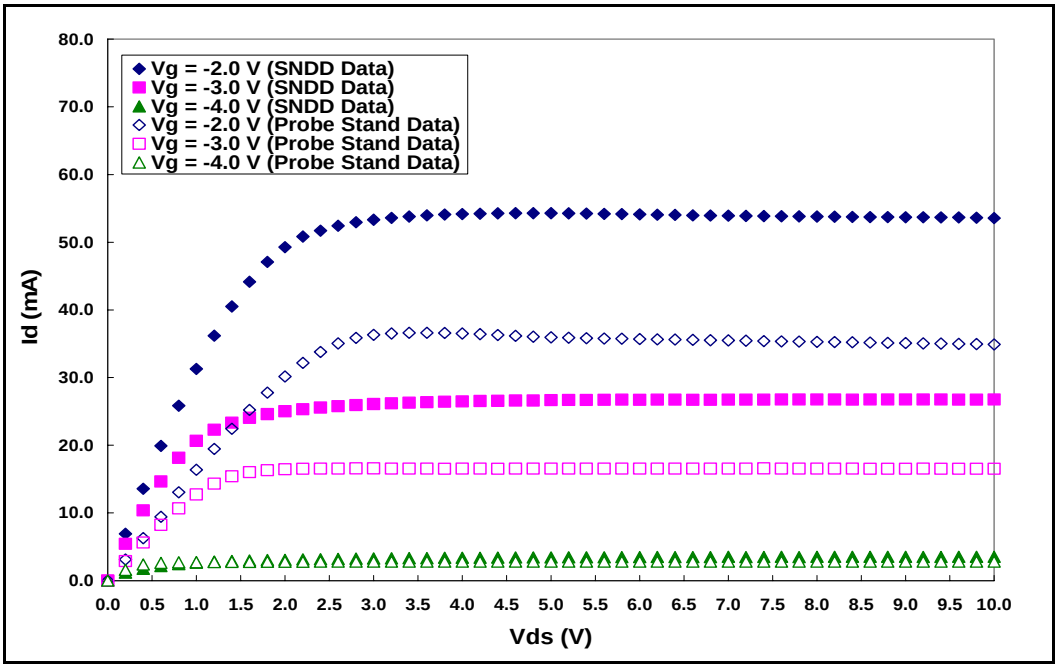

Figure 69. Sample A0408 2X150X1.2 Transistor, SNDD vs. AFIT Room Temperature *I-V* Curves

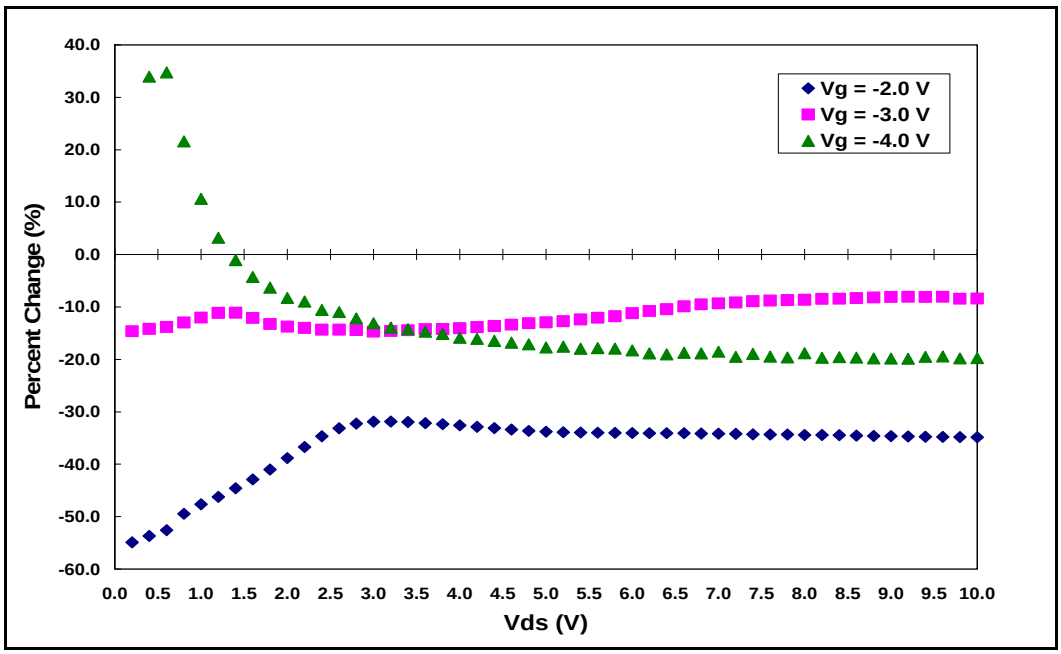

Figure 70. Sample A0408 2X150X1.2 Transistor, Percent Change from SNDD to AFIT Room Temperature *I-V* Curves

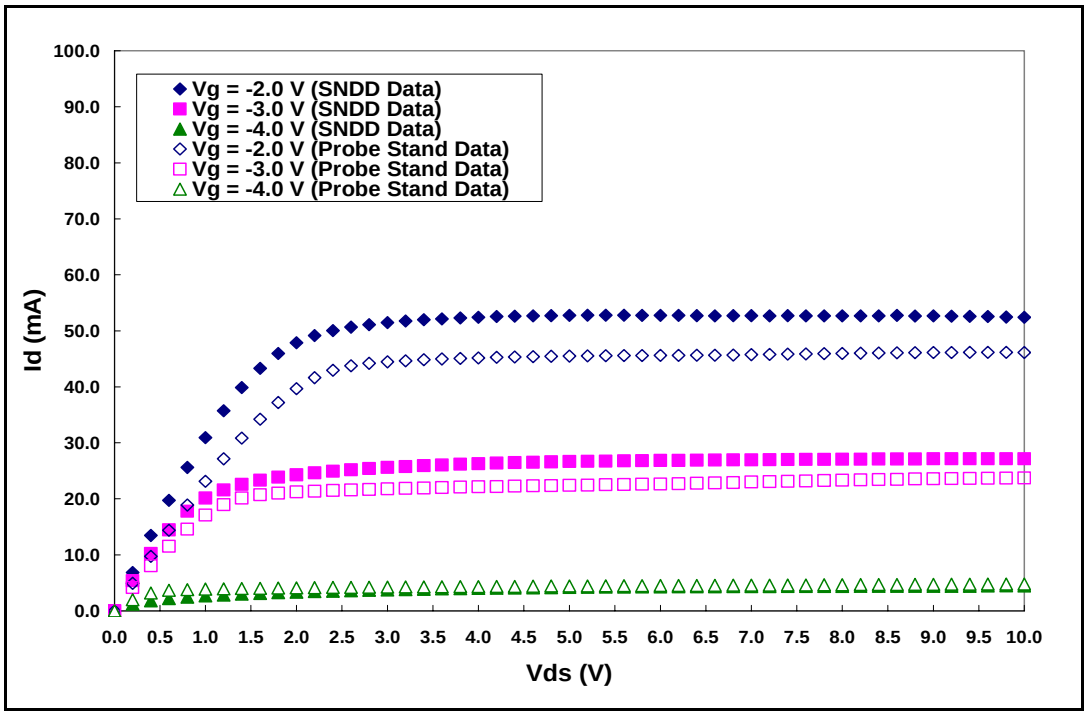

Figure 71. Sample A0409 2X150X1.2 Transistor, SNDD vs. AFIT Room Temperature *I-V* Curves

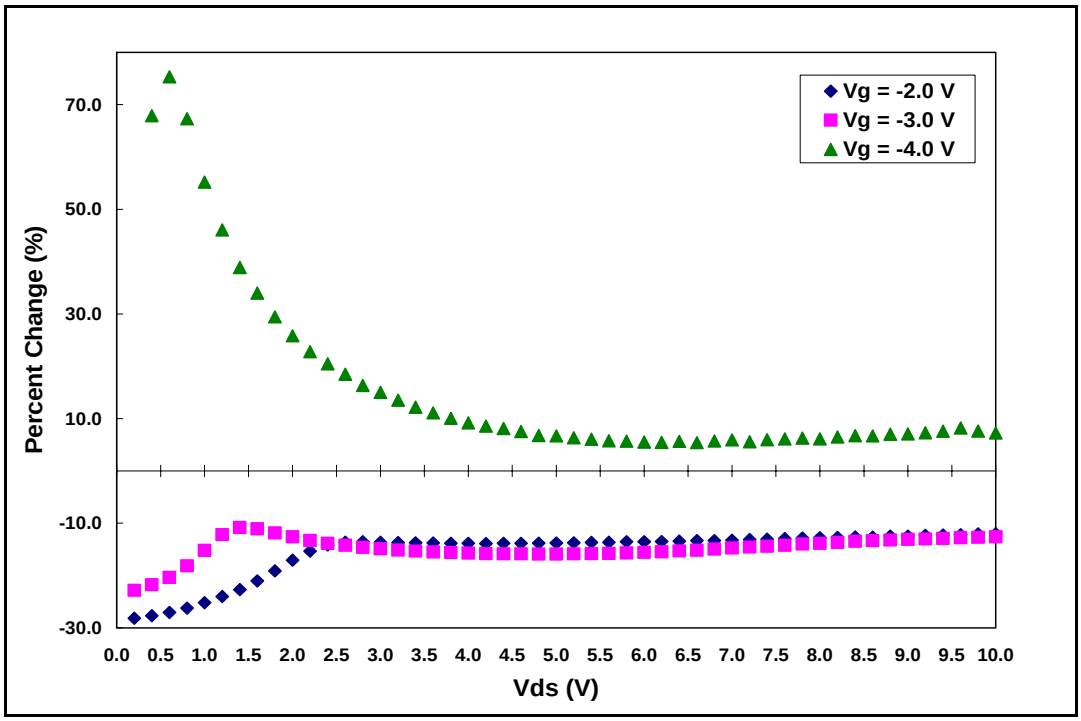

Figure 72. Sample A0409 2X150X1.2 Transistor, Percent Change from SNDD to AFIT Room Temperature *I-V* Curves

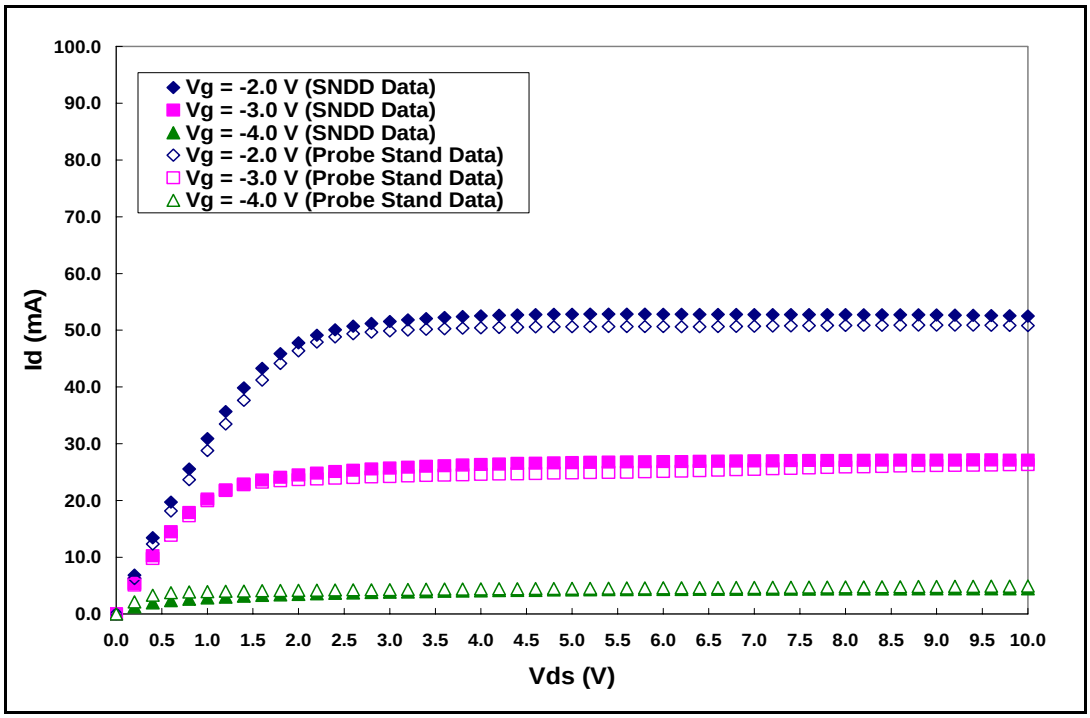

Figure 73. Sample A0411 2X150X1.2 Transistor, SNDD vs. AFIT Room Temperature *I-V* Curves

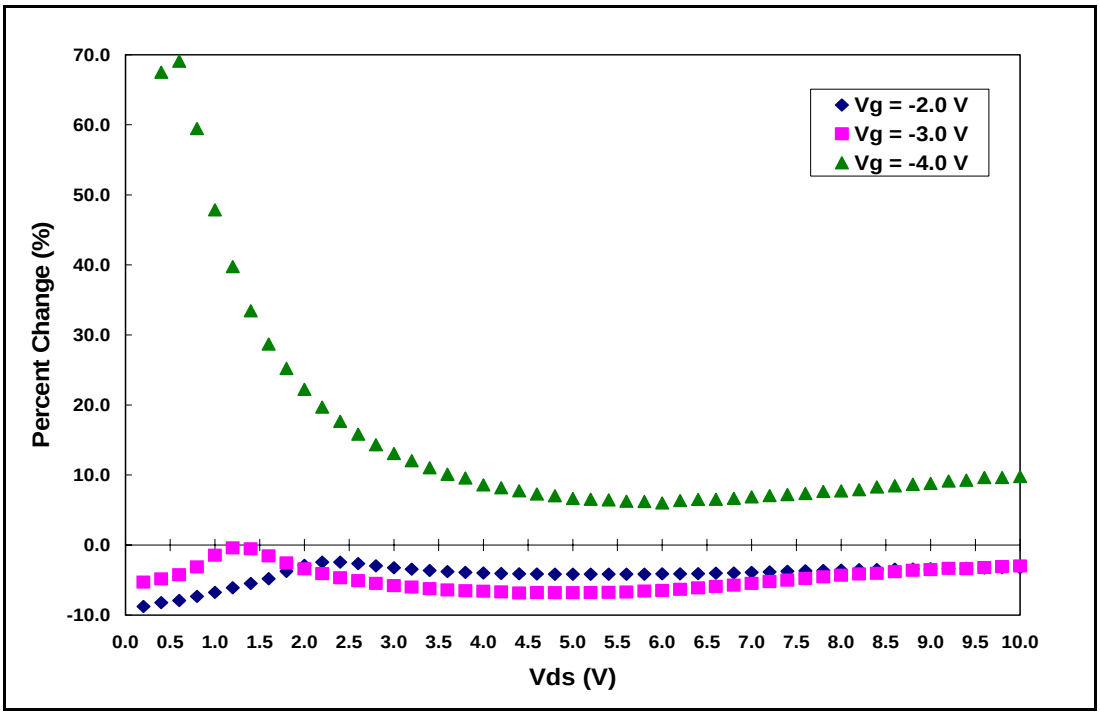

Figure 74. Sample A0411 2X150X1.2 Transistor, Percent Change from SNDD to AFIT Room Temperature *I-V* Curves

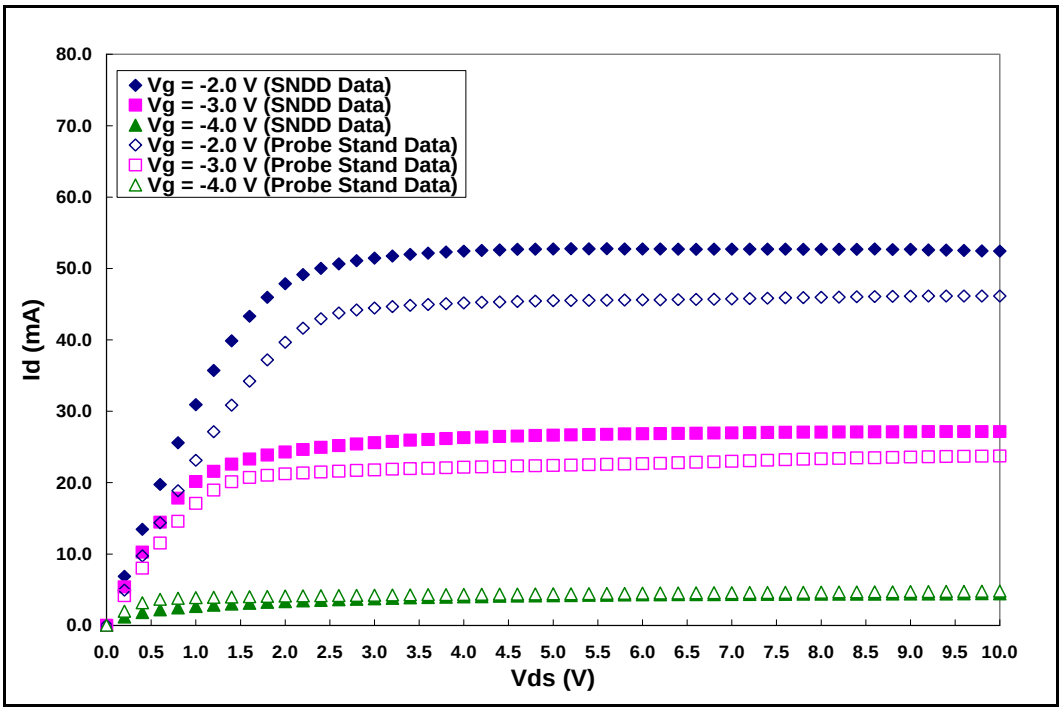

Figure 75. Sample A0412 2X150X1.2 Transistor, SNDD vs. AFIT Room Temperature *I-V* Curves

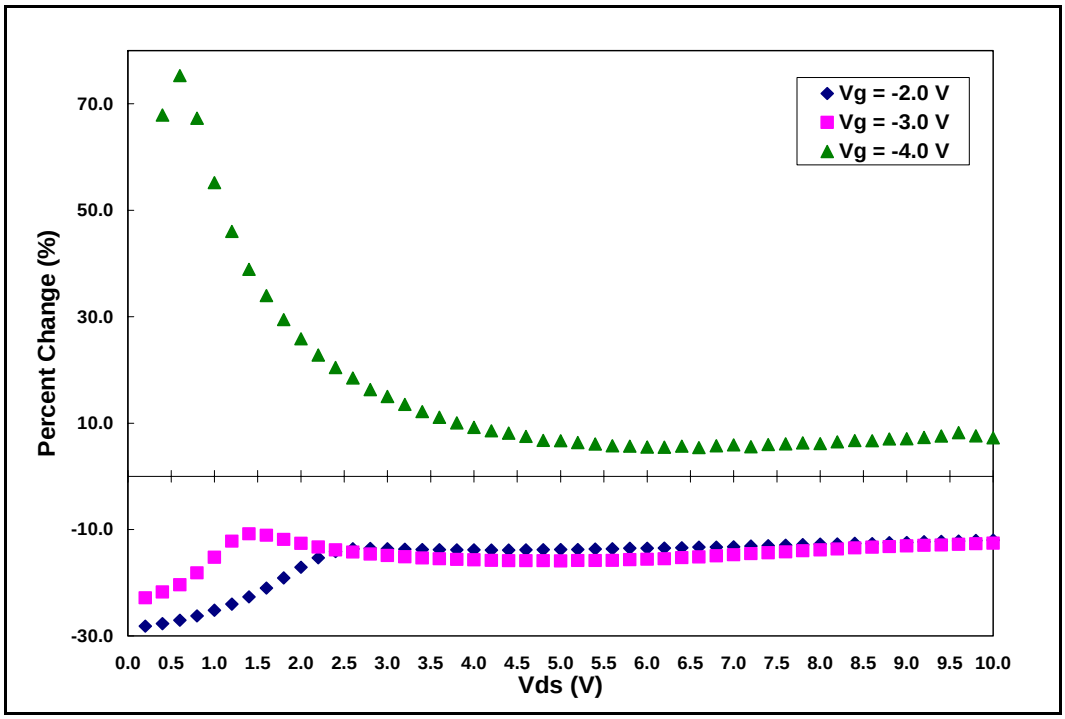

Figure 76. Sample A0412 2X150X1.2 Transistor, Percent Change from SNDD to AFIT Room Temperature *I-V* Curves

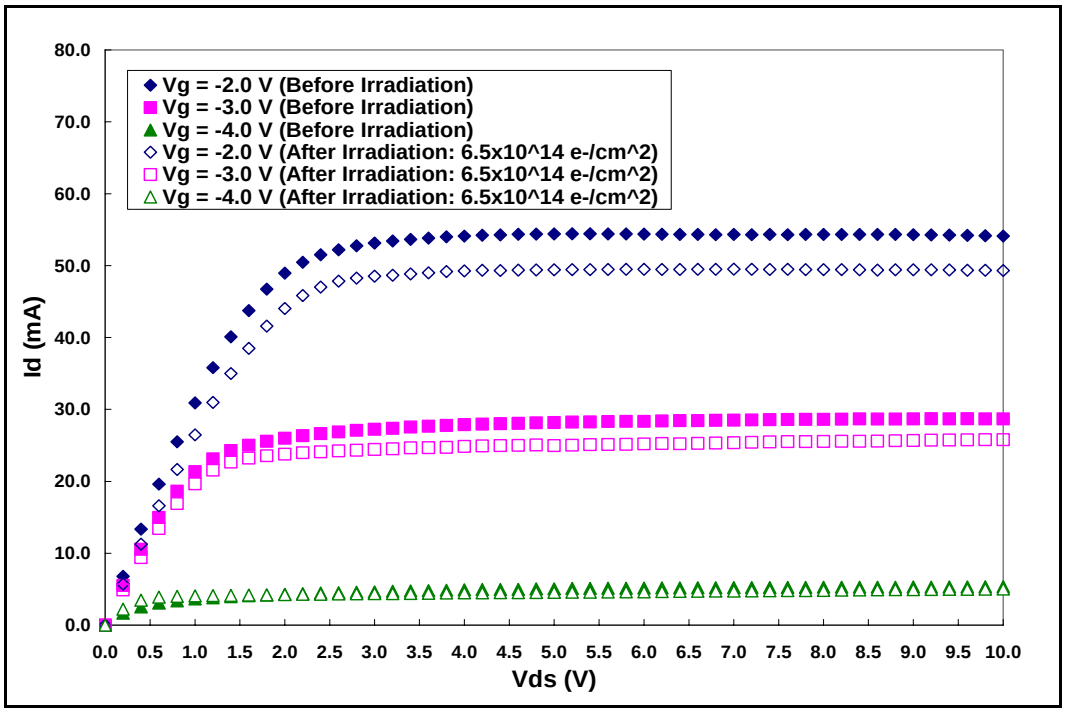

Figure 77. Sample A0314 2X150X1.2 Transistor Pre- and Post-Irradiation Room Temperature *I-V* Curves (0.8 MeV Electrons)

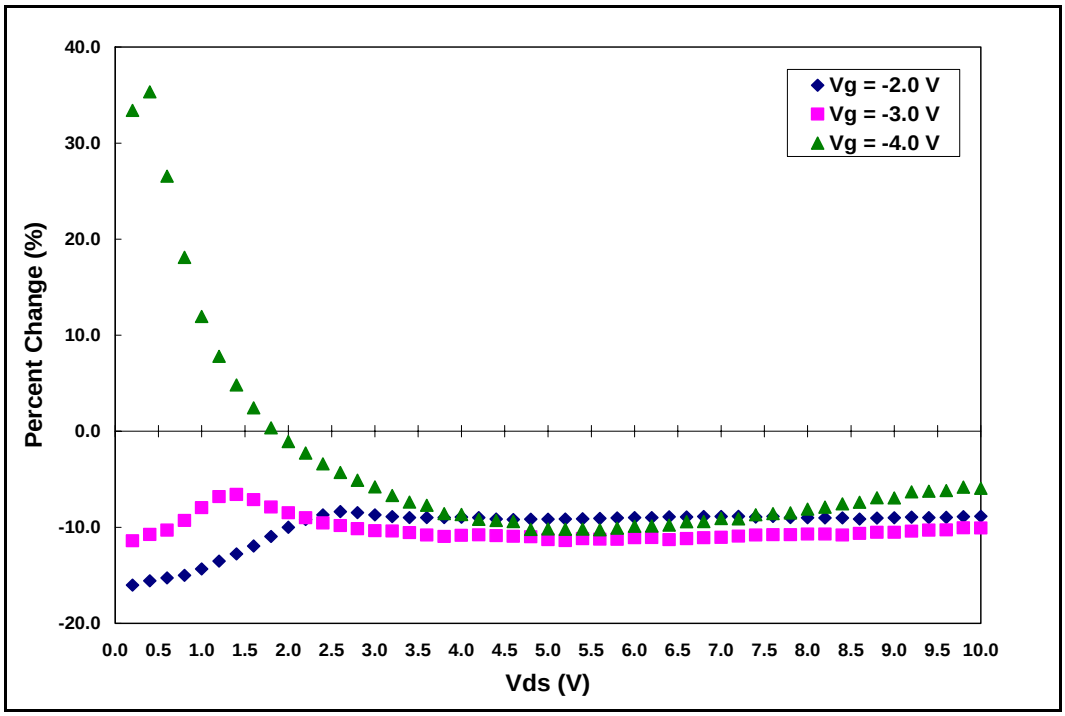

Figure 78. Sample A0314 2X150X1.2 Transistor Percent Change from Pre- to Post-Irradiation Room Temperature *I-V* Plots (0.8 MeV Electrons)

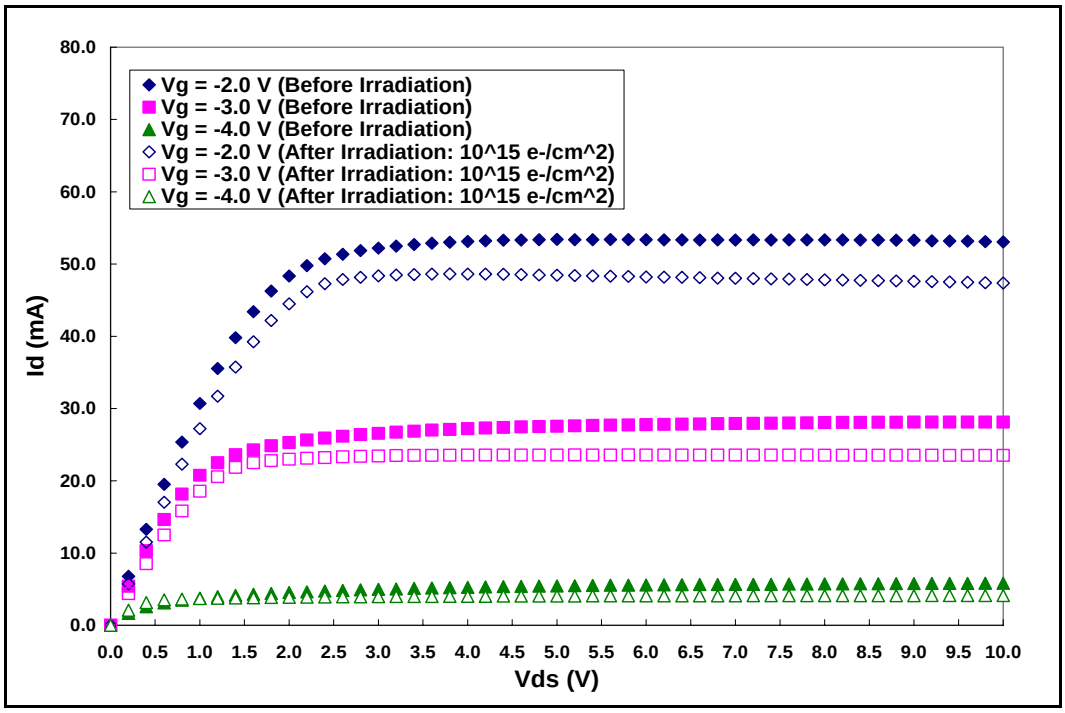

Figure 79. Sample A0315 2X150X1.2 Transistor Pre- and Post-Irradiation Room Temperature *I-V* Curves (0.8 MeV Electrons)

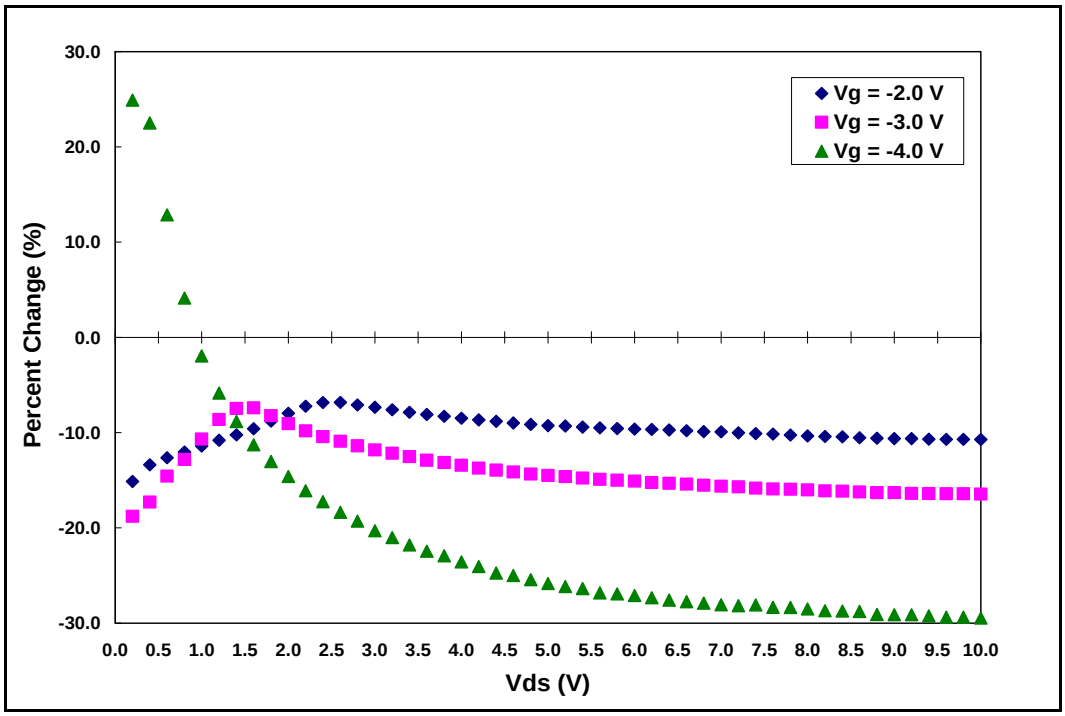

Figure 80. Sample A0315 2X150X1.2 Transistor Percent Change from Pre- to Post-Irradiation Room Temperature *I-V* Plots (0.8 MeV Electrons)

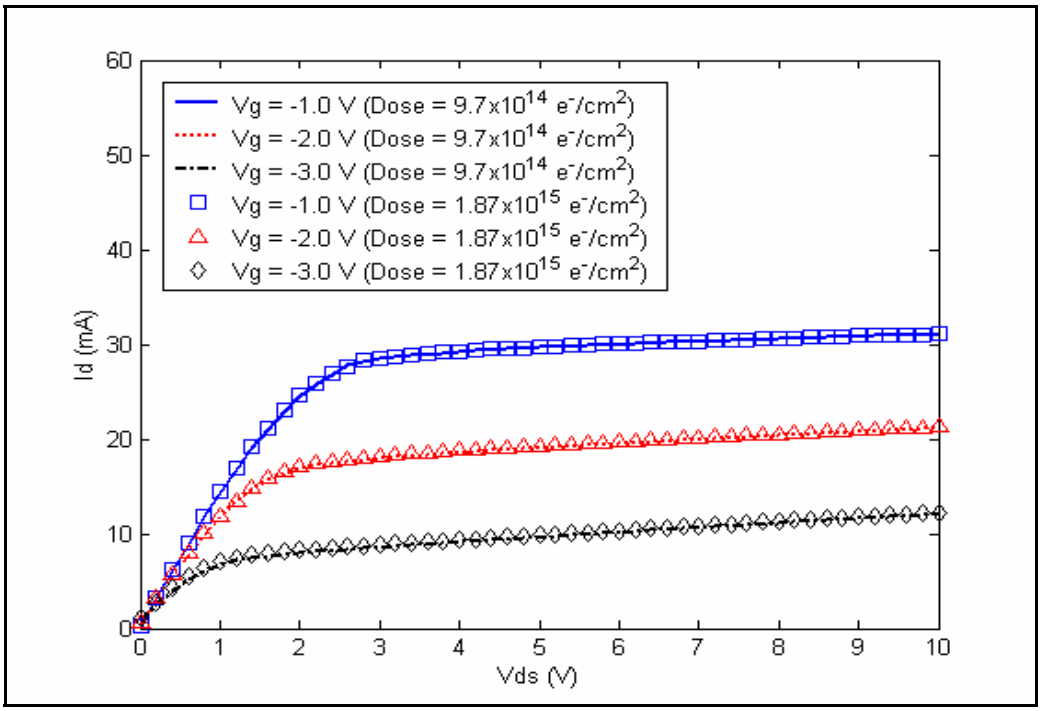

Figure 81. Sample A0409 FatFET Third Irradiation: Change in *I-V* Curves at LiN Temperature (0.45 MeV Electrons)

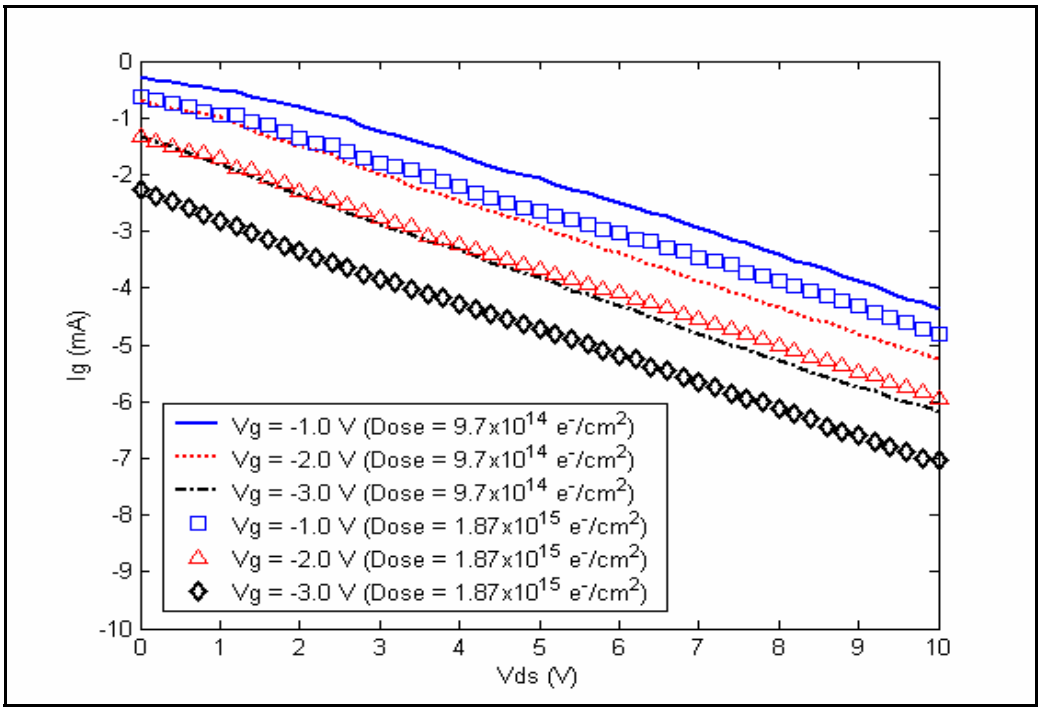

Figure 82. Sample A0409 FatFET Third Irradiation: Change in Gate Leakage Currents at LiN Temperature (0.45 MeV Electrons)

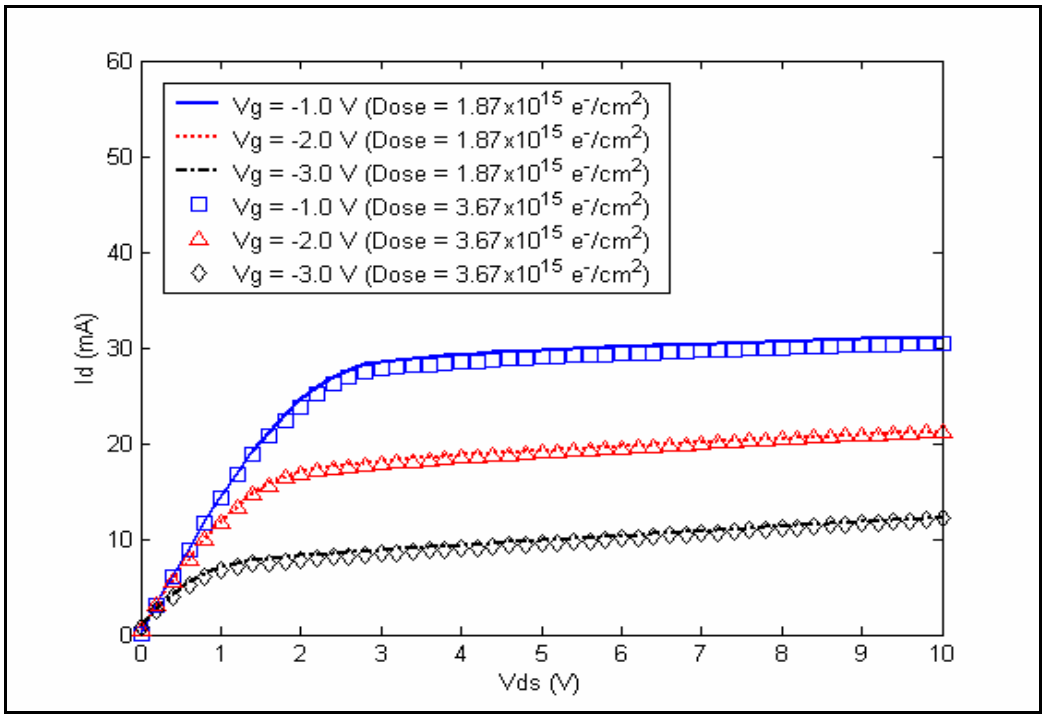

Figure 83. Sample A0409 FatFET Fourth Irradiation: Change in *I-V* Curves at LiN Temperature (0.45 MeV Electrons)

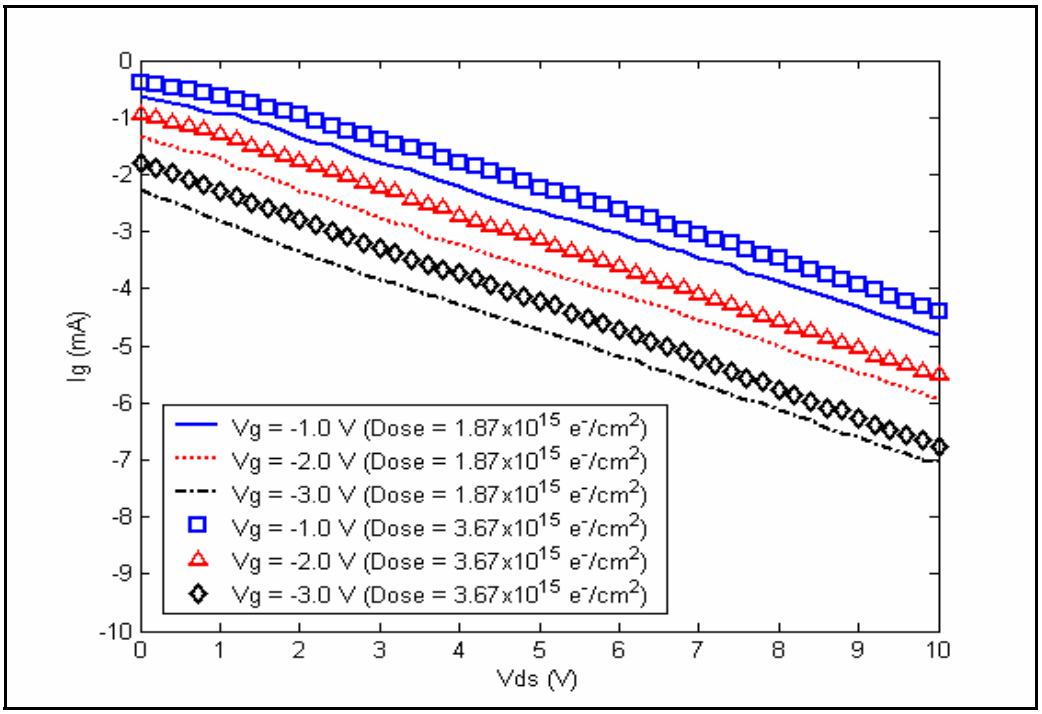

Figure 84. Sample A0409 FatFET Fourth Irradiation: Change in Gate Leakage Currents at LiN Temperature (0.45 MeV Electrons)

Bibliography

[1] Robert F. Pierret. *Semiconductor Device Fundamentals*. Addison-Wesley Publishing Company, Reading, MA, 1996.

[2] Stephen A. Campbell. *The Science and Engineering of Microelectronics Fabrication*. Oxford University Press, New York, 2001.

[3] M. Stutzmann, *et. al*. "GaN-based heterostructures for sensor applications," *Diamond and Related Materials*, 11: 886-891 (2002).

[4] Hadis Markoc. "Potential applications on III-V nitride semiconductors," *Materials Science and Engineering*, B43: 137-146 (1997).

[5] Mohamed Henini. "III-V nitrides for electronic and UV applications," *III-Vs Review*, Vol. 12, No. 5: 28-32 (1999).

[6] Q. Chen, *et. al*. "Microwave Electronic Device Applications of AlGaN/GaN Heterostructures," *Materials Science and Engineering*, B59: 395-400 (1999).

[7] B. Luo, *et. al*. "High-energy proton irradiation effects on AlGaN/GaN high-electron mobility transistors," *Journal of Electronics Materials*, 31: 437-441 (2002).

[8] A. Ionascut-Nedelcescu, *et. al*. "Radiation hardness of gallium nitride," *IEEE Transactions on Nuclear Science*, 49: 2733-2738 (December 2002).

[9] Andrew Holmes-Siedle, Len Adams. *Handbook of Radiation Effects*. 2nd Edition, Oxford University Press, Oxford, 2002.

[10] Greene, Kevin D. *Electron Paramagnetic Resonance Spectroscopy and Hall Effect Studies of the Effects of Low Energy Electron Irradiation on Gallium Nitride (GaN)*. Air Force Institute of Technology (AU), Wright-Patterson AFB OH, September 2003.

[11] Bernard Gil. *Low-Dimensional Nitride Semiconductors*. Oxford University Press, New York, 1999.

[12] Umesh K. Mishra, *et. al*. "AlGaN/GaN HEMTs – An Overview of Device Operation and Applications," *Proceedings of the IEEE*, Vol. 90, No. 6: 1022-1031 (2002).

[13] Robert Fitch. AFRL/SNDD WPAFB, OH. Personal Correspondence. 12 February 2004.

[14] A. Y. Polyakov, *et. al*. "Effects of proton implantation on electrical and recombination properties of n-GaN," *Solid State Electronics*, 44: 1971-1983 (2000).

[15] B. D. White, *et. al*. "Characterization of 1.8 MeV proton-irradiated AlGaN/GaN field-effect transistor structures by nanoscale depth-resolved luminescence spectroscopy," *IEEE Transactions on Nuclear Science* 49: 2695-2701 (December 2002).

[16] Francois Gaudreau, *et. al*. "Transport Properties of Proton-Irradiated Gallium Nitride-Based Two-Dimensional Electron-Gas System," *IEEE Transactions on Nuclear Science*, 49: 2702-2707 (December 2002).

[17] Z-Q. Fang, *et. al*. "Deep centers in as-grown and electron-irradiated n-GaN," *IEEE*, 35-42 (2000).

[18] D. C. Look, *et. al*. "Defect Donor and Acceptor in GaN," *Physical Review Letters*, Vol. 79, No. 6: 2273-2 76 (1997).

[19] D. C. Look, *et. al*. "On the Nitrogen Vacancy in GaN," *Applied Physics Letters*, Vol. 83, No. 17: 3525-3527 (2003).

[20] Ho Won Jang, *et. al*. "Mechanism of two-dimensional electron gas formation in $Al_xGa_{1-x}N$/GaN heterostructures," *Applied Physics Letters*, Vol. 81, No. 7: 1249-1251 (2002).

[21] Hadis Morkoc, *et. al*. "Review: GaN-based modulation doped FETs and UV detectors," *Solid-State Electronics*, 46: 157-202 (2002).

[22] J. Burn and L. F. Eastman. "AlGaN/GaN HFETs/MODFETs," *Properties, Processing and Applications of Gallium Nitride and Related Semiconductors*: 579-581 (1998).

[23] John D. Albrecht, *et. al*. "AlGaN/GaN Heterostructure Field-Effect Transistor Model Including Thermal Effects," *IEEE Transactions on Electron Devices*, Vol. 47, No. 11: 2031-2036 (2000).

[24] S. Nozaki, *et. al*. "Compression of the dc drain current by electron trapping in AlGaN/GaN modulation doped field-effect transistors," *Applied Physics Letters*, Vol. 78, No. 19: 2896-2898 (2001).

[25] S.T. Bradley, *et. al*. "Role of Barrier and Buffer Layer Defect States in AlGaN/GaN HEMT Structures," *Journal of Electronic Materials*, Vol. 30, No. 3: 123-128 (2001).

[26] T. Wang, *et. al*. "Investigation of two-dimensional electron gas in AlGaN/GaN heterostructures grown by metalorganic chemical vapor deposition (MOCVD)," *Journal of Crystal Growth*, Vol. 203: 443-446 (1999).

[27] International Commission on Radiation Units and Measurements. *Stopping Power for Electrons and Positrons*. ICRU Report 37. Bethesda, MD, 1984.

[28] Shreepad Karmalkar, *et. al*. "Mechanism of the reverse gate leakage in AlGaN/GaN high electron mobility transistors," *Applied Physics Letters*, Vol. 82, No. 22: 3976-3978 (2003).

[29] D. Qiao, *et. al*. "Transport properties of the advancing interface ohmic contact to AlGaN/GaN heterostructures," *Applied Physics Letters*, Vol. 80, No. 6: 992-994 (2002).

[30] M. Asif Khan, *et. al*. "AlGaN/GaN metal-oxide-semiconductor heterostructure field-effect transistors on SiC substrates," *Applied Physics Letters*, Vol. 77, No. 9: 1339-1341 (2000).

[31] R. Dietrich, *et. al*. "Current limitation after pinch-off in AlGaN/GaN FETs," *Materials Research Society Journal of Nitride Semiconductor Research*, Res. 5, 2 (2000).

[32] Robert Fitch. AFRL/SNDD WPAFB, OH. Telephone Conversation. 26 February 2004.

[33] S. Arulkumaran, *et. al*. "Temperature dependence of gate-leakage current in AlGaN/GaN high-electron-mobility transistors," *Applied Physics Letters*, Vol. 82, No. 18: 3110-3112 (2003).

Vita

Lieutenant James M. Sattler was born in 1980 in San Antonio, Texas. He graduated from Tom C. Clark High School, San Antonio, Texas in 1998 after which he attended Rensselaer Polytechnic Institute, Troy, New York where he earned his Bachelor of Science in Electrical Engineering in 2002. That same year he was commissioned as a Second Lieutenant in the United States Air Force following his successful completion of the Air Force Reserve Officer Training Program. Lieutenant Sattler entered the School of Engineering, Air Force Institute of Technology, Wright-Patterson Air Force Base, Ohio in August of 2002. Following his graduation from AFIT in the Spring of 2004, Lieutenant Sattler will be stationed at Hanscom Air Force Base, Boston, Massachusetts where he will be working in the Air Force Research Laboratory Sensors Directorate. Lieutenant Sattler is a member of Eta Kappa Nu and Tau Beta Pi.

REPORT DOCUMENTATION PAGE

Form Approved
OMB No. 074-0188

The public reporting burden for this collection of information is estimated to average 1 hour per response, including the time for reviewing instructions, searching existing data sources, gathering and maintaining the data needed, and completing and reviewing the collection of information. Send comments regarding this burden estimate or any other aspect of the collection of information, including suggestions for reducing this burden to Department of Defense, Washington Headquarters Services, Directorate for Information Operations and Reports (0704-0188), 1215 Jefferson Davis Highway, Suite 1204, Arlington, VA 22202-4302. Respondents should be aware that notwithstanding any other provision of law, no person shall be subject to an penalty for failing to comply with a collection of information if it does not display a currently valid OMB control number.
PLEASE DO NOT RETURN YOUR FORM TO THE ABOVE ADDRESS.

1. REPORT DATE *(DD-MM-YYYY)*	2. REPORT TYPE	3. DATES COVERED *(From – To)*
March - 2004	Master's Thesis	Jun 2003 – Mar 2004

4. TITLE AND SUBTITLE

AN ANALYSIS OF THE EFFECTS OF LOW ENERGY ELECTRON RADIATION ON $Al_xGa_{1-x}N$/GaN MODULATION-DOPED FIELD-EFFECT TRANSISTORS

5a. CONTRACT NUMBER

5b. GRANT NUMBER

5c. PROGRAM ELEMENT NUMBER

6. AUTHOR(S)

Sattler, James M., 2d Lt, USAF

5d. PROJECT NUMBER

5e. TASK NUMBER

5f. WORK UNIT NUMBER

7. PERFORMING ORGANIZATION NAMES(S) AND ADDRESS(S)

Air Force Institute of Technology
Graduate School of Engineering and Management (AFIT/EN)
2950 Hobson Way, Building 640
WPAFB OH 45433-7765

8. PERFORMING ORGANIZATION REPORT NUMBER

AFIT/GE/ENP/04-02

9. SPONSORING/MONITORING AGENCY NAME(S) AND ADDRESS(ES)

DTRA/CSNP
DTRA HEADQUARTERS
ATTN: Mr. Gerry Baird/CSNP
8725 John J. Kingman Road
Ft. Belvoir, VA 22060-6201

10. SPONSOR/MONITOR'S ACRONYM(S)

11. SPONSOR/MONITOR'S REPORT NUMBER(S)

12. DISTRIBUTION/AVAILABILITY STATEMENT

APPROVED FOR PUBLIC RELEASE; DISTRIBUTION UNLIMITED.

13. SUPPLEMENTARY NOTES

14. ABSTRACT

The effects of radiation on $Al_xGa_{1-x}N$/GaN MODFETs is an area of increasing interest to the USAF as these devices become developed and integrated in satellite-based systems. Irradiation is also a valuable tool for analyzing the quantum-level characteristics and properties that are responsible for device operation.

$Al_xGa_{1-x}N$/GaN MODFETs were fabricated and irradiated at liquid nitrogen temperatures by 0.45 –1.2 MeV electrons up to doses of 6×10^{16} e^-/cm^2. Following irradiation, low temperature *I-V* measurements were recorded providing dose-dependent measurements. Temperature-dependent *I-V* measurements were also made during room temperature annealing following irradiation.

I-V measurements indicate radiation-induced changes occur in these devices creating increased gate and drain currents. These increased currents are only maintained at low temperatures (T < 300 K). It is believed that the increase in gate current is caused by an increase in the electron trap concentration of the $Al_xGa_{1-x}N$ layer. This increase in trap concentration directly increases the trap-assisted tunneling current resulting in the observed increase in gate current. The mechanism causing the increase in drain current is unknown. Several theories explaining this increase are presented along with the additional research necessary to illuminate the correct theory. This is the first experiment involving electron radiation of $Al_xGa_{1-x}N$/GaN MODFETs.

15. SUBJECT TERMS

Aluminum Gallium Nitrides, Gallium Nitrides, Transistors, Heterojunctions, High Electron Mobility Transistors, Field Effect Transistors, Electron Irradiation, Radiation Effects, Radiation Damage, Semiconductors

16. SECURITY CLASSIFICATION OF:			17. LIMITATION OF ABSTRACT	18. NUMBER OF PAGES	19a. NAME OF RESPONSIBLE PERSON
a. REPORT	b. ABSTRACT	c. THIS PAGE			James C. Petrosky, LTC, USA (ENP)
U	U	U	UU	143	19b. TELEPHONE NUMBER *(Include area code)* (937) 255-6565, ext 4600 (James.Petrosky@afit.edu)

Standard Form 298 (Rev. 8-98)
Prescribed by ANSI Std. Z39-18